IL NUOVO CIMENTO

1958

IL
NUOVO CIMENTO

PERIODICO ITALIANO DI FISICA

fondato a PISA nel 1855 da C. MATTEUCCI e R. PIRIA
dal 1897 Organo della Società Italiana di Fisica
è pubblicato
sotto gli auspici del Consiglio Nazionale delle Ricerche
a cura del Direttore
GIOVANNI POLVANI
Presidente della Società
e
dei Vicedirettori
M. CONVERSI e N. DALLAPORTA
con la collaborazione di un Comitato di redazione
costituito dai professori
G. BERNARDINI, G. BOLLA, A. BORSELLINO, E. CAIANIELLO, P. CALDIROLA,
G. CARERI, M. CINI, R. DEAGLIO, B. FINZI, S. FRANCHETTI,
F. FUMI, A. GIACOMINI, L. GIULOTTO, D. GRAFFI, G. OCCHIALINI,
E. PERUCCA, L. A. RADICATI, C. SALVETTI, G. SALVINI, M. SIMONETTA,
G. TORALDO DI FRANCIA, M. VERDE, G. WATAGHIN.

Segretario di Redazione
R. CORBI

Redazione
Bologna, Via Irnerio n. 46
presso l'Istituto di Fisica dell'Università

Direzione
Milano, Via Saldini n. 50
presso l'Istituto di Fisica dell'Università

IL
NUOVO CIMENTO

ORGANO DELLA SOCIETÀ ITALIANA DI FISICA
SOTTO GLI AUSPICI DEL CONSIGLIO NAZIONALE DELLE RICERCHE

VOLUME VII

Serie decima

Anno centesimoquarto

1958

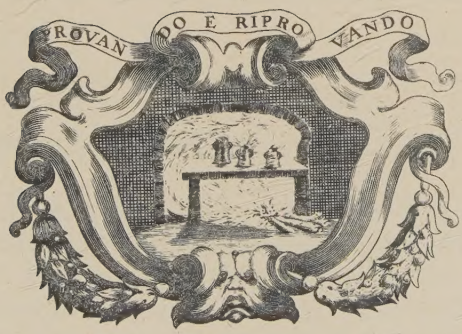

PRINTED IN ITALY

NICOLA ZANICHELLI EDITORE
BOLOGNA

IL
NUOVO CIMENTO
ORGANO DELLA SOCIETÀ ITALIANA DI FISICA
SOTTO GLI AUSPICI DEL CONSIGLIO NAZIONALE DELLE RICERCHE

VOL. VII, N. 1 *Serie decima* 1° Gennaio 1958

Microwave Apparatus for the Measurement of the Refraction, Dispersion and Absorption of Gases at Relatively High Pressure.

A. BATTAGLIA, F. BRUIN (*) and A. GOZZINI
Istituto di Fisica dell'Università - Pisa

(ricevuto il 23 Giugno 1957)

Summary. — An apparatus of high sensitivity is described using a single frequency modulated klystron oscillator. The resonance curve of a sample cavity is compared to the one of a reference cavity by means of an electronic device using microsecond pulse technique. Without special precautions the sensitivity for measurements of the power absorption coefficient is 10^{-5} m^{-1} and 10^{-8} for the refractive index.

1. – General outline of apparatus.

The apparatus described below was designed to search for still unknown microwave absorption bands of gases and vapours at relatively high pressures, when resonance lines are too broad to apply the conventional waveguide techniques of microwave spectroscopy. The application of the latter technique, which is extremely accurate and sensitive but also rather time absorbing, could then be restricted to those frequency regions selected in advance by our apparatus. Apart from this the set-up turned out to be very useful as well to investigate pressure effects of known absorption bands.

For gases at relatively high pressure over a small band in the spectrum the absorption and refraction are independent of frequency so that these

(*) Now at the Natuurkundig Laboratorium. Universiteit van Amsterdam.

quantities may be measured with resonance cavities. The small space required (as compared to a waveguide) has the practical advantage that only relatively little gas is needed and that the device may easily be temperature controlled. Absorption measurements of this kind were first carried out by BLEANEY and PENROSE ([1,2]). Their method was further developed by BIRNBAUM, KRYDER and LYONS ([3]), by ZIEMAN ([4]), by HUGHES and ARMSTRONG ([5]) and by JASINSKY and BERRY ([6]).

One of the main difficulties when using cavities for the measurement of small absorptions or refractions is the drift and the low frequency fluctuation of the frequency and the amplitude of the wave generated by the klystron oscillator: The change in frequency during a comparison of an empty cavity with a cavity containing the sample limits the sensitivity. Of course the sensitivity can be increased when the effect of these fluctuations on the measurement can be diminished. Usually this is done by stabilizing one or two klystron oscillators in frequency against the applied cavity resonators. In the present apparatus, however, high sensitivity is achieved more simply, namely by comparing both cavities in a time interval of only some microseconds. In this way low frequency fluctuations and drift of the klystron are of no importance and no electronic stabilization of the klystron frequency is necessary. Early constructions of the present apparatus may be found in short notes by GOZZINI, POLACCO ([7]) and BATTAGLIA ([8]). We will now give a more detailed and up to date description.

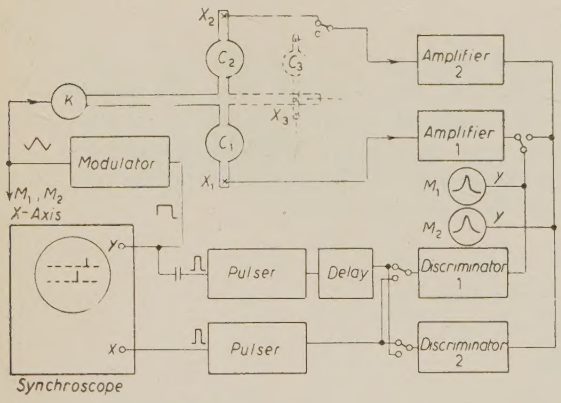

Fig. 1. – Block diagram of the microwave and electronic part of an apparatus used to measure small absorptions and refractions in gases.

A block diagram of a set-up is shown in Fig. 1. A klystron K is modulated in frequency on the reflector by a

(1) B. BLEANEY and R. P. PENROSE: *Proc. Roy. Soc.*, **189**, 358 (1947).
(2) B. BLEANEY and R. P. PENROSE: *Proc. Phys. Soc.*, **60**, 83 (1948).
(3) G. BIRNBAUM, S. J. KRYDER and H. LYONS: *Journ. Appl. Phys.*, **22**, 95 (1951).
(4) C. M. ZIEMAN: *Journ. Appl. Phys.*, **23**, 154, (1952).
(5) J. V. HUGHES and H. L. ARMSTRONG: *Journ. Appl. Phys.*, **23**, 501 (1952).
(6) W. JASINSKY and J. A. BERRY: *Proc. I.E.E.*, **101**, Pt. III, 337 (1954).
(7) A. GOZZINI and E. POLACCO: *Compt. Rend. Acad. Sci.* (*Paris*), **237**, 1497, 1652 (1953).
(8) A. BATTAGLIA and A. GOZZINI: *Onde Elect.*, **35**, 500 (1955).

triangular voltage of small amplitude and of low frequency. A transmission cavity C_1 is tuned to the mean frequency ν_0 and we suppose a second transmission cavity C_3, coupled via a crystal multiplier, to be tuned to a frequency $2\nu_0$. The resonance curves detected by the crystals x_1 and x_3 are amplified considerably. The resulting resonance curves may be viewed on two small monitor oscilloscopes M_1 and M_2. By means of the strongly amplified signals two discriminators both fire a pulse at the moment when the resonance curve of interest passes a certain fraction of its maximum height. These pulses are shaped in the pulsers to have a steep rise and a length of 2 μs. The pulse from channel 1 is used to trigger a synchroscope, the high speed time base of which is calibrated in microseconds by intensity modulation. The pulse from channel 2 is shown on the screen once for increasing and once for decreasing klystron modulation voltage. The pulses on the screen may be distinguished by applying an additional square wave voltage to the y-axis of the synchroscope as is indicated in the block diagram. The pulses may be made coincident by tuning either C_1 or C_3. They may be shifted together along the x-axis by the variation of a delay in channel 1.

When a little gas is introduced into C_1 or C_3 the pulses will be considerably displaced. Using well known formulae for cavity resonators [1] it will be shown that a shift of their « barycentre » is proportional to the power absorption $2\alpha''$ of the gas, whereas a shift of one pulse relative to the other is proportional to the real part of the refractive index n'. Gases could be investigated at two different frequencies, one being twice the other, simply by putting them in either C_1 or C_3.

If sufficient microwave power is available it would be possible to use three cavities instead of C_1 and C_3, two of which could be tuned to the same frequency and one to double this frequency. By means of a switch one could then select the two cavities which would be suited best for a particular experiment. For this reason in Fig. 1 the combination C_1, C_2, C_3 is drawn.

2. – Analysis of operation.

Consider two high Q transmission cavities C_1 and C_2 having resonance frequencies ν_1 and ν_2. For C_1 the relative microwave power transmission is given by [9]

$$\frac{P}{P_0} = 1 \Big/ \left[1 + 4Q_1^2 \left(\frac{\nu - \nu_1}{\nu_1} \right)^2 \right], \tag{1}$$

[9] C. G. Montgomery, R. H. Dijke and E. M. Purcell: *M.I.T. Lab. Series*, Vol. 8.

the same holding for C_2 replacing Q_1 and Q_2 and ν_1 by ν_2. If we assume that both cavities are followed by a matched detector, not necessarily quadratic, and a linear video amplifier, and if we apply linear frequency modulation to the microwave generator, then the output voltages V of the amplifiers will be functions which are symmetryc with respect to the frequencies ν_1 or ν_2, at which they reach maximum values. If the frequency modulation law is triangular the oscillator frequency may be represented by:

$$\nu = \bar{\nu} + vt \qquad \text{when} \qquad 0 < t < T/2 \,, \tag{2a}$$

$$\nu = \bar{\nu} + v(T - t) \qquad \text{when} \qquad T/2 < t < T \,, \tag{2b}$$

$v = |\mathrm{d}\nu/\mathrm{d}t|$ being the modulation velocity and T the repetition time.

If we assume that a pulse is fired each time the amplifier outputs reach preset fractions of their maximum output, for C_1 being $f_1 = V/V(\nu_1)$, and *only after* such a maximum is passed, then for C_1 these pulses are fired at the frequencies

$$\nu_1^+ = \nu_1(1 + k_1/2Q_1) \,, \qquad \text{when} \qquad \mathrm{d}\nu/\mathrm{d}t > 0 \,, \tag{3a}$$

$$\nu_1^- = \nu_1(1 - k_1/2Q_1) \,, \qquad \text{when} \qquad \mathrm{d}\nu/\mathrm{d}t < 0 \,, \tag{3b}$$

which are symmetric with respect to the resonance frequency ν_1. The constant k_1 depends on f_1 and the detector characteristics. Similar relations hold for the second channel (C_2), with as a rule $k_1 \neq k_2$ and $Q_1 \neq Q_2$.

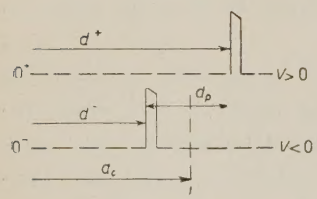

Fig. 2. – Picture on the screen of the synchroscope showing the various distances occurring in the formulae.

As explained in Sect. **1** the pulses from channel 2 trigger the sweep of a synchroscope. The velocity of the spot on the screen, which is very high, we call w. The pulses from channel 1, delayed by and adjustable time τ, produce deflections along the y-axis. One therefore observes on the screen two pulses of which the distances from the starting point of the sweep (O in Fig. 2) will be

$$d^+ = w\tau + \frac{w}{2v}\left[\frac{k_2\nu_2}{Q_2} - \frac{k_1\nu_1}{Q_1}\right] + \frac{w}{v}(\nu_2 - \nu_1) \qquad \text{when} \qquad \frac{\mathrm{d}\nu}{\mathrm{d}t} > 0 \,, \tag{4a}$$

$$d^- = w\tau + \frac{w}{2v}\left[\frac{k_2\nu_2}{Q_2} - \frac{k_1\nu_1}{Q_1}\right] - \frac{w}{v}(\nu_2 - \nu_1) \qquad \text{when} \qquad \frac{\mathrm{d}\nu}{\mathrm{d}t} < 0 \,, \tag{4b}$$

so that the distance between the observed pulses

$$d_p = |d^+ - d^-| = \left|\frac{2w}{v}(\nu_2 - \nu_1)\right| \tag{5}$$

is independent of the constants τ, k_1 and k_2 and the Q-values of the cavities. On the other hand the distance from the starting point O of the sweep to the « barycentre » of the observed pulses is

$$d_c = \frac{(d^+ + d^-)}{2} = w\tau + \frac{w}{2v}\left[\frac{k_2\nu_2}{Q_2} - \frac{k_1\nu_1}{Q_1}\right]. \tag{6}$$

If a gas is let into one or into both cavities, by means of formula (5) one may obtain all quantities related to the refraction of this gas, whereas from (6) one may deduce the absorption. In order to elucidate this we will discuss some examples of practical interest.

2·1. *Refraction and absorption.* – The empty cavities are tuned to the *same* frequency $\nu_0 = \nu_1 = \nu_2$, then pulses appear superimposed on the CRT screen. If a gas is admitted into C_1 the distances d_p and d_c according to (5) and (6) will change by the amounts

$$\delta_p = \frac{2w}{v}\,\delta\nu\,, \tag{7}$$

$$\delta_c = \frac{\omega}{2v}\,k_1\nu_0\left[\frac{1}{Q} - \frac{1}{Q_1}\right], \tag{8}$$

in which $\delta\nu$ is the frequency shift due to the admission of gas and Q is the quality factor of the gas-filled cavity C_1: Now $\delta\nu$ is related to the real part of the refractive index n' by [9]

$$\delta\nu = \nu_0\left(1 - \frac{1}{n'}\right) \approx \nu_0(n' - 1)\,, \tag{9}$$

whereas the power absorption coefficient is given by [9]

$$2\alpha'' = \frac{2\pi\nu_0}{c}\left[\frac{1}{Q} - \frac{1}{Q_1}\right]. \tag{10}$$

It therefore follows that

$$n' - 1 = \frac{v}{2w}\frac{1}{\nu_0}\,\delta_p\,, \tag{11}$$

$$2\alpha'' = \frac{4\pi}{c}\frac{v}{k_1 w}\,\delta_c\,, \tag{12}$$

so that, from the reading of δ_p and δ_c immediately follow the values of n' and $2x'$ at this frequency ν_0. Measurements of this kind will be discussed in a following paper.

2·2. *Strong dispersion.* – By superimposing the observed pulses the empty cavities may also be tuned to frequencies which differ a fixed and accurately known amount $-\Delta\nu_s$ and $+\Delta\nu_s$ respectively (of some MHz only) from a frequency ν_0. If this is done and a gas is admittad into both cavities *simultaneously*, then the change in position of the pulses may be used to measure the dispersion $D = \Delta n'/2\Delta\nu_s$ at frequency ν_0.

This may be done as follows. The triangular modulation voltage is decreased so that the frequency band covered by the frequency modulated klystron is a little less than $2\Delta\nu_s$. If now C_1 is tuned to a frequency just below this band and C_2 to a frequency just above it no pulses will be seen on the synchroscope screen. After this, in addition to the low frequency triangular voltage, a sinusoidal radio wave of frequency $\Delta\nu_s$ from a quartz crystal oscillator is fed to the repeller of the klystron. Apart from microwaves of frequency ν the klystron will then also generate power at the side bands $(\nu \pm m\Delta\nu_s)$, in which m is an integer. The amplitude of the sine-wave is now adjusted to such a value that the larger part of the klystron power is fed into the first pair of side bands, i.e. for $m = 1$ at frequencies $\nu \pm \Delta\nu_s$. Each cavity will then resonate on one of these side bands and the corresponding pulses will be seen on the screen. If these pulses are superimposed then, the cavities will be tuned to frequencies which differ exactly $2\Delta\nu_s$ in frequency. If now a gas is admitted into both cavities, having refractive index n_1' and n_2' at the resonance frequencies $\nu_1 = \nu_0 - \Delta\nu_s$ and $\nu_2 = \nu_0 + \Delta\nu_s$ respectively, then the observed separation of the pulses will be

$$d_v = \frac{2w}{v}\left[\nu_0\left(\frac{1}{n_2'} - \frac{1}{n_1'}\right) + \Delta\nu_s\left(\frac{1}{n_1'} + \frac{1}{n_2'} - 2\right)\right]. \tag{13}$$

or putting $n_1' + n_2' = 2n'$

$$d_v = \frac{2w}{v}\left[\nu_0(n_2' - n_1') + 2\Delta\nu_s(n' - 1)\right]. \tag{14}$$

If $(n' - 1)$ at frequency ν_0 is very small or is known from a previous measurement the dispersion follows immediately from (14).

2·3. *Weak dispersion.* – The empty cavities C_1 and C_3 are tuned to ν_0 and $n\nu_0$ respectively, n being integer. The microwave power at a frequency $n\nu_0$ is obtained by placing an adjusted crystal multiplier between klystron and cavity. The measurements at a frequency ν_0, as listed under 2·1, may now be

repeated for the frequency $n\nu_0$ by admitting the gas into C_2. One may apply the formulae (11) and (12) if the right hand side of (12) is multiplied by n.

If the gas shows little absorption in the frequency region from ν_0 to $n\nu_0$ the relative variation of the refractive index is very small and difficult to detect if the refractive index is measured *directly* at the different frequencies. Such measurements can, however, be carried out easily if the gas, at the same pressure and temperature is admitted into both cavities *simultaneously*. The quantity n' in (11) then denotes the *change* in refractive index over a frequency region $(n\nu_0 - \nu_0)$. Therefore a set-up like this is perfectly suited for the measurement of a small dispersion over a large frequency band.

2·4. *Increased sensitivity for very small absorption.* – Up till now in our discussion the synchroscope sweep was always initiated by the pulses from channel 2, whereas the observed pulses came from channel 1. If alternatively for one period of the modulation one would trigger the sweep with the pulses from channel 2 and the next period one would trigger with the pulses from channel 1, instead of one pulse (Fig. 2) on each of the traces on the screen now two pulses would be seen. In order to achieve this result an electronic switch should be inserted between the discriminators and the pulser outputs. If both cavities are tuned to the same frequency ν_0, and $k_1 = k_2$ and $Q_1 = Q_2$, then $d_1^+ = d_2^-$, $d_1^- = d_2^+$ and $\Delta^+ = \Delta^- = 0$ (see Fig. 3).

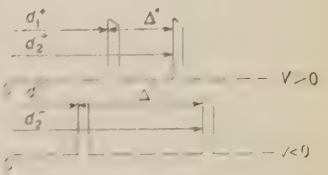

Fig. 3. Picture on the screen of the synchroscope if an auxiliary electronic switch is applied.

If we let gas into one of the cavities and then tune this cavity to have the pulses on one trace coincident again, then it may be easily shown that the distance between the pulses on the other trace is four times as large as the distance δ_ν of formula (8). So by adding an electronic switch as indicated the sensitivity for absorption may be increased by a factor four.

3. – Sensitivity of the apparatus.

The sensitivity of the apparatus is limited by the low frequency noise produced by the crystals detectors and multipliers. Because of this noise there are fluctuations at the output of the amplifiers, causing irregularities in the firing point of each discriminator, so that the pulses on the screen show a jitter.

We have for the indetermination $\Delta\nu$ in the discriminated frequencies ν^+, ν^- produced by this jitter

$$\Delta V = \frac{dV}{dP}\,\frac{dP}{d\nu}\,\Delta\nu = N\,, \tag{15}$$

V and N being the signal and noise voltages at the outputs of the amplifiers.

If the maximum power transmitted by the cavities is of the order of 10^{-6} W then $\Delta\nu$ can be easily calculated. In this case the noise produced by the crystal is essentially the Johnson noise of a resistence equal in value to the d.c. impedence of the crystal, and the crystal operates as a quadratic detector. We have, from (1) and (15) ([10])

$$\frac{\Delta\nu}{\nu_0} = \frac{4\sqrt{3}}{9}\frac{\sqrt{4kTB}}{P_0 MQ},$$

B and M being the bandwidth and the overall figure of merit of the video receiver, and $\mathrm{d}P/\mathrm{d}\nu$ being calculated for frequencies ν^+, ν^- at which $V/V_{max} = 3/4$ ($k_1 = 1/\sqrt{3}$).

With $P_0 \simeq 10^{-6}$ W, $M = 100$, $Q = 30\,000$, we deduce, for the minimum detectable variation of refractive index:

$$(n-1)_{min} = \left(\frac{\Delta\nu}{\nu_0}\right)_{min} \approx 10^{-9}.$$

At present, the sensitivity of the apparatus is of an order of magnitude smaller, being

$$\left(\frac{\Delta\nu}{\nu_0}\right)_{min} \approx 10^{-8}.$$

The sensitivity in the measurement of absorption is proportional to that of refraction, and depends from frequency, because from frequency depends the physical phenomenon from which absorption is deduced. Indeed from (12) we deduce.

$$(2\alpha'')_{min} = \frac{4\pi\nu_0}{ck_1}\left(\frac{\Delta\nu}{\nu_0}\right)_{min}.$$

* * *

This research has been supported by « Consiglio Nazionale delle Ricerche » and by « Centro Microonde » of Florence.

We are grateful to Professors N. Carrara and M. Conversi for valuable suggestions and constant support and for putting at our disposal the facilities of their Laboratories. Thanks are also due to Mr. G. Ciampi and Mr. A. Pecchi,

---

([10]) W. Gordy, W. V. Smith and R. F. Trambarulo: *Microwave Spectroscopy* (New York, 1953), p. 68.

who constructed all parts of the various spectrometers, in particular the waveguide components and cavities, and to Mr. U. Della Croce for building the electronics.

RIASSUNTO

In questa nota viene descritto un apparecchio per misure del coefficiente di assorbimento e dell'indice di rifrazione di gas a pressioni relativamente elevate, costruito nell'Istituto di Fisica dell'Università di Pisa. Confrontando mediante una tecnica ad impulsi due cavità risonanti opportunamente accordate, viene ottenuta una sensibilità di 10^{-8} nelle misure dell'indice di rifrazione e di 10^{-5} m^{-1} nelle misure del coefficiente di assorbimento.

The Electromagnetic Cascade with Tridents.

J. W. Gardner

Atomic Power Division, English Electric Co., Ltd.
Whetstone, Leicester, England

(ricevuto il 16 Luglio 1957)

Summary. — Recent results claiming anomalously large cross-sections for direct pair creation by high energy electrons (mainly above 10 GeV) are discussed with particular reference to their significance in the development of the electron-photon cascade. A qualitative estimate, using an admittedly crude model, suggests that the effect of such large « trident » cross-sections could drastically change the pattern of development in the early stages of a really high energy cascade. The detailed analytical formulation of cascade theory is then modified in such a way that numerical values of the cross-section for trident production, when these are satisfactorily established, can be readily inserted in the formulae used for computing the moments of the number distribution function.

1. – Introduction.

The so-called trident process, i.e. direct creation of electron pairs by interactions of fast charged particles with Coulomb fields, has been studied both experimentally and theoretically by a number of workers (1). Until recently it appeared safe to assume from the available evidence that trident production by electrons, even at the highest cosmic ray energies, was a much less common occurrence than emission of bremsstrahlung or photon materialization. In view of this, and the complexity of cascade theory even without tridents, there has been an understandable reluctance to include terms representing trident production in the diffusion equations describing the multiplication of particles in the electromagnetic cascade—notwithstanding an awareness that even a

(1) Extensive references are given in a paper by M. M. Block *et al.*: *Phys. Rev.* **46**, 1627 (1954).

few tridents might have a non-negligible effect on the initial development of a cascade with energy above 10 GeV, say.

In the past few years, however, the justification for neglecting the trident terms in cascade theory has been somewhat shaken by observations ([2-6]) and calculation ([7,8]) which appear to indicate a distinctly larger cross-section for trident production, especially above 10 GeV, than would have seemed possible from earlier studies. Not all these recent reports have gone unchallenged; for example, BLOCK and KING ([9]) have criticised KOSHIBA and KAPLON's interpretation of their data. [A basic difficulty in the experimental study of tridents arises from the tendency to include in the « trident count » a fraction of those pairs which are due to conversion of bremsstrahlung photons so close to the track of the parent electron that the event cannot be distinguished observationally from direct pair creation by the parent electron. There appears to be some disagreement among experimentalists as to the allowance to be made for such pseudotridents; also for « spurious scattering » and other effects leading to under-estimation of energy.] Nevertheless the persistence of reports of « anomalously » large trident production, coming from a number of independent groups all over the world, does commend a re-assessment of high energy cascade theory to include a significant trident component.

In the present paper we shall first consider qualitatively, in Sect. **2**, how the electromagnetic cascade would develop if the mean free path for trident production were equal to that for bremsstrahlung emission, which at energies above 100 GeV, is about the value indicated by references ([2-4,6]) (*).

Even allowing for the crudeness of the model used, the results are so striking that it has seemed worth while to extend the quantitative formulation of MESSEL and POTTS ([10]) to include tridents. This is done in Sect. **3**, where we set up the matrix equations for the number distribution function and its moments, and compare them with the corresponding equations when tridents

---

([2]) J. E. NAUGLE and P. S. FREIER: *Phys. Rev.*, **92**, 1086 (1953).

([3]) J. E. NAUGLE and P. S. FREIER: *Report of Duke University Cosmic Ray Conference* (1953).

([4]) M. KOSHIBA and M. F. KAPLON: *Phys. Rev.*, **95**, 647 (1954); **97**, 193 (1955); **100**, 327 (1955).

([5]) R. WEILL *et al.*: *Helv. Phys. Acta*, **29**, 437 (1956).

([6]) A. DEBENEDETTI *et al.*: *Nuovo Cimento*, **12**, 954 (1954).

([7]) T. MUROTA *et al.*: *Prog. Theor. Phys.*, **16**, 482 (1956).

([8]) J. W. GARDNER: *Sydney University Research Report*, 1956 (unpublished).

([9]) M. M. BLOCK and D. T. KING: *Phys. Rev.*, **95**, 171 (1954).

(*) Extrapolation of the conventional theory of trident production by electrons (see e.g. reference ([1])) gives a mean free path in emulsion ($Z \sim 40$) of 8 radiation lengths at 100 GeV; however, such extrapolation is shown to be unjustified by MUROTA *et al.* ([7]) who by a more precise calculation obtain a m.f.p. of 3 r.l. at this energy.

([10]) H. MESSEL and R. B. POTTS: *Phys. Rev.*, **86**, 847 (1952).

are neglected. Numerical solution of these equations is not attempted here; while the time and labour involved would of course be greater than for the corresponding calculation without tridents it should not be prohitibive, given a fast electronic computer, to obtain numerical results for the first few moments and use them to construct the distribution function. However, one is deterred from embarking on such a computation until firmer evidence is available on the numerical values to be inserted for the trident production cross-section. It seems likely that further experiments in the course of the next year or so will supply this evidence.

2. – Qualitative considerations.

A qualitative model for the electromagnetic cascade without tridents has been described by HEITLER ([11]). While making no claim to detailed accuracy, the model does give a reasonable picture of the general development of the cascade. In the present section we briefly recapitulate this model and then discuss how it may be modified to include tridents. Some rough estimates of the average numbers of electrons are made, taking the mean free path for trident production to be equal to that for bremsstrahlung emission, and using two alternate assumptions about energy partition among the three trident electrons.

In the Heitler model it is assumed that whenever an electron traverses a distance ln 2 radiation length (*)—the distance in which its energy has on the average dropped by half—it emits just one photon of half its energy and retains the other half. Likewise, a photon in distance ln 2 is assumed to undergo materialization with the photon's energy shared equally between the two electrons. We ignore the fact that the mean free path for photons slightly exceeds that for electrons; both are taken at the high energy limit, where Compton scattering and collision losses may also be ignored. The model readily leads to the following results:

i) The number of particles in the cascade increases exponentially, within limits.

ii) For not too small depths the number of electrons in the cascade is about double the number of photons.

iii) The depth, $t_{\max}$, at which the number of particles in the cascade is a maximum is given by $t_{\max} \approx \ln (E_0/KE_c)$, with $E_0 =$ primary energy, $E_c =$ critical energy, $K =$ a constant of order unity.

iv) The number of electrons at the maximum $\approx 2E_0/3KE_c$.

([11]) W. HEITLER: *Quantum Theory of Radiation* (Oxford, 1954), 3rd ed., Section **38**.

(*) Not *one* radiation length, as erroneously stated in B. ROSSI's: *High Energy Particles* (New York, 1952), Section **5·3**.

To incorporate tridents into the above model let us assume that we have not one, but a large number N_0 of primary particles (electrons and photons) all of the same energy incident at $t = 0$; also in this case it is more convenient to divide the depth into layers of thickness ln 1.5 radiation length instead of ln 2.1 r.l. The solutions for the Heitler model [equations (7) and (8) below] predict that in the first ln 1.5 r.l. half of the primary electrons will emit one photon each, and half of the primary photons will undergo materialization. Now our new model postulates that the bremsstrahlung and photon-materialization mean free paths are unchanged but that, in addition, trident production by electrons occurs with the same mean free path. This, incidentally implies the assumption that the mean free path for trident production is independent of energy in the high energy limit. A further assumption we make is that the probabilities for a given electron to emit a bremsstrahlung and to make a trident in 1.5 r.l. are additive. This greatly simplifies the argument and is consistent with the general level of approximation of the Heitler model. On the present model, then, half of the primary electrons each produce a trident and half each emit a photon in the first ln 1.5 r.l.; the primary photons behave just as on the previous model, half undergoing materialization and half continuing unchanged. Thus in the first ln 1.5 r.l. all the primary electrons and half the primary photons undergo some multiplicative transformation. What happens at subsequent depths is determined by our assumptions about the partition of energy among the three electrons of a trident. We shall consider two opposite assumptions: *a*) each electron receives about one third of the total energy and is therefore itself capable of producing further tridents; *b*) one electron, the « primary », receives the bulk of energy and is the only one capable of producing further tridents, although the two secondaries may still participate in the cascade development by emitting bremsstrahlung. The truth lies somewhere between these two extremes, but probably much nearer to *b*) and *a*), see, for example, reference [1].

Let us denote the numbers of electrons and photons at depth t by $A(t)$, $B(t)$ respectively and also write α for ln 1.5. Then the equations describing the multiplication of particles in the cascade are:

$$2B(t+\alpha) = B(t) + A(t)\,, \tag{1}$$

$$A(t+\alpha) = B(t) + 2A(t)\,, \qquad \text{(Assumption } a)\text{)}, \tag{2a}$$

$$A(t+\alpha) = B(t) + A(t) + A(0)\,, \qquad \text{(Assumption } b)\text{)}. \tag{2b}$$

Equations (1) and (2*a*) taken together are satisfied by:

$$A(t) \approx 0.78\,N_0 \exp[2.03\,t]\,, \tag{3}$$

$$B(t) \approx 0.22\,N_0 \exp[2.03\,t]\,. \tag{4}$$

(1) and (2*b*) taken together yield:

$$A(t) \approx 1.27\, N_0\{\exp[1.42t] - 0.39\}\,, \tag{5}$$

$$B(t) \approx 0.36\, N_0\{\exp[1.42t] - 0.39\}\,. \tag{6}$$

For completeness we also recall the corresponding functions for Heitler's above model which ignores tridents:

$$A(t) \approx 0.67 \exp[t]\,, \tag{7}$$

$$B(t) \approx 0.33 \exp[t]\,. \tag{8}$$

To obtain t_{max} for the cascades represented by the above models one uses the criterion that the average energy per particle (electron or photon) at the maximum is of order KE_c. One finds then, that on either assumption *a*) or assumption *b*), the inclusion of the trident process causes the maximum to be reached in about half the distance that is required if tridents are ignored. To take a specific example, consider a cascade in air initiated by a 100 GeV primary: ignoring tridents $t_{max} \approx 6$ r.l.; with tridents under assumption *a*) $t_{max} \approx 3$ r.l., and under assumption *b*) $t_{max} \approx 3.7$ r.l.

Equations (3) to (8) further show that tridents, besides giving a much faster initial multiplication of particles, also increase the ratio of electrons to photons: without tridents it is 2:1, with tridents (on either assumption) it is just over 3.5:1. The effect on the multiplication of electrons of including the trident process in the cascade is illustrated numerically in Table I, and appears particularly striking, even with due allowance for the crudeness of the models used. The qualitative results of this section thus suggest the need

TABLE I. – *Average numbers of electrons from a single incident primary.*

$A_1(t) = 0.67 \exp[t]$ - tridents ignored,

$A_2(t) = 0.78 \exp[2.03t]$ - tridents included, assumption (*a*),

$A_3(t) = 1.27\{\exp[1.42t] - 0.39\}$ - tridents included, assumption (*b*).

t in radiation lengths	A_1	A_2	A_3	A_2/A_1	A_3/A_1
2	4.95	45.3	21.2	9.15	4.29
3	13.5	343.0	89.5	25.4	6.55

for having available a more quantitative formulation of cascade theory, into which numerical values for trident production cross-sections can be substituted when these are more reliably known. Such a formulation is outlined in the next section.

3. – Quantitative formulation.

In this section we follow closely the method and notation of MESSEL and POTTS in reference ([10]), denoted hereinafter by MP. As is done in that paper we ignore scattering both elastic and inelastic, i.e. we neglect both ionization loss and the lateral spread of the cascade. These approximations are certainly good ones at energies where trident production is expected to be significant. The only other assumption we make is that the cross-section for trident production is, like those for bremsstrahlung and photon materialization, a homogeneous function of degree zero in the primary and secondary energies. More specifically, we assume that the probability for a primary electron of energy E_0 to make in distance $\mathrm{d}x$ a trident with secondary energies in the intervals $\mathrm{d}E_i$ at E_i, $\mathrm{d}E_k$ at E_k and $\mathrm{d}E_l$ at E_l can be written $\omega^{(3)}(\eta_i, \eta_k, \eta_l)\,\mathrm{d}\eta_i\,\mathrm{d}\eta_k\,\mathrm{d}\eta_l\,\mathrm{d}x$ with $\eta_i = E_i/E_0$, $\eta_k = E_k/E_0$, $\eta_l = E_l/E_0$ and, by energy conservation, $\eta_i + \eta_k + \eta_l = 1$. The total cross-section for trident production is then written:

$$\alpha^{(3)} = \int_0^1\int_0^1 \omega^{(3)}(\eta_i, \eta_k, \eta_l)\,\mathrm{d}\eta_k\,\mathrm{d}\eta_l\,.$$

For convenience we recapitulate briefly the more important definitions of MP. The differential cross-sections for bremsstrahlung and for photon materialization (Bethe-Heitler full screening approximation) are respectively

$$\omega^{(1)}(\eta_k, \eta_l)\,\mathrm{d}\eta_k\,\mathrm{d}\eta_l\,\mathrm{d}x \quad \text{and} \quad \omega^{(2)}(\eta_k, \eta_l)\,\mathrm{d}\eta_k\,\mathrm{d}\eta_l\,\mathrm{d}x\,;$$

the corresponding total cross-sections are

$$\alpha^{(1)} = \int_0^1 \omega^{(1)}(\eta_k, \eta_l)\,\mathrm{d}\eta_l \quad \text{and} \quad \alpha^{(2)} = \int_0^1 \omega^{(2)}(\eta_k, \eta_l)\,\mathrm{d}\eta_l\,.$$

The function $p^{(j)}_{n,m}(\eta_1, \ldots, \eta_n, \eta_{n+1}, \ldots, \eta_{n+m}; x)\,\mathrm{d}\eta_1 \ldots \mathrm{d}\eta_{n+m}$ is defined as the differential probability that after a depth x a primary (j) of unit energy has given rise to n electrons with energies in the ranges η_k, $\eta_k + \mathrm{d}\eta_k$, with $k = 1, \ldots, n$, in any order, and m photons with energies in the ranges η_{n+l}, $\eta_{n+l} + \mathrm{d}\eta_{n+l}$, with $l = 1, \ldots, m$ in any order. Further, the function

$$q^{(j)}_{n,m}(\eta_1, \ldots, \eta_n; \eta_{n+1}, \ldots, \eta_{n+m}; x)\,\mathrm{d}\eta_1 \ldots \mathrm{d}\eta_{n+m}$$

is defined as the differential probability that after a depth x a primary (j) of unit energy has given rise to n electrons and m photons with energies specified as above, plus any numbers of electrons and photons with arbitrary energies, including if we wish the same energies specified above. A relation between $q^{(j)}_{n,m}$ and $p^{(j)}_{n,m}$ is given in MP; hence if either $q^{(j)}_{n,m}$ or $p^{(j)}_{n,m}$ is known the other may in principle be determined. However, it is found more expedient to derive diffusion equations for each of $q^{(j)}_{n,m}$ and $p^{(j)}_{n,m}$ and solve them directly.

The usefulness of the quantity $q^{(j)}_{n,m}$, called by some authors the « product density », lies in its very simple relation with the moments of the practically useful function $\varphi_{n,m}(\eta, x)$ expressing the probability that a primary (j) of unit energy has given rise, after a depth x, to n electrons and m photons with energies $> \eta$ and any numbers of electrons and photons with energies $< \eta$. This relation is ([12]):

$$T^{(j)}_{n,m}(\eta; x) = \int_{\eta}^{1} \mathrm{d}\eta_1 \ldots \int_{\eta}^{1} \mathrm{d}\eta_{n+m}\, q^{(j)}_{n,m}(\eta_1, \ldots, \eta_n; \eta_{n+1}, \ldots, \eta_{n+m}; x)\,, \tag{3.1}$$

where $T^{(j)}_{n,m}(\eta; x)$ is the (n, m)-th factorial moment defined by:

$$T^{(j)}_{n,m}(\eta; x) = \sum_{a=0}^{\infty} \sum_{b=0}^{\infty} \frac{(n+a)!}{a!} \frac{(m+b)!}{b!} \varphi^{(j)}_{n+a,\, m+b}(\eta; x)\,. \tag{3.2}$$

Since the enormous complexity of the analytical expression for $\varphi^{(j)}_{n,m}$ makes its direct calculation quite prohibitive, even with an electronic computer ([13]), the value of $q^{(j)}_{n,m}$ for obtaining the moments is immediately apparent; for one can get certain information about the shape of the distribution from its first few moments and may in fact be able to construct a reasonable approximation to $\varphi^{(j)}_{n,m}$ from an expansion in the moments.

We now proceed to set up the matrix recurrence relations giving the $p^{(j)}_{n,m}$ and $q^{(j)}_{n,m}$.

3·1. *Equation for* $p^{(j)}_{n,m}$. – The diffusion equation satisfied by the $p^{(j)}_{n,m}$ is obtained by considering all possible last collisions, just as in MP. It is:

$$\begin{aligned}
\{\partial/\partial x + n(\alpha^{(1)} + \alpha^{(3)}) + m\alpha^{(2)}\} p^{(j)}_{n,m} = \\
= \sum_{C_1^n} \sum_{C_1^m} p^{(j)}_{n,m-1}(\eta_1', \ldots, \eta_{n-1}', \eta_n' + \eta_{n+m}'; \eta_{n+1}', \ldots, \eta_{n+m-1}'; x)\, \omega^{(1)}(\eta_n', \eta_{n+m}') + \\
+ \sum_{C_2^n} p^{(j)}_{n-2,m+1}(\eta_1', \ldots, \eta_{n-2}'; \eta_{n+1}, \ldots, \eta_{n+m}, \eta_{n-1}' + \eta_n'; x)\, \omega^{(2)}(\eta_{n-1}', \eta_n') + \\
+ \sum_{C_3^n} p^{(j)}_{n-2,m}(\eta_1', \ldots, \eta_{n-3}', \eta_{n-2}' + \eta_{n-1}' + \eta_n'; \eta_{n+1}, \ldots, \eta_m)\, \omega^{(3)}(\eta_{n-2}', \eta_{n-1}', \eta_n')\,,
\end{aligned}$$

([12]) H. Messel and R. B. Potts: *Proc. Phys. Soc.* (*London*), **65**, 854 (1952).

([13]) H. Messel and J. W. Gardner: *Phys. Rev.*, **84**, 1256 (1951); **86**, 808 (1952).

with the initial conditions:

$$p^{(j)}_{n,m}(x=0) = \delta_{n+j,2}\,\delta_{m+1,j}\,\delta(1-\eta_1)\,. \tag{3.4}$$

In (3.3) the C^n_1 and C^n_2 signify that the summations are taken over all possible choices of η'_n and η'_{n-1}, η'_n respectively from the η_k, $k=1,\ldots,n$; the C^m_1 signifies summation over all possible choices of η'_{n+m} from the η_{n+1}, $l=1,\ldots,m$; C^n_3 signifies summation over all possible choices of $\eta'_{n\ 2}$, $\eta'_{n\ 1}$, η'_n from the η_k, $k=1,\ldots,n$. The only differences between our equation (3.3) and the corresponding equation (eqn. (8)) of MP are (i) the coefficient of n on the left side is now $\alpha^{(1)}+\alpha^{(3)}$ instead of just $\alpha^{(3)}$; and (ii) the right side now includes a third term representing trident production as well as the original two terms representing bremsstrahlung emission and photon materialization. The initial conditions are exactly as in MP; moreover, since any cascade with tridents cannot contain less than three electrons, the right side of (3.3) must revert to the right side of eqn. (8) of PM for $n<3$.

If we define the Laplace transform of $p^{(j)}_{n,m}$ as:

$$P^{(j)}_{n,m}(\lambda) = \int_0^\infty \exp[-\lambda x]\,p^{(j)}_{n,m}(x)\,\mathrm{d}x\,, \tag{3.5}$$

then (3.3) and (3.4) may be transformed into the following matrix equations:

$$\begin{aligned}[\lambda \boldsymbol{E}_N + \sum_{k=1}^{N} \boldsymbol{\alpha}_N(k)]\,\boldsymbol{P}_N(\eta_1,\ldots,\eta_N;\,\lambda) = \\ = \sum_{C_2} \boldsymbol{w}_{N-1}(\eta_{N-1},\eta_N)\,\boldsymbol{P}_{N-1}(\eta_1,\ldots,\eta_{N-2},\eta_{N-1}+\eta_N;\,\lambda) + \\ + \sum_{C_3} \boldsymbol{v}_{N-2}(\eta_{N-2},\eta_{N-1},\eta_N)\,\boldsymbol{P}_{N-2}(\eta_1,\ldots,\eta_{N-3},\eta_{N-2}+\eta_{N-1}+\eta_N;\,\lambda)\,,\end{aligned} \tag{3.6}$$

and

$$[\lambda E_1 + \boldsymbol{\alpha}_1(1)]\,\boldsymbol{P}_1(\eta_1,\lambda) = \boldsymbol{E}_1\,\delta(1-\eta_1)\,. \tag{3.7}$$

In these equations $\boldsymbol{E}_N$ is the unit matrix of order 2^N. The $\boldsymbol{\alpha}_N(k)$ are given by the direct product of N matrices:

$$\boldsymbol{\alpha}_N(k) = \boldsymbol{E}_1 \times \ldots \times \underset{k\text{-th place}}{\begin{vmatrix} \alpha^{(1)}+\alpha^{(3)} & 0 \\ 0 & \alpha^{(2)} \end{vmatrix}} \times \ldots \times \boldsymbol{E}_1\,. \tag{3.8}$$

The $\boldsymbol{P}_N$ is as $2^N \times 2$ matrix the columns of which correspond to $P^{(1)}$ and $P^{(2)}$ and the rows are ordered by writing $\eta_1 \ldots \eta_N$ as a binary number with digits 1 and 2, standing for an electron and photon respectively. The $\boldsymbol{w}_{N-1}$ is a $2^N \times 2^{N-1}$ matrix in which the only non-zero elements are $\omega^{(1)}(\eta_k,\eta_l)$ and $\omega^{(2)}(\eta_k,\eta_l)$ ordered according to certain rules. The $\boldsymbol{v}_{N\ 2}$ is a $2^N \times 2^{N-2}$ matrix in which

the only non-zero elements are $\omega^{(3)}(\eta_i, \eta_k, \eta_l)$ ordered according to certain rules. The rules for ordering the non-zero elements in $\boldsymbol{w}_{N-1}$ and $\boldsymbol{v}_{N-2}$ can be readily formulated by considering a specific case, say $N = 3$. MP write them out expressly for $\boldsymbol{w}_{N-1}$).

Comparison of (3.6) with the corresponding equation (eqn. (11)) of MP shows that the introduction of tridents into the cascade replaces the simple matrix recurrence relation between $\boldsymbol{P}_N$ and $\boldsymbol{P}_{N-1}$ by a relation between $\boldsymbol{P}_N$, $\boldsymbol{P}_{N-1}$ and $\boldsymbol{P}_{N-2}$.

3·2. *Equation for* $q^{(j)}_{n,m}$. – The « last collision » diffusion equation satisfied by $q^{(j)}_{n,m}$ for the cascade without tridents (eqn. (15) of MP) contains five summation terms on the right side, corresponding to the different types of last collision involving bremsstrahlung emission or photon materialization. When tridents are included three additional terms arise corresponding to the probabilities that the last collision is a trident production with one, two or three of the resulting electron energies falling in the specified intervals. As in the case of $p^{(j)}_{n,m}$ the only change to the left side of the diffusion equation is that n is multiplied now by $\alpha^{(1)}+\alpha^{(3)}$ instead of just $\alpha^{(1)}$. In writing out the new diffusion equation below we omit, for brevity, the arguments of all q's on the right side except the three arising from tridents (*), and in these latter we omit the $\eta_{n+1}, \ldots, \eta_{n+m}$ representing photon energies which of course are all unchanged by the last collision if this is a trident. In this abridged notation the equation becomes:

$$
\begin{aligned}
(3.9)\qquad & \{\partial/\partial x + n(\alpha^{(1)}+\alpha^{(3)}) + m\alpha^{(2)}\} q^{(j)}_{n,m}(\eta_1, \ldots, \eta_n; \eta_{n+1}, \ldots, \eta_{n+m}; x) = \\
& = \sum_{C_1} n \sum_{C_1} m\, q^{(j)}_{n,m-1}\omega^{(1)}(\eta'_n, \eta'_{n+m}) + \sum_{C_2} n\, q^{(j)}_{n-2,\,m+1}\omega^{(2)}(\eta'_{n-1}, \eta'_n) + \\
& + \sum_{C_1} n \int_0^1 q^{(1)}_{n-1,\,m+1} 2\omega^{(2)}(u-\eta'_n, \eta'_n)\,\mathrm{d}u + \sum_{C_1} n \int_0^1 q^{(j)}_{n,m}\,\omega^{(1)}(\eta'_n, u-\eta'_n)\,\mathrm{d}u + \\
& + \sum_{C_1} m \int_0^1 q^{(j)}_{n+1,\,m-1} w^{(1)}(u-\eta'_{n+m}, \eta'_{n+m})\,\mathrm{d}u + \\
& + \sum_{C_3} n\, q^{(j)}_{n-2,m}(\eta'_1, \ldots, \eta'_{n-3}, \eta'_{n-2}+\eta'_n; x)\omega^{(3)}(\eta'_{n-2}, \eta'_{n-1}, \eta'_n) + \\
& + \sum_{C_2} n \int_0^1 q^{(j)}_{n-1,m}(\eta'_n, \ldots, \eta'_{n-2}, u; x) 3\omega^{(3)}(\eta'_{n-1}, \eta'_n, u-\eta'_{n-1}-\eta'_n)\,\mathrm{d}u + \\
& + \sum_{C_1} n \int_0^1 \int_0^1 q^{(j)}_{n,m}(\eta'_1, \ldots, \eta'_{n-1}, u; x) 3\omega^{(3)}(\eta'_n, v, u-\eta'_n-v)\,\mathrm{d}v\,\mathrm{d}u\,.
\end{aligned}
$$

(*) The arguments of the other five q's are exhibited in MP eqn. (15).

Noting that $q^{(j)}_{0,0}(x) = 1$ for all x, our initial conditions are:

$$(3.10) \qquad q^{(j)}_{n,m}(x=0) = \delta_{n+j,2}\delta_{m+1,j}\,\delta(1-\eta_1); \qquad q^{(j)}_{0,0}(x=0) = 1\,.$$

We define the following Mellin-Laplace transform of $q^{(j)}_{n,m}$:

$$(3.11) \qquad Q^{(j)}_{n,m}(s_1, \ldots, s_n; s_{n+1}, \ldots, s_{n+m}; \lambda) =$$

$$= \int_0^1 \mathrm{d}\eta_1 \ldots \int_0^1 \mathrm{d}\eta_{n+m} \int_0^\infty \mathrm{d}x\, \eta_1^{s_1} \ldots \eta_{n+m}^{s_{n+m}} \exp[-\lambda x] q^{(j)}_{n,m}\,,$$

together with the quantities:

$$(3.12) \qquad W^{(j)}(s_1, s_2) = \int_0^1 \left(\frac{\eta_1}{\eta_1+\eta_2}\right)^{s_1} \left(\frac{\eta_2}{\eta_1+\eta_2}\right)^{s_2} \omega^{(j)}(\eta_1, \eta_2)\,\mathrm{d}\eta_2\,,$$

for $j = 1$ or 2, and

$$(3.13) \qquad W^{(3)}(s_1, s_2, s_3) =$$

$$= \int_0^1 \int_0^1 \left(\frac{\eta_1}{\eta_1+\eta_2+\eta_3}\right)^{s_1} \left(\frac{\eta_2}{\eta_1+\eta_2+\eta_3}\right)^{s_2} \left(\frac{\eta_3}{\eta_1+\eta_3+\eta_3}\right)^{s_3} \omega^{(3)}(\eta_1, \eta_2, \eta_3)\,\mathrm{d}\eta_2\,\mathrm{d}\eta_3\,.$$

Operating on (3.9) with (3.11), using (3.10), (3.12) and (3.13), and suppressing for brevity the arguments of the Q's on the right side, we have the following transformed equation:

$$(3.14) \qquad \{\lambda + n(\alpha^{(1)} + \alpha^{(3)}) + m\alpha^{(2)}\} Q^{(j)}_{n,m}(s_1, \ldots, s_n; s_{n+1}, \ldots, s_{n+m}; \lambda) - \delta_{n+j,2}\delta_{m+1,j} =$$

$$= \sum_{\sigma_1}{}_n \sum_{\sigma_1}{}_m Q^{(j)}_{n,m-1} W^{(1)}(s'_n, s'_{n+m}) + \sum_{\sigma_2}{}_n Q^{(j)}_{n-2,m+1} W^{(2)}(s'_{n-1}, s'_n) +$$

$$+ \sum_{\sigma_1}{}_n Q^{(j)}_{n-1,m+1} 2W^{(2)}(s'_n, 0) + \sum_{\sigma_1}{}_n Q^{(j)}_{n,m} W^{(1)}(s'_n, 0) +$$

$$+ \sum_{\sigma_1}{}_m Q^{(j)}_{n+1,m-1} W^{(1)}(0, s'_{n+m}) + \sum_{\sigma_3}{}_n Q^{(j)}_{n-2,m} W^{(3)}(s'_{n-2}, s'_{n-1}, s'_n) +$$

$$+ \sum_{\sigma_2}{}_n Q^{(j)}_{n-1,m} 3W^{(3)}(s'_{n-1}, s'_n, 0) + \sum_{\sigma_1}{}_n Q^{(j)}_{n,m} 3W^{(3)}(s'_n, 0, 0)\,.$$

Again denoting $n+m$ by N we see that each of the Q's in (3.14) refers to either N, $N-1$, $N-2$ particles; the matrix form of (3.12) is then a recurrence relation between $\boldsymbol{Q}_N$, $\boldsymbol{Q}_{N-1}$ and $\boldsymbol{Q}_{N-2}$, which are matrices constructed from the Q's exactly as the $\boldsymbol{P}_N$ in (3.6) are constructed from the P's. The

recurrence formula is: (for $N > 1$)

$$(3.15)\qquad [\lambda \boldsymbol{E}_N + \sum_{k=1}^{N} \boldsymbol{B}_N(s_k)]\boldsymbol{Q}_N(s_1, \ldots, s_N; \lambda) =$$

$$= \sum_{C_2} \boldsymbol{W}_{N-1}(s_{N-1}, s_N)\, \boldsymbol{Q}_{N-1}(s_1, \ldots, s_{N-2}, s_{N-1} + s_N; \lambda) +$$

$$+ \sum_{C_3} \boldsymbol{V}_{N-2}(s_{N-2}, s_{N-1}, s_N)\, \boldsymbol{Q}_{N-2}(s_1, \ldots, s_{N-3}, s_{N-2} + s_{N-1} + s_N, \lambda)\,.$$

The $\boldsymbol{B}_N(s_k)$ are given by the direct product of N matrices:

$$(3.16)\qquad \boldsymbol{B}_N(s_k) = \boldsymbol{E}_1 \times \ldots \times \underset{k\text{-th place}}{\begin{bmatrix} B_1(s_k) & B_2(s_k) \\ B_3(s_k) & B_4(s_k) \end{bmatrix}} \times \ldots \times \boldsymbol{E}_1\,,$$

with

$$(3.17)\qquad \begin{cases} B_1(s) = \alpha^{(1)} + \alpha^{(3)} - W^{(1)}(s, 0) - 3W^{(3)}(s\ 0, 0)\,, \\ B_2(s) = -\,2W^{(2)}(s, 0)\,, \\ B_3(s) = -\,W^{(1)}(0, s)\,, \\ B_4(s) = \alpha^{(2)}\,. \end{cases}$$

The only respect in which $\boldsymbol{B}_N$ differs from the corresponding matrix $\boldsymbol{A}_N$ for the cascade without tridents (MP eqn. (22)–(23)) is in the inclusion of the $\alpha^{(3)}$ and $W^{(3)}$ terms in $B_1(s)$.

The $\boldsymbol{W}_{N-1}$ are $2^N \times 2^{N-1}$ matrices where the only non-zero elements are comprised of $W^{(1)}(s_k, s_l)$, $W^{(2)}(s_k, s_l)$ or $3W^{(3)}(s_k, s_l, 0)$ ordered according to certain rules, readily formulated by analogy with the $\boldsymbol{w}_{N-1}(\eta_{N-1}, \eta_N)$ of (3.6); the $\boldsymbol{V}_{N-2}$ are $2^N \times 2^{N-2}$ matrices and are just the $\boldsymbol{v}_{N-2}$ of (3.6) with $\omega^{(3)}(\eta, \eta_k, \eta_l)$ replaced by $W^{(3)}(s_i, s_k, s_l)$.

For $N = 1$ the recurrence relation assumes the quite simple form:

$$(3.18)\qquad [\lambda \boldsymbol{E}_1 + \boldsymbol{B}_1(s_1)]\, \boldsymbol{Q}_1(s, \lambda) + \boldsymbol{E}_1\,.$$

4. – Discussion.

The relative usefulness of $p^{(j)}_{n,m}$ and $q^{(j)}_{n,m}$ is discussed in MP. The solution for $\boldsymbol{Q}_N$ is the one of direct physical interest because it leads, via the relation (3.1) to the general solution for all the moments, including the correlations between electrons and photons. As an illustration we write out the solution of $N = 1$ explicitly. Equation (3.18) yields, on performing the matrix multiplications,

the following four simultaneous equations:

$$(\lambda + B_1)Q_{10}^{(1)} + B_2 Q_{01}^{(1} \qquad = 1\,, \tag{4.1}$$

$$B_3 Q_{10}^{(1)} + (\lambda + B_4)Q_{01} = 0\,, \tag{4.2}$$

$$(\lambda + B_1)Q_{10}^{(2)} + B_2 Q_{01}^{(2)} \qquad = 0\,, \tag{4.3}$$

$$B_3 Q_{10}^{(2)} + (\lambda + B_4)Q_{01}^{(2)} = 1\,. \tag{4.4}$$

Let us suppose, for example, that we wish to calculate the average number of electrons at depth x and above energy η arising from a single primary electron. For this we require $Q_{10}^{(1)}$, which from (4.1) and (4.2) is found to be:

$$Q_{10}^{(1)} = \frac{\lambda + B_4(s)}{[\lambda + B_1(s)][\lambda + B_4(s)] - B_2(s)B_3(s)}\,. \tag{4.5}$$

The inverse Mellin-Laplace transform of $Q_{10}^{(1)}$ integrated over energy from η to 1 then gives the average number directly:

$$T_{10}^{(1)} = \frac{1}{(2\pi i)^2}\int_{u_0 - i\infty}^{u_0 + i\infty}\frac{\mathrm{d}s}{s}\int_{\lambda_0 - i\infty}^{\lambda_0 + i\infty}\mathrm{d}\lambda\,\exp\,[\lambda x]\eta^{-}\,Q_{10}^{(1)}\,. \tag{4.6}$$

To obtain numerical results from (4.5) and (4.6) one must know the values of the cross-sections occurring in the equations (3.17) which define the B's. Only $B_1(s)$ involves the cross-sections for trident production; the other B's are already known from the Bethe-Heitler full screening cross-sections for bremsstrahlung emission and photon materialization. Computations of average numbers and correlations using these cross-sections, and ignoring tridents, have already been performed on desk machines, using a saddle point approximation for the integrations ([14]). To this approximation it should also be feasible to include the effect of tridents in a desk machine calculation of average numbers, given reliable cross-sections to substitute in $B_1(s)$. Certainly with an electronic computer the inclusion of tridents in average number calculations should present no great difficulty, whether the saddle point approximation or direct numerical integration be employed. To obtain the higher moments, the electronic computer could be programmed to solve (3.15) for $\boldsymbol{Q}_N$, given $\boldsymbol{Q}_{N-1}$ and $\boldsymbol{Q}_{N-2}$, starting with $N = 2$. In practice it may not be

([14]) L. JÁNOSSY and H. MESSEL: *Proc. Phys. Soc.*, A **63**, 1101 (1950).

necessary or desirable to go beyond $N = 2$ or 3 in order to obtain enough information about the distribution function for it to be usefully employed in the interpretation of experimental results.

We have not attempted to give a general analytical solution for Q_N, corresponding to MP's equation (24); such a solution may be obtained by analogy with their procedure but would be even more unwieldy than that of MP. The best hope for obtaining practically useful results appears to be direct numerical solution of the recurrence equation along the lines indicated above.

* * *

Most of the work reported here was performed during the tenure of a research fellowship at the University of Sydney.

RIASSUNTO (*)

Si discutono con particolare riferimento al loro significato nello sviluppo della cascata elettronica fotonica alcuni risultati recenti che segnalano sezioni d'urto anormalmente grandi per la creazione diretta di coppie da parte di elettroni di alta energia (principalmente al disopra di 10 GeV). Un esame qualitativo, con l'ausilio di un modello evidentemente grossolano, suggerisce che l'effetto di tali grandi sezioni d'urto di « tridenti » potrebbe, decisamente cambiare lo schema di sviluppo nei primi stadi di una cascata di energia realmente alta. Si modifica quindi la formulazione dettagliata della teoria della cascata in modo da poter senz'altro inserire nelle formule usate per il calcolo dei momenti della funzione di distribuzione numerica i valori numerici della sezione d'urto per la produzione di tridenti, quando questi siano stati convenientemente accertati.

(*) *Traduzione a cura della Redazione.*

Multiple Scattering Measurements in Nuclear Emulsions.

S. Rosendorff and Y. Eisenberg

Department of Physics, The Weizmann Institute of Science Rehovoth, Israel

(ricevuto il 18 Agosto 1957)

Summary. — The practical use of the new multiple scattering function, $\cos \eta\varphi$, introduced by Lipkin [1] *et al.*, was examined by comparing its theory with experiment. At the same time the mean absolute angle according to Molière's scattering theory was compared with experiment for the second and third difference and the respective dispersions were determined experimentally. (The theoretical dispersion diverges in Molière's theory.) A good agreement between theory and experiment was obtained in the cosine case, both for the mean value and the dispersions, as well as in the mean absolute angle case with cut-off. Writing the relative error of $p\beta$ as $D_{2,3}/\sqrt{n}$ (for the second and third differences, respectively) we have obtained in the cosine case: $D_2=0.976$ and $D_3=1.36$, and in the mean absolute angle case (with cut-off at $4\langle|\varphi|\rangle$): $D_2=0.97$ and $D_3=1.37$. It is shown that, provided one restricts oneself to a certain class of estimates of $p\beta$, the above dispersion values are close to the minimum possible dispersion of $p\beta$. Also, an explanation is suggested for the known experimental fact that the ratio of the « scattering constants » K_3/K_2 is higher by a few percent than the expected value $\sqrt{\frac{3}{2}}$.

1. – Introduction.

Multiple Coulomb scattering measurements of charged particles in nuclear emulsions is very often used in order to estimate the product $p\beta$ of the particle momentum and its velocity. Several detailed multiple scattering theories [2]

[1] H. J. Lipkin, S. Rosendorff and G. Yekutieli: *Nuovo Cimento*, **2**, 1015 (1955).

[2] G. Molière: *Zeits. f. Naturf.*, **2***a*, 133 (1947); **3***a*, 78 (1948); **10***a*, 177 (1955); H. Snyder and W. T. Scott: *Phys. Rev.*, **76**, 220 (1949); S. A. Goudsmidt and J. L. Saunderson: *Phys. Rev.*, **57**, 24; **58**, 36 (1940); H. W. Lewis: *Phys. Rev.*, **78**, 526 (1950). The present work will refer mostly to Molière's calculations.

have been developed, by which it was possible to calculate the value of $p\beta$ from the scattering angles of a particle in matter. In nuclear emulsion practice, it is common to use the mean absolute value of the projected angle φ_i between successive chords along the particle's trajectory for determining the value of $p\beta$ (a summary of the theory and of the experimental situation as of 1953 is given by GOTTSTEIN in HEISENBERG's book ([3])). The angles φ_i are usually determined by measuring the y-co-ordinates at successive equal intervals (equal « cell size »), of a track aligned to be parallel to the x-motion of a microscope, and by taking the second difference of these co-ordinates (this method is known as the « Fowler Co-ordinate Method »). Often, in order to eliminate possible distortions in emulsions, third and higher differences are used.

Recently it has been suggested by LIPKIN *et al.* ([1]) that the value of $p\beta$ could be estimated by using the mean of the cosines of angles proportional to the scattering angles, namely $\langle \cos \eta\varphi_i \rangle$ instead of the conventional use of $\langle |\varphi_i| \rangle$. The constant multiplier η is to be chosen to minimize the dispersion obtained for $p\beta$. It has been shown in I that by using the cosine function one overcomes the main difficulties which are encountered in using the mean absolute angle parameter; namely, one can calculate analytically, without difficulties, both the mean value $\langle \cos \eta\varphi_i \rangle$ and all higher moments. Thus, it is possible to obtain the theoretical dispersion of the measured value of $p\beta$ in the cosine case. This is not possible in the mean absolute angle case due to the divergence of the second and higher moments.

The purpose of this work is to check experimentally the theory of the cosine function as introduced in I, to compare the cosine method with the mean absolute value method and to determine, experimentally, the dispersion in the latter case.

The experimental methods and the range-energy relation used are discussed in Sect. **2**. A comparison between the experimentally measured and the theoretical quantities is given in Sect. **3** for both the first moments and the dispersions. In Sect. **4** an attempt has been made to find out whether or not a better estimation function for $p\beta$ exists, and the conclusions are given in Sect. **5**.

2. – Experimental methods.

In the experimental part of this work we have used a block of 2 in. $\times$ 3 in. $\times$ $\times$ 400 μm Ilford G5 stripped emulsions, exposed to the pion beam of the Nevis Cyclotron at Columbia (*). The average energy of the pions was about 60 MeV,

([3]) *Kosmische Strahlung*, p. 495. Edited by W. HEISENBERG (Berlin 1953).

(*) We are grateful to Dr. G. HARRIS of Columbia University for exposing the plates for us.

and the average range about 53 mm. Thus, most of the pions stopped within the emulsion block and their ranges could be determined exactly. From the known ranges, the value of $p\beta$ was determined accurately and compared with the values obtained from the multiple scattering measurements using the $\langle \cos \eta\varphi_i \rangle$ and the $\langle |\varphi_i| \rangle$ functions.

The range-energy relations used were derived from the measurements of BARKAS *et al.* [4]. We have assumed the usual power low, namely: $R = a \cdot M^{1-b} \cdot E^b$, where R is the range, E the kinetic energy of the particle and M its mass. Using the following values of pion ranges from BARKAS' work:

$$E_1 = 29.80 \text{ MeV}, \qquad \text{for} \quad R_1 = (15\,260 \pm 90)\ \mu\text{m}$$

$$E_2 = 50.64 \text{ MeV}, \qquad \text{for} \quad R_2 = (36\,610 \pm 180)\ \mu\text{m}$$

and correcting them according to the average measured muon range ($\langle R_\mu \rangle$ was $(602.2 \pm 2.5)\ \mu$m in BARKAS' work and $(591.0 \pm 4.4)\ \mu$m in the present experiment) we have obtained for the range-energy relations in our emulsion block the following expression:

$$E\,(\text{MeV}) = 0.186 \cdot R^{0.606} \cdot M^{0.394}, \tag{1}$$

where R is the particle range in microns and M its mass in units of the proton mass. Expression (1) is valid for pions in the range interval $9\,000\ \mu\text{m} < R < 40\,000\ \mu\text{m}$. All the pions we have used were in the above range interval.

A total of 3 960 angles between successive chords have been measured. The cell-size employed was 50 μm. The measurement noise for that cell-size, as determined by calibration against a very energetic cosmic ray particle was: $\langle d_N \rangle = (0.057 \pm 0.006)\ \mu$m. All errors quoted in this work are Standard Deviations.

3. – Comparison with theory.

3·1. *The scattering constant.* – The mean absolute value of the projected scattering angle φ measured between successive tangents or chords (second and third differences) is given by:

$$\langle |\varphi| \rangle_{T.2.3} = \frac{K_{T.2.3}}{p\beta} \cdot \sqrt{t}, \tag{2}$$

[4] W. H. BARKAS, P. H. BARRET, P. CUER, H. H. HECKMAN, F. M. SMITH and H. K. TICHO: *Phys. Rev.*, **102**, 583 (1956).

where $K_{T,2,3}$ is the « scattering constant » for the tangent, second and third difference respectively, and t the cell size. According to the theory of MOLIÈRE [2] (we have used here the notations of Molière), the scattering constant is a slowly varying function of β and t. Explicitly, it is given by the following expression:

$$K_i = X_{ci} \cdot p\beta \cdot \sqrt{B_i/\pi} \left(1 + \frac{0.982}{B_i} - \frac{0.117}{B_i^2} + \ldots\right), \qquad i = T, 2, 3 , \tag{3}$$

X_{ci} is given for the three mentioned cases in terms of the « unit probability angle » per unit length [5] χ_c in the following manner:

$$X_{cT} = X_{c3} = \chi_c , \quad X_{c2} = \sqrt{\frac{2}{3}}\chi_c , \quad \text{where:} \quad \chi_c^2 = \frac{4\pi e^4 Z^2}{p^2 v^2} \cdot \sum_i N_i Z_i^2 \tag{4}$$

or, for G5 nuclear emulsions: $\chi_c = 0.31/p\beta$, if t is 100 μm, $Z^2 = 1$ and $p\beta$ is given in MeV/c.

The parameters B_T, B_2 and B_3 are defined by the transcendental equation:

$$B_i - \ln B_i = (X_{ci}^2 t/X_{ai}^2) - 0.154 . \tag{5}$$

The X_{ai}'s are simply related to Molière's screening angle χ_a:

$$X_{aT}^2 = \chi_a^2 , \qquad \ln X_{a2,3}^2 = \ln \chi_a^2 - 2/3 . \tag{6}$$

The mean number of single scattering processes, Ω_0, occurring in the thickness t of the scattering substance is given by:

$$\Omega_0 = \chi_c^2 t/\chi_a^2 . \tag{7}$$

The B_i's are therefore, according to (4), (5) and (6), related to Ω_0 by the following expressions:

$$\begin{cases} B - \ln B = \ln \Omega_0 - 0.154 & (B_T = B) \\ B_2 - \ln B_2 = \ln (\frac{2}{3}\Omega_0) + \frac{2}{3} - 0.154 \\ B_3 - \ln B_3 = \Omega_0 + \frac{2}{3} - 0.154 . \end{cases} \tag{8}$$

The B_i's as function of $\log_{10} \Omega_0$ are shown in Fig. 1. Curves for Ω_0/t as function of β can be found in the literature [3].

[5] H. A. BETHE: *Phys. Rev.*, **89**, 1256 (1953).

B_2 and B_3 are approximately equal; with this assumption the ratio K_3/K_2 is, according to (3) and (4), given by $\sqrt{\frac{3}{2}}$.

The exact ratio of the third to second difference scattering constants should be:

$$\delta = \frac{K_3}{K_2} = \sqrt{\frac{3}{2}} \cdot \frac{B_3}{B_2} \cdot \frac{1 + 0.982/B_3 - \ldots}{1 + 0.982/B_2 - \ldots},$$

δ is, therefore, greater than $\sqrt{\frac{3}{2}}$ by several percent. Its exact value depends upon the value of B.

For example, for $B = 10$, one obtains $\delta = 1.022\sqrt{\frac{3}{2}}$ and for $B = 5$ one obtains $\delta = 1.046\sqrt{\frac{3}{2}}$. In the present experiment $\delta = 1.028\sqrt{\frac{3}{2}}$. Consequently, this factor explains, in part, the known fact ([6]) that the experimental ratio of K_3/K_2 is a few percent greater than expected according to Molière's theory (in its approximative form), namely $\sqrt{\frac{3}{2}}$.

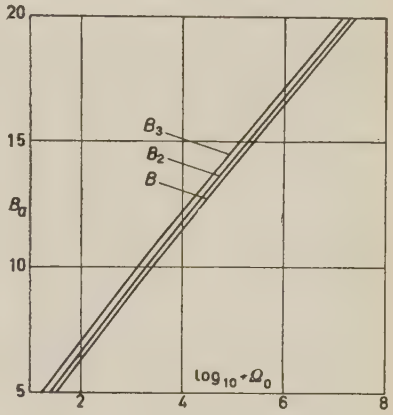

Fig. 1. – The parameters B, B_2 and B_3 as function of $\log_{10} \Omega_0$.

In the present experiment the velocity of the pions β varied between 0.51 and 0.66. The average value of Ω_0 for this velocity range was $\bar{\Omega}_0 = 630$ per 100 μm, and by Fig. 1 the average value of B was $\bar{B} = 7.6$, considering the fact that the cell size we have used in this work was 50 μm. Since the velocity of most of the pions was close to the average value of β and since B changes very slowly with the velocity, it is justified to use the above value for B for all the cases we had. The value of $\bar{B}_2$ and $\bar{B}_3$ according to (8) is found to be:

$$\bar{B}_2 = 7.90\,, \qquad \bar{B}_3 = 8.35\,. \tag{9}$$

This can also be seen from Fig. 1. Let us use, for convenience, the notation: (see (4) above):

$$\begin{cases} \bar{\sigma}_2 = X_{c2} \sqrt{\dfrac{\bar{B}_2 t}{2}} = \chi_c \sqrt{\bar{B}_2 t/3}\,, \\ \bar{\sigma}_3 = X_{c3} \sqrt{\dfrac{\bar{B}_3 t}{2}} = \chi_c \sqrt{\bar{B}_3 t/2}\,. \end{cases} \tag{10}$$

([6]) S. Biswas, E.G. George, B. Peters and M.S. Swami: *Suppl. Nuovo Cimento*, **12**, 369 (1954); M. Di Corato, D. Hirschberg and B. Locatelli: *Suppl. Nuovo Cimento*, **4**, 448 (1956); S. Biswas, B. Peters and Rama: *Proc. Ind. Acad. Sci.*, **4**, 154 (1955).

By (4) and (10) we obtain (for $t = 50\ \mu m$):

$$(10') \qquad \begin{cases} \bar{\sigma}_2 = 0.356/p\beta\ , \\ \bar{\sigma}_3 = 0.448/p\beta\ . \end{cases}$$

3·2. *The grouping of the data.* – As was mentioned in Sect. 2, we have measured a total of 3960 angles. The mean absolute angle and the mean of the cosine function were obtained, as we shall see in Sect. 3·3 and 3·5, by treating the entire data as one group. For obtaining the dispersions, $D/\sqrt{n}$ however, it was necessary to divide the data in a suitable manner. The division we have chosen is the following:

99 groups, each containing 40 successive angles (namely 2000 μm long segments of pion track length for each group) for the dispersion in the mean absolute angle case, and 396 groups each containing 10 successive angles for the cosine case. The reasons for this choice were as follows:

a) In the mean absolute angle case one knows the relative error of the dispersion only for a normal distribution, in which case it is given by: $1/\sqrt{2N}$ (where N is the number of groups). It is reasonable to assume that for $n = 40$ the distribution is close to a normal one, and one can use the above value for the error of the dispersion. On the other hand, in the cosine case one can calculate exactly the errors of the dispersion (see Sect. 3·6) and the requirement of a normal distribution is not necessary. This enables one to choose groups of ten angles ($n = 10$) in which case N becomes 396 and the statistical error of the dispersion becomes smaller.

b) In principle, due to the correlation between the angles, D could depend upon n. In the cosine case, for example, it has been shown in I that:

$$(11) \qquad \left\{\frac{D[\cos(\eta\varphi)]}{\cos\eta\varphi}\right\}^2 = \frac{D_1^2}{n} + \frac{D_2^2}{n^2}\ .$$

For all values of η that we have used, the second term on the right of (11) could be neglected for $n \geqslant 10$. Thus, in the cosine case, one can write the error as $D/\sqrt{n}$,where D is independent of n for n's as small as 10. No such relation can be derived in the mean absolute angle case. One cannot calculate the dispersion in this case, and one does not know to what extent D depends upon n. Choosing $n = 40$ for the mean absolute angle case, makes the dispersion less accurate than in the cosine case, but enables one to write the error also in this case as $D/\sqrt{n}$, where D is probably independent of n.

3·3. *The mean absolute angle.* – In order to compare the experimental results with the theory, it is convenient to define an angle whose distribution is independent of the particles' energy. Such an angle, for example, is:

$$x = \varphi/\bar{\sigma} \,, \tag{12}$$

where φ is the scattering angle and $\bar{\sigma}$ is defined by (10). Using (10′) we obtain

$$\begin{cases} x_2 = \varphi_2 p\beta/0.356 \,, \\ x_3 = \varphi_3 p\beta/0.448 \,. \end{cases} \tag{12′}$$

The mean of (12′) has to be compared with the theoretical value:

$$\langle |x_{2,3}| \rangle = \sqrt{2/\pi}\,(1 + 0.982/\bar{B}_{2,3} - 0.117/\bar{B}^2_{2,3} + \ldots) \,, \tag{13}$$

which can be derived from (2), (3) and (4).

This comparison is not straightforward, however, since, as was mentioned in Sect. 2, (12′) contains the scattering noise. The noise determination was carried out in the following way: the calibration track (see Sect. 2) was rotated slightly so that it formed a small angle with the X-direction of the scattering microscope. By this procedure a condition was reached which was similar to that under which the actual measurements of the pions were performed, The noise increased by about 20% in this case. The value finally used in the noise elimination was the one given in Sect. 2 increased by 18%, since it gave best agreement between theory and experiment for the case $\langle |x_2| \rangle$ with cut-off. It should be emphasized that $\langle |x| \rangle$ is quite insensitive to the exact value of the noise. A change of 5% in the noise corresponds to a change of merely 0.3% in $\langle |x| \rangle$.

Assuming a normal noise distribution, one gets ([6]) for the ratio of the noise in the second and third differences:

$$\langle D_N \rangle_3 / \langle D_N \rangle_2 = 1.825 \,.$$

In the present experiment we have obtained for the above ratio: 1.76 ± 0.25. Assuming both the noise and the true scattering to have normal distributions, one gets the following relation between the mean absolute values of the observed angle x_0, the true angle x_t and the noise x_N.

$$\langle |x_t| \rangle = \left\{ \langle |x_0| \rangle^2 - \langle |x_N| \rangle^2 \right\}^{\frac{1}{2}} . \tag{14}$$

The final results of the mean absolute value $\langle|x_t|\rangle$ are given in Table I, with and without cut-off at $4\ \langle|x_0|\rangle$. The agreement with cut-off is much better than without cut-off, indicating too large a contribution to the result from large angle scattering in the theory of Molière.

TABLE I. – *The mean absolute angle.*

Difference	$\langle\|x_t\|\rangle_2$		$\langle\|x_t\|\rangle_3$	
	Observed	Calculated	Observed	Calculated
No cut-off	0.855 ± 0.013	0.895	0.864 ± 0.017	0.891
With cut-off	0.820 ± 0.011	0.823	0.833 ± 0.013	0.822

In order to reduce the numerical work, $p\beta$ was assumed to be constant in each 500 μm interval. Actually it varied by about 1%. However, the error introduced by this assumption was much less than the statistical error and could therefore be neglected.

3·4. *The dispersion of $p\beta$. Absolute value case.* – In order to know how good an estimate of $p\beta$ is obtained from eq. (2), one has to calculate the dispersion of $p\beta$ in the theory of Molière. However, such a calculation is impossible (*) since the second moment of η_t diverges in Molière's theory [1]. One can, therefore, only determine the experimental value of the dispersion, whereas in the cosine case it is also possible to calculate it, as was shown in I.

Using (14) we obtain for the dispersion of X_t:

$$\frac{D(|x|)}{|x_t|} = \frac{[\langle|x_0|\rangle^4(D(|x_0|)/|x_0|)^2 + \langle|x_N|\rangle^4(D(|x_N|)/|x_N|)^2]^{\frac{1}{2}}}{\langle|x_0|\rangle^2 - \langle|x_N|\rangle^2}. \tag{15}$$

We have assumed that the noise has a normal distribution, therefore

$$D(|x_N|)/|x_N| = 0.755/\sqrt{n}\,.$$

If n is a large number and if the ratio $\langle|x_N|\rangle/\langle|x_0|\rangle$ is small, the distribution of $\langle|X_t|\rangle$ becomes approximately normal and the dispersion of $|X_t|$

(*) *Note added in proof:* It should be noted, however, that it is possible to calculate the dispersion if an appropriate cut-off is applied. For example, HUYBRECHTS (*Suppl. Nuovo Cimento*, 4, 903 (1956)) calculated numerically the dispersion in the mean absolute angle with cut-off at $4\langle\varphi_i\rangle$ for $B \simeq 8$, and got $D_{t_2} = 0.93$, in agreement with the experimental value obtained in this work (see Table II).

given by (14) becomes the ordinary standard error. It can be written as $D_t/\sqrt{n}$, where D_t is the desired coefficient to be determined by experiment (as was mentioned above, D_t diverges in Molière's theory). It should be noted that the dispersion of $p\beta$ is the same as that of $|X_t|$. In Table II are given the results of D_t determined experimentally, of the second and third differences, for the cases of no cut-off (NCO), overall cut-off (CO) and local cut-off (LCO). The overall cut-off (a cut-off by using the average of all 3960 angles) is less useful than the local cuto-off (determined separately for each group of 40 angles), since the latter is of more practical importance. So, for ordinary emulsion work, the value of the dispersion for the LCO case should be used (see Table II).

TABLE II. – *The dispersion of $p\beta$ in the mean absolute angle case.*

	$D_{t2}=\sqrt{n}\,[D(p\beta)/p\beta)]_2$	$D_{t3}=\sqrt{n}\,[D(p\beta)/p\beta]_3$
No cut-off	1.020 ± 0.074	1.435 ± 0.106
With cut-off	0.878 ± 0.065	1.216 ± 0.090
Local cut-off	0.973 ± 0.073	$1,372 \pm 0.102$

3·5. *The mean of the cosine function.* – The comparison between theory and experiment in the case of the cosine function has been performed for three different values of the multiplier η for the second as well as for the third difference. The values of η used were $\eta/\eta_{\text{opt}} = \frac{1}{4}$, 1, 2, where η_{opt} is the optimal value of η which minimizes the dispersion of $p\beta$ (see I).

In I the same parameter B has been used for both the tangent and second difference cases. A simpler and more general expression for the mean value of the cosine function can be derived by using the various parameters B_i and X_{ci} defined in (4) and (8). The result is:

$$\langle \cos \eta\varphi \rangle = \exp\left[-\frac{1}{2}(\eta\sigma_i)^2\left(1 - \frac{1}{B_i}\ln\tfrac{1}{2}(\eta\sigma_i)^2\right)\right], \tag{16}$$

where

$$\sigma_i^2 = \tfrac{1}{2}x_{ci}^2{}' B_i \,.$$

This expression is valid for the tangent case as well as for the second, third, etc., difference cases (see Fig. 5 of I for the graphical representation of (16)). The minimum dispersion of $p\beta$ in the case of the second difference occurs at the point

$$(\eta_{\text{opt}_2}\sigma_2)^2 = 1.04 \,, \tag{17}$$

which yields for the present experiment

$$\eta_{\mathrm{opt}_2} = 2.87\, p\beta\,, \tag{17'}$$

and in the case of the third difference occurs at the point

$$(\eta_{\mathrm{opt}_3}\sigma_3)^2 = 1.32\,, \tag{18}$$

which yields

$$\eta_{\mathrm{opt}_3} = 2.57\, p\beta\,, \tag{18'}$$

where $p\beta$ is expressed in MeV/c.

The noise elimination in the case of the cosine function is somewhat different from the noise elimination in the absolute angle case. In the latter we have to assume a normal distribution for the true scattering whereas in the cosine case no such assumption is necessary. The relation between the means of the cosine functions of the three scattering angles φ_t, φ_0 and φ_N is simply given by

$$\langle \cos \eta\varphi_t \rangle = \langle \cos \eta\varphi_0 \rangle / \langle \cos \eta\varphi_N \rangle\,. \tag{19}$$

(19) is the analogous expression to (14). We shall assume again a normal noise distribution. Therefore we have:

$$\langle \cos \eta\varphi_N \rangle = \exp\left[-\tfrac{1}{2}(\eta\sigma_N)^2\right], \tag{20}$$

where

$$\sigma_N^2 = \frac{\pi}{2}\langle |\varphi_N|^2 \rangle\,.$$

The expression to be compared to the theory is:

$$\frac{1}{N}\sum_i \langle \cos \eta\varphi_t \rangle_i = \frac{1}{N}\exp\left[(\bar{\eta}\sigma_N)^2/2\right]\sum_i \langle \cos \eta\varphi_0 \rangle_i\,, \tag{21}$$

where N is the number of groups. In the cosine case we had $N = 396$, each group contained $n = 10$ angles. The variation of the exponential function is very small compared to the standard deviation of the cosine function. It is therefore permitted to take it out of the sum in (21).

Table III shows the results of the mean value of the cosine function for three different values of the multiplier η. The agreement with theory is very good at all points.

TABLE III. – *The mean value of the cosine function.*

η/η_{opt}	$\langle\cos\eta\varphi_t\rangle_2$		$\langle\cos\eta\varphi_t\rangle_3$	
	Observed	Calculated	Observed	Calculated
$\frac{1}{4}$	0.957 ± 0.002	0.955	0.948 ± 0.003	0.945
1	0.572 ± 0.009	0.570	0.490 ± 0.013	0.500
2	0.137 ± 0.015	0.152	0.094 ± 0.018	0.097

3·6. *The dispersion of the cosine function.* – The dispersion of $\langle\cos\eta\varphi_0\rangle$ is given by

$$\frac{s}{\langle m\rangle} = \sqrt{\frac{1}{N}\sum_i (m_i - \langle m\rangle)^2}/\langle m\rangle = D_0/\sqrt{n}\,,$$

where

$$m_i = \frac{1}{n}\sum_j \cos\eta_i\varphi_j,$$

is the mean of the cosine function in a group containing n angles, and N is the number of groups.

The theoretical value derived in I cannot be compared directly with the measured one, as it does not include the noise. Therefore we have calculated the dispersion of the expression

$$\cos\eta\varphi_0 = \tfrac{1}{2}\{\exp[i\eta(\varphi_t+\varphi_N)] + \exp[-i\eta(\varphi_t+\varphi_N)]\}\,.$$

The standard deviation σ_0^2 of $\cos\eta\varphi_0$ is found to be

$$\sigma_0^2 = \sigma_t^2 - \tfrac{1}{2}\langle\cos 2\eta\varphi_t\rangle(1 - \langle\cos 2\eta\varphi_N\rangle) + \langle\cos\eta\varphi_t\rangle^2(1 - \langle\cos\eta\varphi_N\rangle^2)\,. \tag{22}$$

σ_t is the standard deviation of $\cos\eta\varphi_t$. As the influence of the noise on σ_0 is small, it has been decided to neglect the statistical correlation in the derivation of (22). However, in the numerical calculation of σ_0^2, according to (22), the exact value of σ_t^2 including correlation, as derived in I, eq. (4.9) (for the second difference) has been used.

Taking into account (19), the dispersion of $\cos\eta\varphi_0$ becomes

$$\frac{D(\cos\eta\varphi_0)}{\cos\eta\varphi_0} = \frac{\sigma_0}{\langle\cos\eta\varphi_t\rangle\langle\cos\eta\varphi_N\rangle}\,,$$

and the dispersion of $\langle \cos \eta\varphi_t \rangle$ becomes

$$\frac{D(\cos \eta\varphi)}{\cos \eta\varphi_t} = \left\{ \left[\frac{D(\cos \eta\varphi_0)}{\cos \eta\varphi_0} \right]^2 + \left[\frac{D(\cos \eta\varphi_N)}{\cos \eta\varphi_N} \right]^2 \right\}^{\frac{1}{2}} . \tag{23}$$

Because of the assumption of normal noise distribution we have

$$\frac{D(\cos \eta\varphi_N)}{\cos \eta\varphi_N} = \sqrt{\frac{2}{n}} \sinh \frac{1}{2} (\eta\sigma_N)^2 .$$

The dispersion of $p\beta$ is equal to (23) divided by the derivative

$$\mathrm{d}(\ln \langle \cos \eta\varphi_t \rangle) / \mathrm{d}(\ln p\beta) .$$

In Table IV the measured and calculated dispersion of $p\beta$ of the second and third difference for three different values of η are presented.

TABLE IV. – *The dispersion of $p\beta$ obtained by the cosine function.*

η/η_{opt}	$D_{t2}=\sqrt{n}\,[D(p\beta)/p\beta]_2$		$D_{t3}=\sqrt{n}\,[D(p\beta)/p\beta]_3$	
	Observed	Calculated	Observed	Calculated
$\frac{1}{4}$	1.349 ± 0.120	1.614	1.488 ± 0.144	1.756
1	0.976 ± 0.039	1.022	1.362 ± 0.061	1.229
2	2.013 ± 0.222	1.741	3.061 ± 0.612	3.038

The theoretical dispersion of $p\beta$ for the second difference is given in I, eq. (4.10). For the third difference the calculation is similar but more tedious. We shall give here only the final results, namely

$$\frac{D(p\beta)}{p\beta} = \left\{ \sinh^2 \Omega + \frac{1}{4} \exp[2\Omega](\exp[\varepsilon_1 - 1]) + 2 \sinh^2 (\Omega/6) + \right.$$
$$+ \frac{1}{2} \exp[\Omega/3](\exp[\varepsilon_2 - 1]) + 2 \sinh^2 (\Omega/3) +$$
$$\left. + \frac{1}{2} \exp[2\Omega/3](\exp[\varepsilon_3 - 1]) \right\}^{\frac{1}{2}} \Big/ \sqrt{2n}\,(\Omega + 3\varepsilon_2/2) ,$$

where

$$\Omega = -\tfrac{1}{2}(\sigma\eta)^2[1 - (1/B) \ln (\tfrac{1}{2}\sigma^2\eta^2)] ,$$

$$\varepsilon_1 = 2\eta^2\sigma_3^2 \ln 4/B_3 , \quad \varepsilon_2 = (\eta\sigma_3)^2/3B_3 \quad \text{and} \quad \varepsilon_3 = 8\eta^2\sigma_3^2 \ln 4/9B_3 .$$

A graphical representation of $\sqrt{n}\cdot(D_3(p\beta))/p\beta$ as a function of $(\eta\sigma_3)^2$ is given in Fig. 2.

The agreement with theory is quite good, but less than in the mean cosine case. The statistical errors have been found with the help of known statistical methods (7). Explicitly the relative standard error of s is given by the expression

$$\frac{\sigma(s)}{s} = \left\{\left[\frac{1}{2} + \frac{1}{4n}(\mu_4/\sigma^4 - 3)\right]/N\right\}^{\frac{1}{2}},$$

where σ^2 is the standard deviation of the cosine function and μ_4 its fourth (central) moment. The factor $(1/n)(\mu_4/\sigma^4 - 3)$ measures the deviation of the cosine function from normality. (Note that for a normal distribution the error of the dispersion is $1/\sqrt{2N}$). For relatively small values of η this factor is quite big and therefore cannot be neglected. Let us remark here that in the case of the absolute angle it is impossible, according to the theory of Molière, to estimate this factor. This is the main reason why in the absolute angle case the number of angles n in each group has been chosen much bigger than in the cosine case (40 instead of 10; see Sect. 3·2).

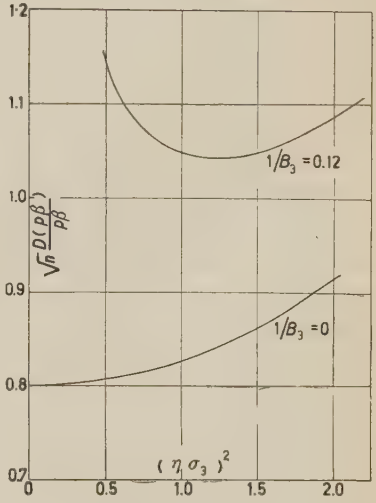

Fig. 2. – The dispersion of $p\beta$ in the third difference case.

4. – The minimum possible dispersion of $p\beta$.

In the previous section we have obtained the dispersion of $p\beta$ by using the mean absolute angle and the cosine function of the scattering angles φ_i. In order to check this point we have made use of the following statistical theorem (8): Let $\varphi_1, \ldots, \varphi_n$ be a set of n independent random variables and let A be a parameter which is to be estimated by the φ_i's. Let $f(\varphi; A)$ be the distribution function of φ_i and $A^*(\varphi_1, \ldots, \varphi_n)$ be the estimation function of A. Then if A^* fulfils the following conditions: (1) A^* is independent of A, (2) A^* is a continuous function and has continuous derivatives $\partial A^*/\partial\varphi_i$ at all points $\varphi = (\varphi_1, \ldots, \varphi_n)$, (except perhaps at a finite number of points), (3) the expectation value of A^* is A: $E[A^*(\varphi_1, \ldots, \varphi_n)] = A$ and (4) if the de-

(7) H. Cramer: *Mathematical Methods of Statistics* (Princeton, 1946).
(8) Ref. (7), p. 477.

rivative $\partial f/\partial A$ is bound, then, the following inequality holds:

$$E[(A^* - A)^2] \geqslant \left\{ n \int_0^\infty f(\varphi; A)(\partial \ln f/\partial A)^2 \, d\varphi \right\}^{-1} . \tag{24}$$

Since we are interested in estimating $p\beta$ we shall choose A to be:

$$A = \sigma = \chi_c \sqrt{B/2} .$$

Not all possible estimates of A fulfil the conditions (1)-(4) above. For example, the mean absolute angle with cut-off (see Sect. 3·3) does not fulfil conditions (1) and (4), and the cosine function does not fulfil condition (3). (In the cosine case this difficulty can easily be removed). Thus the conclusions which will be drawn by using the above theorem will not apply to all possible estimates of $p\beta$ only to a certain class of estimates.

We shall restrict ourselves to the calculation of the minimum dispersion in the case of no correlation between the φ_i's and compare the results to the calculated dispersion for the cosine function. The actual experimental dispersion, as we have seen in I and in Sect. 3 of this work is about 14% greater. (About half of the 14% increase is due to the fact that the angles φ_i measured by the Fowler Co-ordinate Method are correlated, and the other half is contributed by the scattering noise). In the case where there is correlation the dispersion is increased somewhat, but the same holds for the minimum dispersion. Therefore, the above restriction will not affect very much the relative position of the dispersions and comparison of the calculated minimum dispersion with the dispersion of the idealized cosine case will indeed show whether or not a better estimate of $p\beta$ exists. For the distribution function we shall choose Molière's function, neglecting the correction function $f^{(2)}(\varphi)$ and higher order terms, namely:

$$f(\varphi; A) = (1/\sqrt{2}A)\left[(2/\sqrt{\pi}) \cdot \exp\left[-\varphi^2/2A^2\right] + (1/B) f^{(1)}(\varphi/\sqrt{2}A)\right] , \tag{25}$$

$$f^{(1)}(x) = \Phi'(x) \cdot \left[(x^2 - \tfrac{1}{2})(\ln 4\gamma + 2I(x) + 1\right] - 2x\Phi(x) ,$$

where: $x = \varphi/\sqrt{2} \cdot A$, $\Phi(x)$ is the error function and $I(x)$ is defined by the integral:

$$I(x) = \int_0^1 \frac{dZ}{1 - Z^2} \left(\exp\left[1 - Z^2\right]x^2 - 1\right) .$$

The minimum dispersion, using (24) and (25), is obtained by a straightforward but tedious calculation, which involves also numerical integration (9).

(9) S. ROSENDORFF: *Ph.D. thesis* (unpublished), The Hebrew University, Jerusalem (1957).

The results for various values of the parameter B are given in Table V. By inspecting the table it becomes evident that the dispersion of $p\beta$ obtained by the cosine method is very close to the minimum possible dispersion. Since, as we have seen in Sect. 3, the dispersion of $p\beta$ in the cosine case is very close

TABLE V. – *The minimum dispersion of $p\beta$ and the dispersion in the cosine case with no correlation, as a function of $1/B$.*

$1/B$	0	0.05	0.10	0.125	0.20
Minimum possible dispersion	0.707	0.789	0.845	0.872	0.960
Dispersion optained by USING the cosine function . . .	0.707	0.790	0.850	0.882	0.976

to that obtained from the mean absolute angle parameter, it can be concluded that among the class of functions considered here, no better estimate of $p\beta$ than the existing ones can be found.

5. – Conclusion.

On the basis of the present work it can be concluded that the cosine function as an estimate of $p\beta$ rests on a simple theoretical foundation and its theory agrees very well with experiment. In this theory it is possible to calculate all necessary moments and therefore to determine exactly the errors of the second, third and even higher differences. This is not possible in the case of the mean absolute angle because of the divergence of the second and higher moments. On the other hand, it is less convenient to use the cosine function than the mean absolute angle for two reasons:

(*a*) The optimum value of the multiplier η depends upon the value of $p\beta$. It is therefore necessary to begin with a trial value of η and to iterate several times. Because, however, of the insensitivity of the dispersion with variation in η, it should be possible to find a good value of η by one or two iterations. An alternative way of finding the optimal η is to first find an estimate of $p\beta$ by the mean absolute angle method.

(*b*) The determination of the experimental mean of the cosine function involves much numerical work (our analysis was performed on the WEIZAC (*)) whereas the experimental mean of the absolute angle is found almost immediately.

(*) Weizmann Institute Automatic Computer.

We have seen that in the mean absolute angle case one gets good agreement with theory by introducing an appropriate cut-off and that the dispersion in that case is close to the one obtained using the cosine parameter. This shows that both the absolute angle and the cosine function are good estimating functions for $p\beta$ from the statistical point of view.

* * *

We are grateful to Dr. G. YEKUTIELI and Dr. H. J. LIPKIN for many clarifying discussions and to Dr. J. GILLIS and Mr. S. BRUDNO for programming and actually performing the calculation on the WEIZAC. We are also thankful to C. CIVIDALLI and R. PARDO for performing the scanning and part of the numerical calculations.

RIASSUNTO (*)

Confrontando la teoria con l'esperienza abbiamo esaminato l'uso pratico della nuova funzione di scattering multiplo $\cos \eta\varphi$ introdotta da LIPKIN [1] *et al.* Contemporaneamente abbiamo confrontato con l'esperienza le differenze seconde e terze dell'angolo assoluto medio risultante dalla teoria dello scattering di Molière e determinato sperimentalmente le rispettive dispersioni. (Nella teoria di Molière la dispersione teorica diverge). Un buon accordo tra teoria ed esperienza si trova per il coseno, sia per il valor medio e le dispersioni sia per l'angolo assoluto medio con cut-off. Esprimendo l'errore relativo di $p\beta$ con $D_{2,3}/\sqrt{n}$ (per le differenze seconde e terze rispettivamente) abbiamo ottenuto per la funzione coseno: $D_2 = 0.976$ e $D_3 = 1.36$, e per l'angolo assoluto medio (con cut-off a $4\langle|\varphi|\rangle$): $D_2 = 0.97$ e $D_3 = 1.37$. Si dimostra che, limitandosi a una determinata classe di valutazioni di $p\beta$, i suddetti valori di dispersione sono vicini alla dispersione minima possibile di $p\beta$. Si suggerisce anche una spiegazione del noto fatto sperimentale che il rapporto delle « costanti di scattering » K_3/K_2 è di qualche percento maggiore del valore atteso $\sqrt{\frac{3}{2}}$.

(*) *Traduzione a cura della Redazione.*

IL NUOVO CIMENTO Vol. VII, N. 1 1° Gennaio 1958

Analysis of Bursts Produced by Mesons.

M. R. Gupta

Department of Mathematics and Geophysics, Bengal Engineering College Howrah, India

(ricevuto il 28 Agosto 1957)

Summary. — The contributions made by the μ and π^0-mesons to the frequency of burst production under a thick shield of materials have been calculated by making use of the recent results of the soft cascade shower theory. The theoretical results thus obtained have been compared with the observational data given by various authors. Satisfactory agreements between the theoretical and observational results are found everywhere, at high altitude, at sea-level and also underground, using Poisson's distribution for the fluctuation, and taking $\bar{N}(E = 2mc^2, t)$, as the average number of particles in a shower. Further it is seen that the burst calculations made with the above modifications lead us to decide unambiguously in favour of the $\frac{1}{2}$ spin theory of the μ-meson, in contradistinction to the uncertainties met with previously while trying to determine the spin of the μ-meson from the observed burst rates. The effects of taking $N(E=0, t)$ for the average number of particles in a shower or of using a Furry distribution for the fluctuation, have also been estimated.

1. – Introduction.

Large ionization bursts produced in an ion-chamber under a thick shield of materials have been observed by different investigators. The size frequency of such bursts has been calculated by Christy and Kusaka (1) and Chakrabarty (2). Their calculations are based on the assumption that a μ-meson while traversing the thick layer of materials over the ionization chamber ra-

(1) R. F. Christy and S. Kusaka: *Phys. Rev.*, **59**, 414 (1941).
(2) S. K. Chakrabarty: *Ind. Journ. Phys.*, **16**, 377 (1942).

diates a high energy photon which in turn produces the ionization burst through cascade multiplication in the material. The knock-on process contributes only a very small portion of the large bursts which they considered, and as such was not taken into consideration. Apart from the fact that the mass of the μ-meson taken was smaller and the absolute intensity of the μ-meson higher than their values now accepted as probable, there are also other sources of uncertainty in their results. This arises mainly from lack of exact knowledge about $\bar{N}(E, t)$, the average number of particles in a shower and the cascade distribution function. CHRISTY and KUSAKA have based their calculations on the Furry distribution formula and Serber and Snyder's values for $\bar{N}(E, t)$ which except for $E = 0$, is not very dependable as has been discussed previously ([3]). On the other hand CHAKRABARTY has used values for $\bar{N}(E, t)$ as obtained by BHABHA and CHAKRABARTY which again are rather too low for iron. In other respects we have, however, followed CHAKRABARTY in assuming that the probability of N particles appearing in a cascade shower instead of the average number $\bar{N}$ is given by Poisson's distribution. Further we have taken the average of the total number of electrons that can be detected experimentally in a shower at depth t to be equal to $\bar{N}(E=2mc^2, t)$ rather than $\bar{N}(E=0, t)$ or $N_0(0, t)$. A comparison with the results obtained recently by some authors ([4]) while studying the development of cascade showers in multiplate cloud chambers justifies this assumption ([5]). With this modification the calculation of the size frequency of burst production gives consistent results irrespective of the shielding material over the ionization chamber and definitely supports the $\frac{1}{2}$ spin theory of the μ-meson which is now accepted as correct because of the evidences from the decay spectrum ([6]).

At higher altitudes, the frequency of burst production is much larger than at sea-level, while the intensity of the μ-mesonic radiation does not correspondingly increase. This indicates that there must be some additional mechanism which will contribute a major part to the frequency of burst production at high altitudes. It is believed that bursts recorded at high altitudes under thick layers of material are primarily due to the nuclear interaction of the N-rays. The π^0-mesons produced within the shield by such interactions will, on account of their very short life-time, decay almost instantaneously giving two photons which in their turn will produce the ionization bursts through cascade multiplication. FAHY ([7]) has given a rough estimate of the

([3]) S. K. CHAKRABARTY and M. R. GUPTA: *Phys. Rev.*, **101**, 813 (1956).

([4]) W. E. HAZEN: *Phys. Rev.*, **99**, 911 (1955); P. A. BENDER: *Nuovo Cimento*, **2**, 980 (1955).

([5]) M. R. GUPTA: *Proc. Nat. Inst. Sci.* (*Ind.*) **23** A, 217 (1957).

([6]) R. SAGANE, W. L. GARDNER and H. W. HUBBARD: *Phys. Rev.*, **82**, 557 (1951).

([7]) E. F. FAHY: *Phys. Rev.*, **83**, 413 (1951).

bursts size-frequency based on the neutral meson hypothesis. In the present paper, we have made an attempt to determine the contribution to the burst frequency from π^0-mesons at high altitudes and also at sea-level.

2. – Bursts produced by μ-mesons.

It has been shown previously by CHAKRABARTY that for large bursts containing more than 100 particles the contribution from the knock-on electrons produced by the μ-mesons is negligible. The μ-meson may, however, radiate a high energy photon in the field of the atomic nucleus. The cross-section for this process (assuming spin $\frac{1}{2}$ and magnetic moment $e\hbar/2Mc$) is given by

$$(1a) \qquad Q(\omega, E_0)\,\mathrm{d}E_0 = \frac{16}{3}\cdot\frac{Z^2 r_0^2}{137}\left(\frac{m}{M}\right)^2\left[\frac{\omega - E_0}{E_0} + \frac{3}{4}\cdot\frac{E_0}{\omega}\right]\left[\ln\frac{2\omega(\omega - E_0)}{Mc^2 E_0} - \frac{1}{2}\right]\frac{\mathrm{d}E_0}{\omega},$$

when the screening of the nucleus by the orbital electrons is incomplete and

$$(1b) \qquad Q(\omega, E_0)\,\mathrm{d}E_0 = \frac{16}{3}\,\frac{Z^2 r_0^2}{137}\left(\frac{m}{M}\right)^2 \ln\left(183\,\frac{M}{m}\,Z^{-\frac{1}{3}}\right)\left[\frac{\omega - E_0}{E_0} + \frac{3}{4}\cdot\frac{E_0}{\omega}\right]\frac{\mathrm{d}E_0}{\omega},$$

for complete screening.

If $\bar{N}(E, t)$ is the average number of particles of energy $\geqslant E$ at a depth t in a cascade shower initiated by a primary of energy E_0, then assuming Poissonian distribution, the probability of finding more than N particles when the average is $\bar{N}$ is given by

$$(2) \qquad P(N+1, \bar{N}) = \sum_{r=N+1}^{\infty} \frac{\bar{N}^r}{\Gamma(\bar{N}+1)} \exp[-\bar{N}] - \frac{\bar{N}^{N+1}}{\Gamma(N+1)} \int_0^1 z^N \exp[-z\bar{N}]\,\mathrm{d}z\,.$$

Thus the probability that a μ-meson after traversing a thickness T_0 of the shielding material above the ionization chamber will register a burst consisting of more than N particles (electrons or positrons) is

$$(3) \qquad \sigma \int_0^{\omega} \mathrm{d}E_0\, Q(\omega, E_0)\cdot l \int_0^{T_0} \mathrm{d}t\, P(N+1, \bar{N})\,.$$

where l (in cm) is the thickness of the material of the shield corresponding to one radiation unit and σ is the number of atoms per cm^3 in the materials.

The differential spectrum of the μ-mesons is given by ([8])

$$S(\omega)\,\mathrm{d}\omega = \delta \cdot I_0 \frac{(2\cdot 10^9\ \mathrm{eV})^\delta}{(\varepsilon T + \omega)^{\delta+1}}\,\mathrm{d}\omega\,, \tag{4}$$

where $\delta = 1.87$, $\varepsilon T = 1.8\cdot 10^9$ eV at sea level and the absolute intensity I_0 as given by PUPPI and DALLAPORTA ([9]) is $8.3\cdot 10^{-3}\ \mathrm{s^{-1}\,(cm^2)^{-1}\,sr^{-1}}$. Hence the frequency per cm² per s of bursts containing more than N particles is

$$B_\mu(N) = \sigma l \int_0^\infty 2\pi S(\omega)\,\mathrm{d}\omega \int_0^\infty \mathrm{d}E_0\, Q(\omega, B_0) \int_0^{T_0} \mathrm{d}t\, P(N+1, \bar{N}) \ldots\,. \tag{5}$$

To evaluate the integral on the right hand side we require the values of $\bar{N}$ for different values of E_0 and t. This has been given in closed analytic form by CHAKRABARTY and GUPTA ([3]). Since the exact expressions for $\bar{N}$ are too complicated to be used here, we have, following CHAKRABARTY ([2]) tried to set up empirical relations which give values in close agreement with the numerical values they have given. We have taken

$$\begin{cases} \bar{N}(E, t) = N_m \exp\left[-\alpha_1 t_m (1 - t/t_m)^2\right]\,; & t < t_m \\ \qquad\quad = N_m \exp\left[-\alpha_2 t_m (t/t_m - 1)^2\right]\,; & t > t_m \end{cases} \tag{6}$$

$$N_m = x_0 [y_0 - \zeta]^{-\frac{1}{2}} e^{y_0} \tag{7}$$

$$t_m = 1.01\, y_0 - \zeta_1\,, \tag{8}$$

$$y_0 = \ln E_0/\beta\,,$$

where α_1, α_2, x_0, etc., will depend on the cut-off energy E and also on the material in which the shower develops.

For $E = 2mc^2$, we have (for lead)

$$\alpha_1 = \cdot 57\,; \quad \alpha_2 = \cdot 20\,; \quad x_0 = \cdot 20\,; \quad \zeta = -\cdot 40\,; \quad \zeta_1 = \cdot 51 \tag{9a}$$

while for iron we have for the same energy value,

$$\alpha_1 = \cdot 56\,; \quad \alpha_2 = \cdot 20\,; \quad x_0 = \cdot 25\,; \quad \zeta = -\cdot 38\,; \quad \zeta_1 = \cdot 42\,. \tag{9b}$$

For $E = 0$, we have both for Pb and Fe

$$\alpha_1 = \cdot 55\,; \quad \alpha_2 = \cdot 20\,; \quad x_0 = \cdot 32\,; \quad \zeta = -\cdot 36\,; \quad \zeta_1 = \cdot 20\,. \tag{9c}$$

([8]) H. EULER and W. HEISENBERG: *Ergeb. Exakt. Naturwiss.*, **17**, 1 (1938).
([9]) G. PUPPI and N. DALLAPORTA: *Progr. Cosm. Rays Phys.*, Vol. **1**, p. 336.

For sufficiently thick shields, i.e., for large values of T_0 we may now write the integral over t in (5) as

$$(10)\qquad \int_0^\infty \mathrm{d}t\ \frac{\bar{N}^{N+1}}{\Gamma(N+1)} \int_0^1 z^N \exp[-z\bar{N}]\,\mathrm{d}z =$$

$$= \frac{N_m^{N+1}}{\Gamma(N+1)} \int_0^{t_m} \mathrm{d}t \exp[-\alpha_1 t_m (N+1)(1-t/t_m)^2] \cdot$$

$$\cdot \int_0^1 \mathrm{d}z z^N \sum_{r=0}^{\infty} \frac{(-)^r z^r}{\Gamma(r+1)} N_m^r \exp[-\alpha_1 t_m r (1-t/t_m)^2] +$$

$$+ \frac{N_m^{N+1}}{\Gamma(N+1)} \int_{t_m}^{\infty} \mathrm{d}t \exp[-\alpha_2 t_m (N+1)(t/t_m - 1)^2] \cdot$$

$$\cdot \int_0^1 \mathrm{d}z z^N \sum_{r=0}^{\infty} \frac{(-)^r z^r}{\Gamma(r+1)} N_m^r \exp[-\alpha_2 t_m r (t/t_m - 1)^2] =$$

$$= \frac{N_m^{N+1}}{\Gamma(N+1)} \cdot \frac{\sqrt{\pi}}{2} (\alpha_1^{-\frac{1}{2}} + \alpha_2^{-\frac{1}{2}}) t_m^{\frac{1}{2}} \sum_{r=0} \frac{(-)^r z^r}{\Gamma(r+1)} \cdot \frac{1}{(N+r+1)^{\frac{3}{2}}} =$$

$$= \frac{\sqrt{\pi}}{2} (\alpha_1^{-\frac{1}{2}} + \alpha_2^{-\frac{1}{2}}) \cdot \frac{1}{2\pi i L} \int_{C-i\alpha}^{C+i\alpha} \mathrm{d}z \frac{\Gamma(z) N_m^{N-z+1} t_m^{\frac{1}{2}}}{\Gamma(N+1)(N-z+1)^{\frac{3}{2}}} .$$

For $N > N_m$, the value of the integral (10) is insignificant as pointed out by CHAKRABARTY. Since we are interested in large bursts containing more than 200 particles, this means that an appreciable contribution to $B_\mu(N)$ will come only from energies $E_0 \geq E_N$, where $E_0 = E_N$ corresponds to $N_m = 200$. For the different cases that we are considering here, $y_N = \ln(E_N/\beta)$ will be between 7.5 and 8.0. Further as the meson energy $\omega \geq E_0 \geq E_N$, we may approximate the meson spectrum $S(\omega)$ by taking $\omega^{-(\delta+1)}$ instead of $(\varepsilon T + \omega)^{-(\delta+1)}$.

Interchanging the ω and E_0 integration, substituting for N_m and t_m, (5) may now be written (for incomplete screening) as follows

$$(11)\qquad B_\mu(N) = \beta^{-\delta} \cdot A \cdot \frac{16}{3} \int_\varepsilon^\infty \mathrm{d}E_0 \int_{E_0}^\infty \frac{\mathrm{d}\omega}{\omega^{\delta+2}} \left[\frac{\omega}{E_0} + \frac{3}{4} \cdot \frac{E_0}{\omega} - 1\right] \cdot$$

$$\cdot \left[\ln \frac{2\beta}{Mc^2} + \ln \frac{E_0}{\beta} + \ln \frac{\omega}{E_0}\left(\frac{\omega}{E_0} - 1\right) - \frac{1}{2}\right] \cdot$$

$$\cdot \frac{1}{2\pi i} \int_{C-i\alpha}^{C+i\alpha} \mathrm{d}z \frac{\Gamma(z)(y_0-\zeta)^{-\frac{1}{2}(N-z)} (x_0 e^{y_0})^{N-z+1}}{\Gamma(N+1)(N-z+1)^{\frac{3}{2}}} \cdot \left(\frac{y_0 - \zeta_1}{y_0 - \zeta}\right)^{\frac{1}{2}},$$

$$A = \frac{\sqrt{\pi}}{2}\,(\alpha_1^{-\frac{1}{2}} + \alpha_2^{-\frac{1}{2}})2\pi l\sigma\,\delta I_0\,\frac{Z^2 r_0^2}{137}\cdot\left(\frac{2\cdot 10^9\ \mathrm{eV}}{\beta}\right)^8 . \tag{12}$$

For reasons mentioned in the previous section, we may put $(y_0 - \zeta_1)/(y_0 - \zeta))^{\frac{1}{2}} \approx 1$ and take the lower limit $\varepsilon = \beta e^{\zeta}$ in the integral over E_0. (11) can now be easily evaluated and we have finally for the case of incomplete screening,

$$B_{\mu}(N) = A\,\exp\,[-\,\delta\zeta]\{(K + \zeta L) f_1(N,\,\delta) + L f_2(N,\,\delta)\} \tag{13a}$$

and similarly for complete screening

$$B_{\mu}(N) = A\,\exp\,[-\,\delta\zeta] K' f_1(N,\,\delta)\,, \tag{13b}$$

where

$$L = L_0 + \frac{4}{\delta + 2}\,; \qquad L_0 = \frac{16}{3}\cdot\frac{1}{\delta(\delta+1)}\,. \tag{14a}$$

$$\left\{\begin{aligned} K &= K_0 + 4\left[\frac{1}{\delta+2}\left\{\ln\frac{2\beta}{Mc^2} - \frac{1}{2}\right\} + \frac{2}{(\delta+2)^2} - \frac{1}{\delta+2}\left\{\frac{\mathrm{d}}{\mathrm{d}\delta}\ln\Gamma(\delta+3) + \gamma\right\}\right], \\ K_0 &= L_0\left[\left\{\ln\frac{Mc^2}{2\beta} - \frac{1}{2}\right\} + \frac{2(2\delta+1)}{\delta(\delta+1)} + \right. \\ &\qquad \left. + \delta\,\frac{\delta}{\mathrm{d}\delta}\ln\Gamma(\delta+2) - (\delta+1)\,\frac{\mathrm{d}}{\mathrm{d}\delta}\ln\Gamma(\delta+1) - \gamma\right], \\ K' &= \frac{16}{3}\ln\left(183\,\frac{M}{m}\,Z^{-\frac{1}{3}}\right)\left\{\frac{1}{\delta(\delta+1)} + \frac{3}{4}\,\frac{1}{\delta+2}\right\}, \end{aligned}\right. \tag{14b}$$

and γ is the Euler constant.

The function $f_1(N, \delta)$ and $f_2(N, \delta)$ are in the same form as given by CHAKRABARTY except that values of the constants x_0 and ζ are different.

$$f_1(N,\,\delta) = \frac{1}{2\pi i}\int_{C-\iota\alpha}^{C+\iota\alpha}\mathrm{d}z\,\frac{\Gamma(z)(x_0 e^{\zeta})^{N-z+1}}{\Gamma(N+1)(N-z+1)^{\frac{3}{2}}}\cdot \tag{15a}$$

$$\cdot\,\Gamma\left(1 - \frac{N-z}{2}\right)(\delta + z - N - 1)^{-\frac{1}{2}(2+z-N)}\,,$$

$$f_2(N,\,\delta) = \frac{1}{2\pi i}\int_{C-\iota\alpha}^{C+\iota\alpha}\mathrm{d}z\,\frac{\Gamma(z)(x_0 e^{\zeta})^{N-z+1}}{\Gamma(N+1)(N-z+1)^{\frac{3}{2}}}\cdot \tag{15b}$$

$$\cdot\,\Gamma\left(2 - \frac{N-z}{2}\right)(\delta + z - N - 1)^{-\frac{1}{2}(4+z-N)}\,.$$

$B_{\mu}(N)$ as given by (13) cannot be directly used for the calculation of the frequency of small bursts ($50 \leqslant N \leqslant 100$) produced underground. The reason for this is that at large depths (say at a depth of 60 m w.e.) the differential μ-spectrum is given by

$$S(\omega)\,\mathrm{d}\omega = \delta I_0 \frac{(2\cdot 10^9)^{\delta}}{(12\cdot 10^9 + \omega)^{\delta+1}}\,\mathrm{d}\omega\,,$$

so that for the burst size under consideration we are no longer justified in replacing $(12\cdot 10^9 + \omega)^{-(\delta+1)}$ simply by $\omega^{-(\delta+1)}$. We have therefore taken

$$S(\omega) = \cdot 079\cdot \delta I_0 \frac{(2\cdot 10^9\ \mathrm{eV})^{\delta}}{\omega^{\delta+1}}\,,$$

with $\delta = 1.55$, which gives a fairly good fit with the actual value for $S(\omega)$ for energies down to ~ 6 GeV. The contribution to the underground small bursts through the bremsstrahlung process can now be evaluated by multiplying the right hand side of (13) by the factor .079 and putting $\delta = 1.55$.

For small bursts the contribution from the knock-on electrons produced by the μ-mesons by direct collision is also important. The cross-section for the knock-on process is

$$Q(\omega, E_0)\,\mathrm{d}E_0 = 2\pi r_0^2 mc^2 Z\left[1 - \frac{E_0}{\varepsilon_m} + \frac{1}{2}\cdot\frac{E_0^2}{\omega^2}\right]\frac{\mathrm{d}F_0}{F_0^2} \qquad r_0 = e^2/mc^2, \tag{16}$$

where ε_m is the maximum energy transferable to the electron in a direct collision, and is given by

$$\varepsilon_m = \omega\left[1 + \mu\frac{Mc^2}{2\omega}\right]^{-1}; \qquad \mu = M/m\,.$$

Substituting for $Q(\omega, E_0)$ in (5) and proceeding as before, the contribution of the knock-on electrons can now be determined. The results have been shown in Fig. 3 and are discussed in a subsequent section.

3. – Bursts produced in π^0-mesons.

For the calculation of the size frequency of bursts produced by π^0-mesons it is necessary to have a knowledge of its differential energy spectrum at different heights above sea-level. But sufficient direct observational data regarding this are not available. Following the theory of nucleonic cascades

based on the hypothesis of plural production of mesons ([10]), we may however obtain it from the spectrum of the primary cosmic ray component. The differential spectrum of the primary cosmic-ray component ([11]) may be approximated by a power law of the form $E^{-(\delta+1)}$. The value of δ is however not constant but varies from 1·1 (in the low energy region $E \lesssim 10$ GeV) to the value 1.67 for sufficiently high energies. In the energy range in which we are interested we may put $\delta = 1.67$ and write the primary cosmic ray component in the form

$$S(E)\,\mathrm{d}E = a \cdot \frac{(10^9\ \mathrm{eV})^{\delta}}{E^{\delta+1}}\ \mathrm{s}^{-1}\,(\mathrm{cm}^2)^{-1}\,\mathrm{sr}^{-1}\,, \tag{17}$$

where $a = 1.67$.

It has been shown by MESSEL that for $E > E_c$ the latitude cut-off energy, the primary component is absorbed exponentially in the atmosphere so that the spectrum at a depth x g/cm² below the top of the atmosphere is

$$S(E, x)\,\mathrm{d}E = S(E)\,\exp\,[-x/X]\,\mathrm{d}E\,,$$

where X g/cm² is the absorption mean free path in the atmosphere.

Assuming the top of the atmosphere to be horizontal the intensity per cm² per s at depth x is

$$\mathrm{d}E \int_0^{2\pi} \mathrm{d}\varphi \int_0^{\pi/2} S(E, x/\cos\theta)\,\sin\theta\,\mathrm{d}\theta = 2\pi S(E)\,\mathrm{d}E \int_0^{\pi/2} \exp\,[-x\sec\theta/X]\,\sin\theta\,\mathrm{d}\theta = \tag{18}$$

$$= 2\pi\left[\exp\,[-x/X)] - \frac{x}{X}\int_{x/X}^{\infty} \exp\,[-t]\,\mathrm{d}t/t\right] = 2\pi f(x/X)\,.$$

At a depth t (in radiation units) within the shield over the ionization chamber, the intensity of the incident nucleonic component is

$$2\pi f(x/X)\,S(E)\,\mathrm{d}E\,\exp\,[-t/T]\,,$$

where T is the absorption mean free path in radiation units for the material of the shield. Now, the probability per collision length of a nucleon of energy E colliding with another nucleon and giving rise to a fast nucleon in the energy range ε, $\varepsilon+\mathrm{d}\varepsilon$, a meson in the range ω, $\omega+\mathrm{d}\omega$ and a second

([10]) W. HEITLER and L. JÁNOSSY: *Proc. Phys. Soc.*, A **62**, 374 (1949); H. MESSEL: *Proc. Phys. Soc.*, A **64**, 726 (1951).

([11]) H. V. NEHER: *Progr. Cosm. Ray Phys.*, Vol. **1**, p. 301.

nucleon of energy $E-\varepsilon-\omega$ is [12]

$$\omega(E,\varepsilon,\omega)\,\mathrm{d}\omega = 120\,\frac{\varepsilon}{E}\cdot\frac{\omega}{E}\left(1-\frac{\varepsilon}{E}-\frac{\omega}{E}\right)\mathrm{d}\left(\frac{\varepsilon}{E}\right)\mathrm{d}\left(\frac{\omega}{E}\right).$$

Then the total number of mesons produced within a thickness $\mathrm{d}(T_0-t)$ (T_0 is the total thickness of the shield) within the shield is

$$(19)\qquad 2\pi f(x/X)\exp\left[-(T_0-t)/T\right]l\,\mathrm{d}(T_0-t)\cdot\int_{\omega}^{\infty}S(E)\,\mathrm{d}E\cdot$$

$$\cdot\left[\frac{120}{L}\,\mathrm{d}\left(\frac{\omega}{E}\right)\cdot\frac{\omega}{E}\int_0^{1-\omega/E}\frac{\varepsilon}{E}\left(1-\frac{\omega}{E}-\frac{\varepsilon}{E}\right)\mathrm{d}\left(\frac{\varepsilon}{E}\right)\right]=$$

$$=\frac{40\pi l}{L}\,f(x/X)\left[\frac{1}{\delta+2}-\frac{3}{\delta+3}+\frac{3}{\delta+4}-\frac{1}{\delta+5}\right]\cdot$$

$$\cdot a\cdot\frac{(10^9\ \mathrm{eV})^{\delta}}{\omega^{\delta+1}}\,\mathrm{d}\omega\exp\left[-(T_0-t)/T\right]\mathrm{d}(T_0-t),$$

where l and L are respectively the radiation and collision unit for the material of the shield. Of these mesons, one-third are neutral π^0-mesons which decay almost instantaneously into photons. Assuming that the decay photons are emitted isotropically in a co-ordinate system moving with the velocity of the neutral meson, it may be easily shown that the probability that a decay photon will have energy in the range E_0, $E_0+\mathrm{d}E_0$ is [13]

$$Q(\omega,E_0)\,\mathrm{d}E_0=\frac{\mathrm{d}E_0}{\sqrt{\omega^2-\omega_0^2}},$$

for

$$\tfrac{1}{2}\left(\omega-\sqrt{\omega^2-\omega_0^2}\right)\leqslant E_0\leqslant\tfrac{1}{2}\left(\omega+\sqrt{\omega^2-\omega_0^2}\right)$$

and is zero outside this interval, where W is the energy of the meson and ω_0 is its rest energy. For $\omega\ll\omega_0$ we may put

$$(20)\qquad Q(\omega,E_0)\,\mathrm{d}E_0=\frac{\mathrm{d}E_0}{\omega}.$$

[12] H. Messel, R. B. Potts and C. B. A. McCusker: *Phil. Mag.*, **43**, 889 (1592).
[13] A. G. Carlson, J. E. Hooper and D. T. King: *Phil. Mag.*, **41**, 701 (1950).

Combining (2), (19) and (20) and remembering that two photons are obtained from a single decay event, we find that the frequency of bursts produced by the neutral mesons is given by

$$B_{\pi^0}(N) = c_1 a(10^9 \text{ eV})^{\delta} \int_0^{\infty} \frac{\mathrm{d}\omega}{\omega^{\delta+1}} \int_0^{\omega} \mathrm{d}E_0 Q(\omega, E_0) \cdot \cdot \int_{T_0}^{0} \mathrm{d}(T_0 - t) \exp\left[-(T_0 - t)/T\right] P(N+1, \bar{N}) , \tag{21}$$

where

$$c_1 = \frac{80\pi l}{3L} f(x/X) \left[\frac{1}{\delta+2} - \frac{3}{\delta+3} + \frac{3}{\delta+4} - \frac{1}{\delta+5}\right] . \tag{22}$$

For large thicknesses of the shielding material, the integral over t may be written as

$$\exp\left[-T_0/T\right] \int_0^{\infty} \mathrm{d}t \exp\left[t/T\right] \frac{\bar{N}^{N+1}}{\Gamma(N+1)} \int_0^1 z^N \exp\left[-z\bar{N}\right] \mathrm{d}z . \tag{23}$$

Substituting for N and proceeding as in (10) the expression (23) may be shown to be equal to

$$\frac{\sqrt{\pi}}{2} (\alpha_1^{-\frac{1}{2}} + \alpha_2^{-\frac{1}{2}}) \exp\left[-T_0/T\right] t_m^{\frac{1}{2}} \exp\left[t_m/T\right] \cdot \frac{1}{2\pi i} \int_{C-\iota\alpha}^{C+\iota\alpha} \mathrm{d}z \frac{\Gamma(z) N_m^{N-z+1}}{(N-z+1)^{\frac{3}{2}}} \frac{1}{\Gamma(N+1)} . \tag{24}$$

From (8)

$$\exp\left[t_m/T\right] = \exp\left[\frac{1}{T}(1.01 y_0 - \zeta_1)\right] \approx \left(\frac{E_0}{\beta}\right)^{1-0.1/T} = \left(\frac{E_0}{\beta}\right)^{\alpha}, \quad \text{say.}$$

Substituting (24) for the integral over t in (20) we finally get

$$B_{\pi^0}(N) = c_1 c_2 f_1(N, \delta - \alpha) . \tag{25}$$

where

$$c_2 = \exp\left[-T_0/T\right] \frac{a}{\delta+1} \left(\frac{10^9}{\beta}\right)^{\delta} \frac{\sqrt{\pi}}{2} (\alpha_1^{-\frac{1}{2}} + \alpha_2^{-\frac{1}{2}}) \exp\left[-(\delta - \alpha)\zeta\right] . \tag{26}$$

4. – Numerical results.

The integrals $f_1(N, \delta)$ and $f_2(N, \delta)$ have been evaluated numerically by the saddle point method and then from equations (13*a*) numerical values for $B_\mu(N)$ have been obtained. This has been done both for iron and lead shields over the ionization chamber and the two sets of results thus obtained have been compared with the sea-level data given by LAPP [14]. It should be mentioned here that while Lapp's burst data for iron are obtained with a 35 cm homogeneous iron-shield, it is not so for lead (10.7 cm thick shield) because of the presence of the 1.25 cm thick iron-wall of the ionization chamber. The effect of the iron which is to reduce the number of cascade particles produced in the lead shield, may be taken into consideration by choosing a value of β intermediate between those for pure lead and iron. Following the arguments given by CHRISTY and KUSAKA we find that this effective value $\beta_{\text{Pb-Fe}}$ is 12 MeV in this case. For the iron-shield, there is, however no such difficulty and we have β_{Fe} equal to 25.9 MeV as usual.

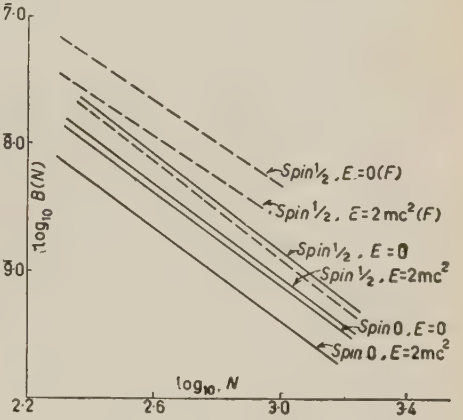

Fig. 1. – Plot of $\log_{10} B_\mu(N)$ against $\log_{10} N$. Dashed curve shows Lapp's sea-level data. *F* indicates Furry distribution. The screening is taken to be incomplete.

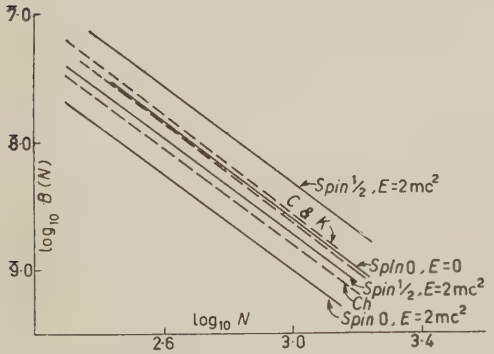

Fig. 2. – Dashed curve shows Lapp's sea-level data under 10.7 cm Pb + 1.25 cm Fe shield. All the other curves indicate the calculated results (Eqn. (13*a*)) under the same shield. *C* and *K* → Christy and Kusaka's curve; *Ch* → Chakrabarty's curve.

In Fig. 1 and Fig. 2 we have plotted $\log_{10} B_\mu(N)$ against $\log_{10} N$ for different assumptions regarding the spin of the μ-meson and the average number of particles. Comparison with Lapp's sea-level data (shown in the same figures) show that the $\frac{1}{2}$ spin theory of the μ-meson is the most plausible one, provided we take $\bar{N}(E = 2mc^2, t)$ as the average number of particles. If however, we use $\bar{N}(E = 0, t)$ the theore-

[14] R. E. LAPP: *Phys. Rev.*, **69**, 321 (1946).

tical burst frequencies (for spin $\frac{1}{2}$) become larger than the observed ones. In this case the spin zero curve gives a better agreement. The reason for this discrepancy is that the cascade shower theory in its usual B-approximation form gives too large a multiplication near zero energy (as the assumptions regarding constant ionization loss etc., are no longer valid.) Further, below a certain energy the particles will escape detection and finally it is to be remembered that the energy of a particle (electron) at minimum ionization is nearer to $2mc^2$ rather than to zero energy.

In Fig. 2 we find that, as expected, the values given by CHAKRABARTY are somewhat less than those given by us for $E = 2mc^2$. On the other hand, contrary to expectation, CHRISTY and KUSAKA's values (after introducing the necessary corrections for the mass of the μ-meson etc.) are less than ours for $E = 0$. The reason for this is that at a later stage in their analysis they have introduced a modification which is equivalent to taking $E_0/15\beta$ as the maximum number of particles, while it is nearly $E_0/9\beta$ according to SERBER and SNYDER (which corresponds to our values for $\overline{N}_{\max}$ when $E = 0$). Moreover the empirical expression for $N(E, t)$ which they have used gives $t_{\max} = 7$ independently of the primary energy while actuallly it varies nearly linearly with $\ln(E_0/\beta)$. According to their analysis the contribution to the burst frequencies for any particle of energy E_0 is proportional to $t_{\max}$ and hence the resulting frequency is thus further under-estimated.

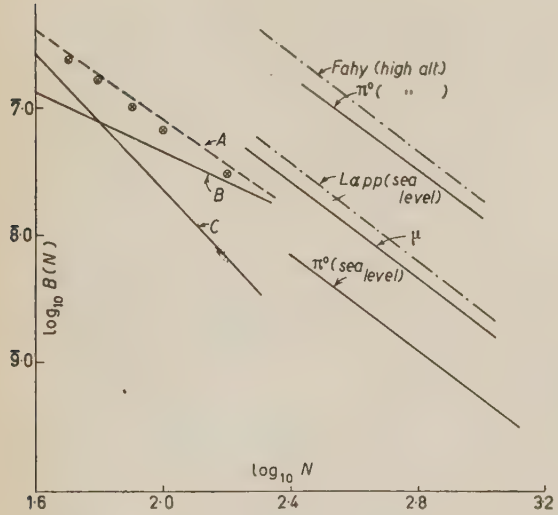

Fig. 3. – $A \rightarrow$ George and Trent's underground bursts data under 15 cm Pb shield; B and $C \rightarrow$ contributions from bremsstrahlung, knock-on electrons respectively; Pts. $\otimes \rightarrow$ combined contribution from the two processes.

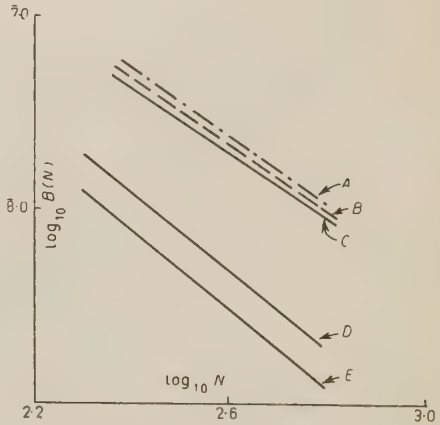

Fig. 4. – A, $B \rightarrow$ from Carmichael and Steltje's sea-level burst data under 12 cm and 27 cm Pb respectively; C, D, $E \rightarrow$ from μ and π^0-mesons at sea level under 12 cm and 27 cm of Pb respectively.

In Fig. 3 and 4 we have compared our results with the experimental data given by LAPP, FAHY and GEROGE and TRENT ([15]). It is seen that according to our analysis nearly 75% of the bursts at sea-level (under 10.7 cm Pb + + 1.25 cm Fe) should be ascribed to μ-mesons, while the π^0-mesons contribute (16 to 20)% of the total under the same shield. At an altitude of 3500 m above the sea-level, the μ-mesons contribute about 10% of the total while (70 to 75)% comes from the π^0-mesons. As regards the small bursts observed under ground (at a depth 60 m w.e.) it is found that (90 to 95)% of the total burst frequency may be accounted for by considering the combined effect of the knock-on electrons and the bremsstrahlung photons emitted by the μ-mesons. As expected the contribution from the π^0-mesons at this depth is negligible.

In Fig. 4 we have also compared our results with those given by CARMICHAEL and STELJES ([16]) at sea-level under lead shields of different thicknesses. The contribution from the μ-mesons amounts to nearly 79% of the bursts observed under a 12 cm thick Pb shield, while under a thickness of 27 cm of Pb nearly 85% of the total may be accounted for in this way. For these two cases the contribution from the π^0-mesons has also been worked out and is found to be $\approx 21\%$ and 12% respectively. Our analysis thus gives results which are fairly consistent with the experimental ones at different heights and depths and also under different thicknesses of material.

5. – Dependence on the form of fluctuations.

So long we have only used the Poissonian distribution in our calculations. To have an idea of the effect of fluctuation on the frequency of burst production we shall now calculate the burst frequency by assuming the Furry distribution. In this case

$$P(N-1,\ N) = \left[1 - \frac{1}{\bar{N}}\right]^N .$$

For convenience in numerical calculation we have used a different empirical form for $N(E, t)$. Following CHRISTY and KUSAKA we have taken

$$\bar{N}(E, t) = \left\{1 - \left(1 - \frac{a\beta}{E}\right)\left(\frac{t}{t_m}\right)^{58\beta/E} \exp\left[\frac{58\beta}{E}(1 - t/t_m)\right]\right\}^{-1}, \tag{27}$$

where t_m is the same as given by (8) and (9) and

$$\begin{cases} a = 15 & \text{for lead } (E = 2mc^2)\,, \\ = 11.5 & \text{for iron } (E = 2mc^2)\,, \\ = 9.0 & \text{for both Pb and Fe } (E = 0)\,. \end{cases} \tag{28}$$

([15]) E. P. GEORGE and P. T. TRENT: *Proc. Phys. Soc.*, A **64**, 733 (1951).
([16]) H. CARMICHAEL and J. F. STELJES: *Phys. Rev.*, **99**, 1542 (1955); **105**, 1626 (1957).

Substituting for $P(N+1, \bar{N})$ and $\bar{N}(E, t)$ from the above equations in (5) it may be easily shown that

$$(29) \qquad B_\mu(N) = \frac{A'}{S^\delta}\left[L\frac{\mathrm{d}^2}{\mathrm{d}\delta^2}\Gamma\left(\delta-\frac{1}{2}\right) - \{(2L-\zeta_1)\ln S + K\}\frac{\mathrm{d}}{\mathrm{d}\delta}\Gamma\left(\delta-\frac{1}{2}\right) + \right.$$

$$\left. + (\ln S - \zeta_1)(K + \ln S)\,\Gamma\left(\delta-\frac{1}{2}\right)\right].$$

$$A' = 2\pi l\sigma\,\delta I_0\,\frac{Z^2 r_0^2}{137}\left(\frac{m}{M}\right)^2\left(\frac{2\cdot 10^9}{\beta}\right)^\delta$$

$$S = aN$$

and K and L are the same as given by equations (14 *a*, *b*).

In Fig. 1 we have plotted $\log_1 B_\mu(N)$ as given by (29) for the two different cases viz., $E = 2mc^2$ and $E = 0$. It is quite evident from the graphs that whatever be the form for fluctuation, $\bar{N}(E = 0, t)$ cannot be taken as the average number. However, for $E = 2mc^2$, the experimental curve lies in between the two extreme cases given by the Poisson and the Furry distribution and the former is to be used for this value of the cut-off energy. But the Furry distribution may also be successfully used if a higher value of the cut-off energy is chosen.

* * *

I am indebted to Dr. S. K. Chakrabarty, F.N.I. for help and guidance in this work.

The author is also thankful to the Atomic Energy Department, Govt. of India for the financial support during the progress of this work.

RIASSUNTO (*)

Si è calcolato il contributo dato dai mesoni μ e π^0 alla frequenza della produzione di burst sotto uno spesso schermo di materia servendosi di recenti risultati della teoria della cascata molle. I risultati teorici così ottenuti sono stati confrontati con i dati d'osservazione forniti da vari autori. Si è trovato dappertutto un soddisfacente accordo tra i risultati delle osservazioni e la teoria, sia a grande altezza, sia al livello del mare, sia sotto terra, adottando per la fluttuazione della distribuzione di Poisson e prendendo $\bar{N}(E = 2mc^2, t)$ per il numero medio di particelle in uno sciame. Si vede inoltre che i calcoli sui burst fatti con le modificazioni di cui sopra ci portano senza ambiguità a preferire la teoria dello spin $\frac{1}{2}$ del mesone μ a differenza della incertezze incontrate prima nel cercare di determinare lo spin del mesone μ dalla frequenza dei burst osservati. Si sono anche valutati gli effetti del prendere $N(E=0, t)$ per il numero medio di particelle in uno sciame o dell'usare una distribuzione di Furry per la fluttuazione.

(*) *Traduzione a cura della Redazione.*

IL NUOVO CIMENTO Vol. VII, N. 1 1° Gennaio 1958

The Average Multiplicity and Inelasticity in π-Meson Production in the Atmosphere.

G. Ishikawa and K. Maeda (*)

Meteorological Research Institute - Tokyo

(ricevuto il 29 Agosto 1957)

Summary. — The energy spectra of primary and secondary cosmic radiation are analysed to find the multiplicity-energy relation in the π-meson production in the atmosphere at the energy region from several GeV to some thousands GeV with the help of simplified considerations on the meson production by nucleus-nucleus collisions. The results being subjected to the assumed values of inelasticity suggest that the multiplicity-energy relation agrees with the formula of the type given by Fermi and Landau under the condition of a practically constant small inelasticity.

1. – Introduction.

Using the data of the integral energy spectrum of the N-component averaged over the atmospheric depth $J(E_p)$, and that of charged π-mesons $\Pi(E_0, E_p)$ the empirical multiplicity of π-meson production averaged throughout the atmosphere $\bar{m}(E_0, E_p)$ is given by Olbert in the simplified expression

$$m(E_0, E_p) = \frac{\partial \Pi}{\partial E_p} \Big/ \frac{\partial J}{\partial E_p},$$

where E_p is the so-called cut-off energy which is well defined by the geomagnetic latitude λ [1].

For the evaluation of $\Pi(E_0, E_p)$ the number of charged π-mesons produced

(*) Now at University of Nebraska, Lincoln, Nebraska.

(1) S. Olbert: *Phys. Rev.*, **96**, 1400 (1954).

downwards throughout the atmosphere with kinetic energy greater than E_0 at the geomagnetic latitude λ, OLBERT made use of his corrected spectrum of μ-meson production under the condition of $E_0 = 260$ MeV. And $J(E_p)$ is taken from the data compiled by G. PUPPI and N. DALLAPORTA (2).

Since his results are derived from the latitude effect of cosmic-rays, the obtained multiplicity covers only the low energy region of primary radiation i. e. less than about 15 GeV. It is obvious, however, that the estimation of multiplicities of meson production in the atmosphere can be extended to higher energies as long as both the energy spectra of primary particles and of the produced π-mesons are known.

Therefore, we have tried to estimate the average multiplicities of meson production in the higher energy region up to 10^3 GeV, making simplified assumptions for the meson production by nuclear collisions to get the energy relations between the spectra of primary and of secondary cosmic-rays.

2. – The energy relation of primary particles and produced π-mesons.

We consider the general casea nucleus-nucleus collision in which one of the nuclei of mass A_1M, has a total energy A_1U_p in the laboratory system and the other of mass A_2M is originally at rest, where M is the mass of the nucleon and U_p is the total energy of the incident particles per nucleon. As we consider such a high energy collision that the binding energy is negligible, the total energy carried by both nuclei before collision in the center of mass system, U^*, is written as

$$U^* = \left\{ Mc^2[2A_1A_2U_p + (A_1^2 + A_2^2)Mc^2] \right\}^{\frac{1}{2}} \tag{2.1}$$

and the velocity of the center of mass of the two nuclei, β_c, is

$$\beta_c = (U_p^2 - M^2c^4)^{\frac{1}{2}} \Big/ \left(U_p + \frac{A_2}{A_1} Mc^2 \right). \tag{2.2}$$

Now let $m(U_p; A_1, A_2)$ and $\eta(U_p; A_1, A_2)$ be the multiplicity and inelasticity respectively for the meson production in the above nuclear interaction, then the total energy of a meson produced in the center of mass system, U_π^*, is by definition

$$U_\pi^* = \frac{\eta(U_p; A_1, A_2)}{m(U_p; A_1, A_2)} U^*. \tag{2.3}$$

(2) *Progress in Cosmic Ray Physics*, **1**, 317 (1952).

It can be assumed that one half of the emitted mesons have the average angle of emission, θ_{π}^{*}, measured from the line o fflight of the incident particle, and the rest are emitted symmetrically backwards, and that the transferable energy for meson production is equally distributed to each π-meson in the center of mass.

Hence, using the above equations, the energy of a π-meson, U_{π}, with respect to the laboratory system is given as a function of the incident energy U_p by

$$U_{\pi}^{\pm} = \frac{\eta(U_p;\, A_1, A_2)}{m(U_p;\, A_1, A_2)} \left[A_1 U_p + A_2 M c^2 \pm A_1 \cos\theta_{\pi}^{*} \sqrt{U_p^2 - M^2 c^4} \right] \quad \theta \leqslant \theta_{\pi}^{*} < \pi/2, \tag{2.4}$$

where $\pm$ indicates the emission of the mesons respectively forward and backward in respect to the direction of the incident particle (see Appendix).

3. - The energy spectra of primary particles and of produced π-mesons.

The production spectrum of π-mesons is directly related to the energy spectrum of the parent N-rays. The actual relationship of these two quantities might be very complicated, but this complexity can be reduced by considering the statistical quantities of averaged multiplicity $\overline{m}$ as follows.

Let $f(U_{\pi})$ be the effective energy spectrum of charged π-mesons at production and $P(U_p)$ be the energy spectrum of N-rays, then the relation of these two quantities is given by

$$f(U_{\pi}) = \tfrac{1}{3}\overline{m}(U_p) \cdot P(U_p)\,. \tag{3.1}$$

The factor $\frac{1}{3}$ in (3.1) arises from the fact that on the average only $\frac{2}{3}$ among the produced mesons are charged and among them only $\frac{1}{2}$ is directed forward. As shown in Appendix II, the contribution of the primary particles which produces π-mesons backwards in the center of mass system is in this case negligible.

N-rays include protons, neutrons, π-mesons, α-particles and heavy nuclei contribute meson production colliding with the air nuclei. The amount of heavy particles in cosmic-rays is very small so that we can neglect its contribution to meson production. On the other hand, the contribution of α-particles to meson production is not to be ignored especially in the topmost layers of the earth's atmosphere where the abundance of α-particles is considerable. We assume here, for simplicity, that the secondary nucleons and π-mesons do not play an important role in the meson production. Then, we may write

$$\overline{m}(U_p) = \varepsilon_p m(U_p;\, 1, A_2) + \varepsilon_{\alpha} m(U_p;\, 4, A_2) \qquad \varepsilon_p + \varepsilon_{\alpha} = 1, \tag{3.2}$$

where ε_p and ε_α are the ratio of protons and α-particles to the total number of N-components of cosmic-rays in the atmosphere, respectively. The maximum value of ε_α may not exceed 10 percent ([3]), then the expression for $\overline{m}(U_p)$ may be written in first approximation,

$$\overline{m}(U_p) = \bar{A}_1 \cdot m(U_p; 1, A_2) , \tag{3.3}$$

where

$$\bar{A}_1 = \varepsilon_p + 4\varepsilon_\alpha .$$

ε_p and ε_α depend not only on the atmospheric depth owing to their different attenuation mean free path in the air, but also on the magnetic latitude, because the magnetic cut-off energy of these particles is not the same. In a similar fashion, the average inelasticity for meson production in a nucleus-nucleus collision can be approximated by

$$\bar{\eta}(U_p) = \bar{A}_1 \cdot \eta(U_p; 1, A_2) . \tag{3.4}$$

Hence, the average total energy of the energy of a π-meson produced by the primary particle of energy U_p, can be written from (2.4)

$$U_\pi = \frac{\bar{\eta}(U_p)}{\overline{m}(U_p)} [\bar{A}_1 U_p + \bar{A}_2 M c^2 + \bar{A}_1 \cos\theta_\pi^* \sqrt{U_p^2 - M^2 c^4}] , \tag{3.5}$$

where U_π is U_π^+ in the expression of (2.4).

The equation (3.5) shows that the average multiplicity in a nucleus-nucleus collision can be obtained from the knowledge of the energy spectrum of primary particles and the production spectrum of π-mesons, provided that the unknown quantity is determined in some other way.

4. – The production spectrum of π-mesons and μ-mesons, and their energy relation.

The effective production spectrum of π-mesons $f(U_\pi)$ in the equation (3.1) is not obtained directly from observation. Therefore, instead of the direct use of $f(U_\pi)$, we introduce a more convenient quantity, the production spectrum of μ-mesons.

The relation between the energy spectrum of π-mesons and that of μ-mesons

([3]) *Progress in Cosmic Ray Physics*, **1** 232 (1952).

at production is given with sufficient accuracy in the high energy region by

$$\mu_s(U_\mu, x) = \frac{B_\pi(x)}{rU_\pi}\,\pi(U_\pi, x)\,, \tag{4.1}$$

where $U_\mu = rU_\pi$ and r is the ratio of the mass of the μ-meson to that of the π-meson and is taken as 0.76 ([4]). (Because of the two body-decay of the π-meson, the energy relation of U_μ and U_π is given definitely, and the above expression is obtained with extreme relativistic approximation).

On the other hand, the energy spectrum of π-mesons is given as a solution of the diffusion equation,

$$\frac{\partial\pi(U_\pi, x)}{\partial x} = \frac{f(U_\pi)}{\Lambda}\exp\left[-\frac{x}{L}\right] - \left(\frac{1}{\lambda_\pi} + \frac{B_\pi}{\beta_\pi U_\pi x}\right)\pi(U_\pi, x)\,, \tag{4.2}$$

where Λ and L are the collision and absorption mean thicknesses of the primary particles respectively, and λ_π is the nuclear absorption mean free path of π-mesons. In what follows, we shall assume that Λ is equal to L, having the constant value of 120 g/cm², and that λ_π is 60 g/cm² in the air. $c\beta_\pi$ is the velocity of π-mesons in the laboratory system and $B_\pi(x)$ is the characteristic energy for the decay of π-mesons at the atmospheric depth x, which is given by

$$B_\pi(x) = \frac{M_\pi c}{\tau_\pi}\cdot\frac{x}{\varrho(x)}\,, \tag{4.3}$$

where M_π and τ_π are the mass and the mean life of π-mesons and $\varrho(x)$ is the air density at the atmospheric depth x g/cm².

The solution of (4.2) was numerically calculated disregarding the multiplicity in meson production and assuming $B_\pi(x)$ to be a constant ([4]). In the actual atmosphere $x/\varrho(x)$ is not necessarily constant and should be carefully examined in particular when one considers the temperature effect at low altitude. Therefore, we have improved this point as shown in Appendix III and obtained the solution in the form

$$\pi(U_\pi, x) = f(U_\pi)\cdot S(U_\pi, x)\,, \tag{4.4}$$

where

$$S(U_\pi, x) = \frac{1}{\Lambda}\int_0^x \left(\frac{Z}{x}\right)^{HT_1/\beta_\pi U_\pi}\exp\left[\left(\frac{1}{\lambda_\pi} - \frac{1}{\Lambda}\right)Z - \frac{x}{\lambda_\pi}\right]\mathrm{d}Z \qquad \text{for } x \leqslant x_1 \tag{4.5}$$

([4]) K. Maeda and M. Wada: *Journ. Sci. Res. Inst.*, **48**, 71 (1954).

and

$$S(U_\pi, x) = \frac{1}{\Lambda}\left\{\int_0^{x_1}\left(\frac{x}{x_1}\right)^{H\alpha x_1/\beta_\pi U_\pi}\left(\frac{Z}{x}\right)^{HT_1/\beta_\pi U_\pi}\cdot\right.$$
$$\cdot\exp\left[\frac{H\alpha x_1}{\beta_\pi U_\pi}-\left(\frac{1}{\lambda_\pi}+\frac{H\alpha}{\beta_\pi U_\pi}\right)x+\left(\frac{1}{\lambda_\pi}-\frac{1}{\Lambda}\right)Z\right]\mathrm{d}Z+ \tag{4.5}$$
$$\left.+\int_{x_1}^{x}\left(\frac{Z}{x}\right)^{H(T_1-\alpha x_1)/\beta_\pi U_\pi}\exp\left[-\left(\frac{1}{\lambda_\pi}+\frac{H\alpha}{\beta_\pi U_\pi}\right)x+\left(\frac{1}{\lambda_\pi}-\frac{H\alpha}{\beta_\pi U_\pi}-\frac{1}{\Lambda}\right)Z\right]\mathrm{d}Z\right\}$$
for $x > x_1$.

Then, the relation (4.1) can be written

$$\mu_s(rU_\pi, x) = f(U_\pi)\,\frac{B_\pi(x)}{rU_\pi}\,S(U_\pi, x)\,. \tag{4.6}$$

In Fig. 1 and Fig. 2, the values of $\pi(U_\pi, x)$ and $\mu_s(rU_\pi, x)$ under the above assumption are shown for the atmospheric depth x, with three different

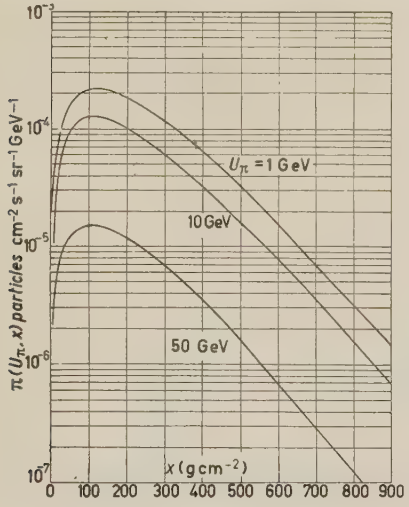

Fig. 1.

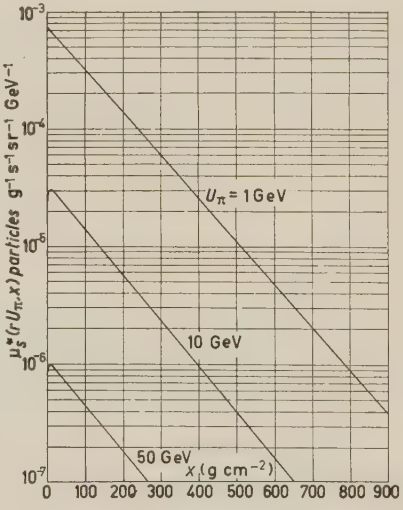

Fig. 2.

values of the energy U_π. In these calculations, we made use of the empirical formula of the energy spectrum of primary particles given by BARRET *et al.* [5] for $P(U)$, which is expressed by the following formula

$$\frac{P(U)}{A} = 7.813\cdot 10^{-4}\left(\frac{3.2}{U+3.2}\right)^{2.25+0.02\ln((U+3.2)/3.2)}\left[1.35+0.04\ln\left(\frac{U+3.2}{3.2}\right)\right], \tag{4.7}$$

where U is measured in GeV.

[5] P. H. BARRET, L. M. BOLLINGER, G. COCCONI, Y. EISENBERG and K. GREISEN: *Rev. Mod. Phys.*, **24**, 133 (1952).

From Fig. 2, one can see that the production spectrum of the μ-mesons is well expressed by the following form in the region of the atmospheric depth larger than 10 g/cm²,

$$\mu_s(rU_\pi, x) = \mu_s(rU_\pi)\cdot\exp(-x/L)\,. \tag{4.8}$$

The attenuation length L, is found to be nearly equal to that of the primary particles, ~ 120 g/cm².

The fact, that the depth where the production of μ-mesons reaches its maximum value is shifted up to around 10 g/cm² whereas that of the π-mesons is in the vicinity of the effective absorption depth of primary particles, can be understood by considering that the production of μ-mesons is proportional not only to the intensity, but also to the decay rate of the π-mesons, and that the latter increases exponentially with the altitude.

Hence, we get the following expression for the production spectrum of μ-mesons with the help of equations (3.1), (4.6) and (4.8),

$$\mu_s(rU_\pi) = \mu_s^*(rU_\pi)\,\frac{\overline{m}(U_p)\cdot P(U_p)}{3P(U_\pi)}\,, \tag{4.9}$$

where $\mu_s^*(rU_\pi)$ is the vertical production spectrum of μ-mesons calculated with the assmption of $f(U) = P(U)$.

5. – Calculation of the average multiplicity.

The above considerations show that the multiplicity of π-meson production can be obtained as a function of the energy U_p, using the equations (2.4), (4.7), (4.9) and the calculated values of $\mu_s^*(rU_\pi)$ provided that $\mu_s(rU_\pi)$ is known.

For this purpose the empirical production spectrum of μ-mesons given by OLBERT expressed in range spectrum ([1]) has been used for numerical calculation of $\mu_s(rU_\pi)$ with the help of an energy-range relation.

In Fig. 3, $\mu_s(rU_\pi)$ and $\mu_s^*(rU_\pi)$ are shown together with the primary energy spectrum given by (4.7).

Letting

$$\xi(U_\pi) = 3P(U_\pi)\,\frac{\mu_s(rU_\pi)}{\mu_s^*(rU_\pi)}\,. \tag{5.1}$$

The average multiplicity of π-mesons, $\overline{m}(U_p)$ becomes

$$\overline{m}(U_p) = \frac{\xi(U_\pi)}{p(U_p)}\,. \tag{5.2}$$

The relation between U_p and U_π is given by the equation (2.4). The actual procedure is rather tedious, namely, first, in order to calculate $\xi(U_\pi)$

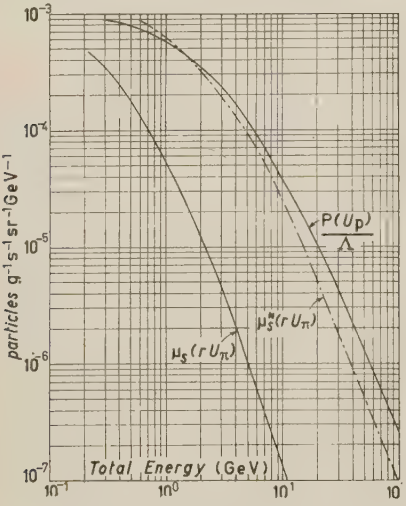

Fig. 3*a*.

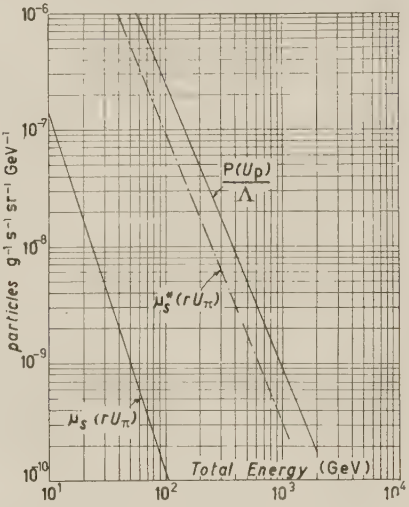

Fig. 3*b*.

for a certain value of U_p, we adopt arbitrary values of U_p being considered eventually as the energy of N-rays which produce forward directed π-mesons of energy U_π.

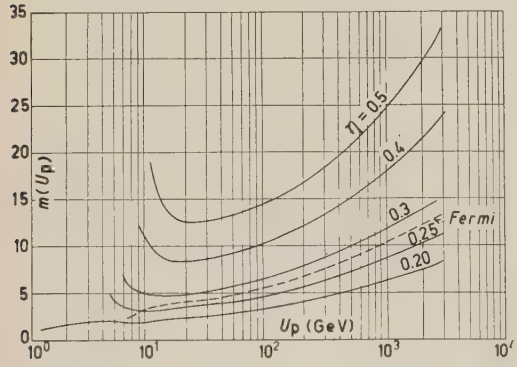

Fig. 4.

With these values of U_p, we get $\overline{m}(U_p)$'s by the equation (5.2). Next, in order to check which of these $\overline{m}(U_p)$'s thus obtained is correct, we put them back into the equation (2.4). If one of the values of U_π coincides with the one formerly assigned, the corresponding U_p, and consequently $\overline{m}(U_p)$, is adopted as the real one.

The second procedure has been carried out actually for several different values of $\eta(U_p)$ under the assumption that η is independent of U_p. The numerical values we used are: $Mc^2 = 0.938$ GeV, $M_\pi c^2 = 0.141$ GeV.

$$\overline{A}_1 = 1.15\,, \qquad \overline{A}_2 = 14.4$$

and

$$\cos\theta_\pi^* = 0.786\,.$$

The results obtained are shown in Fig. 4. For a comparison, the theoretical values computed by Fermi's formula of the multiplicity-energy relation is shown by a dashed line which is expressed by

$$m(U_p) = 1.8(U_p/Mc^2)^{\frac{1}{4}}, \tag{5.3}$$

provided that the ratio of the number of charged mesons to the total is two thirds.

6. – Concluding remarks.

The multiplicity calculated by our model depends on the assumed inelasticity. As one can see from Fig. 4, our evaluated multiplicity increases with decreasing primary energy below around 20 GeV if η is larger than 0.2. This apparent increase of multiplicity at lower energies for large values of inelasticity seems absurd, because in the actual case the emission of π-mesons should be suppressed by the threshold energy of multiple meson production. As it is plausible to assume that the multiplicity is a monotone increasing function of the primary energy, our results indicate either that the inelasticity decreases with the U_p decrease in this low energy region, or that it has a practically constant value less than 0.3.

It is interesting to notice that the recent analysis by VERNOV and GRIGOROV shows that the inelasticity in the energy region below 20 GeV is about $0.2 \sim 0.3$, increasing with the primary energy ([6]).

With respect to the multiplicity in meson production, several theoretical estimations have been given especially for the analysis of high energy events such as jet phenomena in nuclear emulsions and air showers ([7-10]).

However, recent experiments shows that the energy dependence of multiplicity in meson production is favourable to the results given by Fermi's statistical theory and Landau's relativistic-hydrodynamic theory as long as the energy dependence of the multiplicity is concerned.

([6]) S. N. VERNOV and N. L. GRIGOROV: *Suppl. Nuovo Cimento*, **4**, 879 (1956).
([7]) E. FERMI: *Prog. Theor. Phys.*, **5**, 570 (1950).
([8]) W. HEISENBERG: *Zeits. f. Phys.*, **126**, 569 (1949).
([9]) H. W. LEWIS, J. R. OPPENHEIMER and S. A. WOUTHUYSEN: *Phys. Rev.*, **73**, 127 (1948).
([10]) S. Z. BELEN'KJI and L. D. LANDAU: *Suppl. Nuovo Cimento*, **3**, 15 (1956).

If we express our results in an empirical formula of the type

$$m(U_p) = \alpha(\eta U_p)^{\gamma}\,, \tag{6.1}$$

where α and γ will be determined for a certain value of η by means of a least squares calculation, we get for the case of $\eta = 0.2$, as an example, $\alpha = 1.665$ $\gamma = 0.249$, and the equation (6.1) is written in this case

$$m(U_p) = 1.665 \cdot (0.2 \cdot U_p)^{\frac{1}{4}}\,. \tag{6.2}$$

This is practically consistent with Fermi's formula (5.3). Although, in Fermi's theory, the inelasticity is not explicitly described, it is obvious that the inelasticity is small because among the secondary particles are considered not only π-mesons, but nucleons and anti-nucleons. If one of the secondary nucleons is emitted with large energy, this corresponds to the low inelasticity because this secondary nucleon is undistinguishable with the incident primary nucleon.

On the other hand, Landau's formula for the multiplicity in a nucleon-nucleus collisions is a little different from that of Fermi's nucleon-nucleon collision and is expressed by [10]

$$m(U_p) = KA_2^{0.19}\left(\frac{U_p}{2Mc^2}\right)^{\frac{1}{4}}\,. \tag{6.3}$$

Comparing our results with this formula, we get

$$K = 0.658\,.$$

* * *

We would like to thank to Dr. MARCEL SCHEIN for his kind advice and comment on this subject at the Midwest Cosmic Ray Conference at Iowa City. We are also very grateful to Prof. ROBERT CHASSON in the University of Nebraska and to Dr. JUN NISHIMURA of Tokyo University for their helpful discussions.

Appendix

I. – The relations (2.1), (2.2) and (2.4) are derived as follows.

The Lorentz invariance with respect to both systems of center of mass (C.M. system) and laboratory (L. system) is

$$c^2p^2 - U^2 = c^2p^{*2} - U^{*2}\,. \tag{I-1}$$

The C.M. system is defined so that p^* is zero, and if $c\beta$ be the velocity of the incident particle with respect to the L. system, then its momentum is given by

$$cp = A_1 U_p \cdot \beta \tag{I-2}$$

and this can be also written

$$\beta^2 = 1 - (Mc^2/U_p)^2 \tag{I-3}$$

and

$$U = A_1 U_p + A_2 Mc^2\,. \tag{I-4}$$

Putting above relation into (I-1), the equation (2.1) is obtained.

Since p^* is zero with respect to the C.M. system, the Lorentz transformation of the total energy U^* to the L. system is given by

$$U = U^*/\sqrt{1-\beta_c^2}\,, \tag{I-5}$$

where $c\beta_c$ is the velocity of the center of mass in the L. system. This is written also,

$$\beta_c^2 = 1 - (U^*/U)^2\,. \tag{I-6}$$

Putting (2.1) and (I-4) into (I-6), the equation (2.2) is obtained.

Similarly, the Lorentz transformation of total energy of each π-meson, U_π^*, emitted at an angle θ_π^* with the direction of the incident particle in the C.M. system, to the total energy in the L. system U_π, is written as

$$U_\pi = (U_\pi^* + \beta_c c p_\pi^* \cos\theta_\pi^*)/\sqrt{1-\beta_c^2}\,, \tag{I-7}$$

where $cp_\pi^* = U_\pi^*\beta_\pi^*$ and β_c is given by the equation (2.2). Using (I-5), this can be written further

$$U_\pi = \frac{U}{U^*}\, U_\pi^*[1 + \beta_c\beta_\pi^* \cos\theta_\pi^*]\,. \tag{I-8}$$

Since we are considering the extremely high energetic case of U_p, the relative velocity of the emitted π-mesons with respect to the C.M. system β_π^*, can be

regarded as unity. Then this equation becomes (2.4), where the corresponding terms of β_c and U_π^*/U^* are substituted by (2.2) and (2.3), respectively.

II. – The actual production of π-mesons, $f_a(U_\pi)$, can be expressed by two terms, i.e. the one due to the mesons emitted forwards and the other due to those emitted backwards in the C.M. system of colliding particles.

Let $f^+(U_\pi)$ and $f^-(U_\pi)$ be the production spectra corresponding to these two terms respectively, then we can write

$$f_a(U_\pi) = f^+(U_\pi) + f^-(U_\pi) .$$

As the emission of π-mesons in the C.M. system is regarded to be symmetrical with respect to the direction of the incident particle, we get

$$f^+(U_\pi) = \tfrac{1}{3}\overline{m}(U_p^+)\cdot P(U_p^+)$$

and

$$f^-(U_\pi) = \tfrac{1}{3}\overline{m}(U_p^-)P(U_p^-)\Theta(U_p^-) \qquad \Theta(U_p^-) \leqslant 1,$$

where $U_p^{\pm}$ is the energy of a primary particle which produces π-mesons of energy U_π in the L. system originally emitted forward and backward in the C.M. system respectively $\Theta(U_p^-)$ is a correction factor for angular spread in the case of originally backward emitted mesons.

Then from the equation (2.4), we get the following ratio for the extreme relativistic case,

$$\frac{U_p^+}{U_p^-} \sim \frac{1 - \cos\theta_\pi^*}{1 + \cos\theta_\pi^*} \frac{\eta(U_p^-)}{\eta(U_p^+)} \frac{m(U_p^+)}{m(U_p^-)} .$$

The inelasticity might be almost independent of energy and the multiplicity can be regarded as a slowly increasing function of energy, i.e.

$$\frac{\eta(U_p^-)}{\eta(U_p^+)} \sim 1 , \quad \frac{m(U_p^+)}{m(U_p^-)} < 1 , \qquad (\text{as it is obvious } U_p^+ < U_p^-) .$$

Therefore, we can write

$$\frac{U_p^+}{U_p^-} < \frac{1 - \cos\theta_\pi^*}{1 + \cos\theta_\pi^*} .$$

According to the Fermi's statistical theory of multiple meson production, the angular distribution of π-mesons in the C.M. system is a function of the impact parameter of colliding nucleons and is shown approximately be const. $\cos\theta_\pi^*$. For this case, we get $\theta_\pi^* = \cos^{-1} 0.79$ as the average angle of emission. Put $\theta_\pi^* = \bar{\theta}_\pi^*$ in the above inequality, then we get

$$\frac{U_p^+}{U_p^-} < \frac{0.21}{1.79} \sim 0.12 \ldots$$

This ratio is an overestimation, because the recent analysis of jet showers in nuclear emulsions shows that the seconadry particles are more concentrated within the narrow cone around the axis than shown by the above expression, consenting with Landau's theory which gives very sharp forward angular distribution in C.M. system. Consequently, the mean angle of emission θ^*_{π} should be far smaller than the above estimation. It follows, therefore, that the ratio of U_p^+ to U_p^- might be less than of order 0.1.

Now, the differential energy spectrum of primary ray is approximately shown by

$$P(U_p) \sim U_p^{-2.4} \qquad \text{for } U_p > 20 \text{ GeV}.$$

Then, the ratio of the primary flux which contributes to the backward and forward production of π-mesons of energy U_π is

$$\frac{P(U_p^-)}{P(U_p^+)} \sim \left(\frac{U_p^+}{U_p^-}\right)^{2.4} \lesssim 10^{-2.4}.$$

On the other hand, the ratio $m(U_p^+)/m(U_p^-)$ is not so small compared with the above quantity.

Therefore, the contribution of the parent particles corresponding to the backward produced π-mesons can be neglected as compared with that of producing forward primaries.

III. – The atmospheric depth x (in g/cm²) is equal to the barometric pressure P (in dyne/cm²) divided by the acceleration of earth's gravity, g, i.e.

$$P = x \cdot g$$

and the pressure P is also given by $P = \varrho RT$, where $\varrho = \varrho(x)$ and $T = T(x)$ are the density of air and the temperature at the atmospheric depth x, respectively. Thus we get

$$\frac{x}{\varrho(x)} = \frac{R}{g} T(x). \tag{III-1}$$

Therefore, the characteristic energy for the decay of π-mesons (4.3) is written by

$$B_\pi(x) = \frac{M_\pi}{\tau_\pi} \frac{CR}{g} T(x) \tag{III-2}$$

$$= H \cdot T(x),$$

where $H = 0.521$ GeV deg^{-1} in our case.

In order to get the rigorous solution of the diffusion equation (4.2), we made the following assumption of the vertical temperature distribution in

the atmosphere,

$$\text{(III-3)} \qquad \begin{cases} T(x) = T_1 & \text{for } x < x_1 \\ \quad = T_1 + \alpha(x - x_1) & \text{for } x \geqslant x_1 \end{cases}$$

with the numerical values,

$$T_1 = 217\ ^\circ\text{K}\,, \qquad \alpha = 7/90\ \text{deg/g}\cdot\text{cm}^2\,, \qquad x_1 = 150\ \text{g/cm}^2\,.$$

Putting the conditions (III-3) into the equation (4.2), we get the two different equations for $x \lesseqgtr x_1$, and consequently the two solutions (4.5) and (4.5′).

RIASSUNTO (*)

Si analizzano gli spettri energetici della radiazione cosmica primaria e secondaria per trovare la relazione molteplicità-energia nella produzione di mesoni π nell'atmosfera nell'intervallo energetico da alcuni GeV ad alcune migliaia di GeV con l'ausilio di considerazioni semplificate sulla produzione di mesoni per collisione nucleo-nucleo. Dai risultati, confrontati coi valori assunti per l'inelasticità, si rileva che la relazione molteplicità-energia si accorda con una formula del tipo di quella data da Fermi e Landau a condizione di avere debole inelasticità, praticamente costante.

(*) *Traduzione a cura della Redazione.*

IL NUOVO CIMENTO Vol. VII, N. 1 1° Gennaio 1958

Shrinkage of Nuclear Research Emulsions.

W. M. Gibson and J. G. McEwen

Physics Department, Queen's University
Belfast, North Ireland

(ricevuto il 31 Agosto 1957)

Summary. — A method is described for obtaining accurate values for the shrinkage factor of nuclear research emulsions, and for testing the uniformity of the shrinkage with depth. The results obtained from one plate show a shrinkage factor near the surface 6% greater than near the glass. The importance of avoiding such variations, when accurate depth measurements are required, is stressed.

Nuclear research emulsions contain a large proportion of silver bromide, removal of which in processing reduces their thickness by a factor of 2 or more. If accurate measurements in three dimensions are to be made on events recorded in the emulsion, this factor must be known. Several methods of measuring it have been used, the most accurate being that described by Duke, Lock, March and Munir [1]: they used a mechanical gauge to measure the difference between the unprocessed and processed thicknesses, while the thickness of the processed emulsion was measured with a calibrated microscope.

The present work was undertaken partly to check the accuracy of measurements made by the method of Duke *et al.*, and partly to study the uniformity of shrinkage throughout the depth of the emulsion.

A beam of 925 MeV protons from the Birmingham synchrotron was ar-

[1] P. J. Duke, W. O. Lock, P. V. March and B. A. Munir: *Journ. Sci. Instr.*, **32**, 365 (1955).

ranged to pass through emulsions, nominally 400 μm thick, held on a frame which could be rotated about an axis at right angles to the beam. The plates were set at approximately 45° from the beam direction for one pulse from the synchrotron, and then turned through exactly 90° for a second pulse. The average angle of dip of the two beams was thus 45°, within about 0.1°, even if the plates were exposed in their original wrappings and with 1° uncertainty in their orientation.

The results from three sets of plates are described here: plates A were kept in the manufacturer's wrapping until a short time before exposure; B were unwrapped and kept in an atmosphere at (58 ± 5)% relative humidity for 10 days before exposure; C were kept in this atmosphere for 7 days, then sealed with a sheet of thin lacquered copper, and left for a further 7 days before exposure.

The plates were processed in the usual manner ([2]), and were examined on a microscope whose fine-focus scale had been shown to be reliable by an interference method ([3]).

The examination was carried out in a room with controlled relative humidity (58 ± 5)%, after the plates had been kept there for some days to reach equilibrium. The vertical setting was noted at horizontal intervals of 50 μm along about 50 tracks of each of the two beams, starting 10 μm from the end nearest to the glass.

Since the beam was not perfectly parallel, and the emulsions were originally about 420 μm thick, some tracks gave 7 intervals and some 8: in the latter case the middle two intervals were grouped together. The average of the angles of dip of the two beams in the processed emulsion was obtained for each interval, and the shrinkage factor calculated. Other values were obtained by measurements over the whole length of each track, and by the gauge method of DUKE *et al.* The results are shown in Table I, for three sets of plates exposed, processed and examined at different times. The statistical uncertainty in the figures from the gauge method is 0.02, and in each of the other figures 0.01.

It will be seen that there is very satisfactory agreement between the means of the measurements throughout the depth, the independent measurements over the whole length, and the gauge measurement where this was made. But there is strong evidence of a systematic variation of shrinkage factor throughout the depth of plate A. In plate B there is a low value for the layer next to the glass, but this might possibly result from a systematic error in the method of using the microscope, and would need to be confirmed. In plate C, slightly lower values are found for the layers closer to the centre of the emulsion.

([2]) A. D. DAINTON, A. R. GATTIKER and W. O. LOCK: *Phil. Mag.*, **42**, 396 (1951).
([3]) J. B. ENGLAND: *Journ. Sci. Instr.*, **34**, 208 (1957).

The variations observed could in principle be due to any of three causes:

a) a non-uniform response of the gelatine to the changes involved in processing, or

b) a change in atmospheric humidity some time before exposure, or

c) a change in atmospheric humidity some time before observation.

TABLE I.

Part of tracks used	Mean depth of interval (microns above glass)	Shrinkage factor		
		Plate A	Plate B	Plate C
First 50 μm (near glass) .	35	2.38	2.25	2.34
Second 50 μm	85	2.44	2.31	2.35
Third 50 μm	135	2.44	2.29	2.30
Middle 50 μm or 100 μm .	200	2.48	2.31	2.30
Second from last 50 μm .	265	2.46	2.32	2.33
Next to last 50 μm . . .	315	2.51	2.32	2.36
Last 50 μm (near surface)	365	2.53	2.33	2.35
Whole length	208	2.46	2.31	2.34
Emulsion measurements by gauge and microscope		—	2.33	2.33

The procedure used prevented *b*) and *c*) from playing any significant part: *b*) might have contributed slightly in plate A, but the whole effect would have required a very large and sudden change in atmospheric humidity ([4]). But in this connection it should be pointed out that the characteristic time for the diffusion of water into or out of a 400 μm thick emulsion is 64 hours; this represents the time which must elapse after a change in surface conditions before the change in mean density of an emulsion reaches 93% of its final value, or before the change in density at the bottom reaches 89% of its final value (see the analogous theory for conduction of heat, developed for example by CARSLAW and JAEGER ([5])). It was obtained by measurements in conditions where water vapour was removed rapidly from the surface, and a longer effective time constant would be observed in a stagnant atmosphere. Careful planning is therefore needed before any exposure in which uniformity of the shrinkage with depth is required. In some conditions it may be easier to sacrifice some of the advantages of thick emulsion for the sake of the smaller time constant of a thinner layer ($\propto t^2$ where t = thickness).

([4]) A. J. OLIVER: *Rev. Sci. Instr.*, **25**, 326 (1954).

([5]) H. S. CARSLAW and J. C. JAEGER: *Conduction of Heat in Solids* (Oxford, 1947).

Once an emulsion has reached equilibrium, however, the slow rate of diffusion of water vapour through the surrounding air thereafter helps to keep the distribution of water within the emulsion uniform. In experiments analogous to those described above, but with deliberate extreme alteration of the humidity 12-24 hours before exposure, no systematic non-uniformity was found. Little would be expected unless conditions allowed unusually rapid transport of water vapour.

If *a*) is responsible for the observed effect, it would represent a type of distortion not previously observed, but by no means unlikely. It could perhaps be reduced by the same precautions as are used to minimize distortion in the horizontal plane.

The large effect observed in plates A, and in some others not described here, might, however, be due to slight solubility of one of the components of the gelatine; this could lead to a reduction of the thickness of the upper layer of the processed emulsion, and a greater shrinkage factor for these layers. This could be prevented, or compensated, only by specially designed procedures.

It may be concluded, therefore, that if depth measurements are required to be accurate to better than $\pm 3\%$, not only the actual shrinkage factor but also the uniformity of shrinkage should be checked: care should be taken to ensure that no diffusion of moisture is taking place at the time of the exposure, and a plate from the same batch should be exposed in some apparatus similar to that described here and processed with the plates under test. If this shows that the shrinkage is not sufficiently uniform the processing procedure should be modified.

* * *

The authors wish to thank Dr. W. O. LOCK and Mr. P. J. DUKE for arranging the exposures, and Mrs. S. E. BAKER and Mrs. D. E. ANDERSON for examining the plates.

RIASSUNTO (*)

Si descrive un metodo per ottenere accurati valori del fattore di contrazione delle emulsioni per ricerche nucleari e per saggiare l'uniformità della contrazione con la profondità. I risultati ottenuti con una lastra rivelano un fattore di contrazione del 6% maggiore presso la superficie che non vicino al vetro. Si mette in rilievo l'importanza di evitare tali variazioni quando sono richieste precise misure in profondità.

(*) *Traduzione a cura della Redazione.*

Relativistic Increase of Energy Loss by Ionization in Gases (*).

R. G. Kepler (+), C. A. d'Andlau (×), W. B. Fretter and L. F. Hansen
University of California - Berkeley

(ricevuto il 7 Settembre 1957)

Summary. — Measurements of ionization loss by relativistic charged particles have been made in helium, argon and xenon. The experimental results agree well with theory in the case of helium. In argon, and particularly in xenon, the relativistic rise in ionization found experimentally is less than that predicted theoretically. The measurements were made by the method of counting drops in a cloud chamber.

1. – Introduction.

The theory of energy loss by ionization was first developed by Bohr (1) in 1913. In the early 1930's Bethe (2) and Bloch (3), improved the treatment by using quantum mechanical methods. The theory they developed indicated that the energy loss per unit path length would decrease as $1/\beta^2$ where $\beta = v/c$, v is the velocity of the particle and c is the velocity of light, until $\beta = .97$. At this velocity the energy loss per unit path length would begin increasing as $\log \beta\gamma$, where $\gamma = 1/(1-\beta^2)^{\frac{1}{2}}$, and would increase indefinitely as the velocity increased. The increase is caused by the relativistic lateral extension of the electric field of the moving particle. The lateral extension

(*) Supported in part by the joint program of the U.S. Office of Naval Research and the U.S. Atomic Energy Commission.

(+) Now at E. I. duPont de Nemours and Company, Wilmington, Delaware.

(×) On leave of absence from the Laboratoire de Physique, Ecole Polytechnique, Paris.

(1) N. Bohr: *Phil. Mag.*, **25**, 10 (1913); **30**, 581 (1915).

(2) H. A. Bethe: *Zeits. f. Phys.*, **76**, 293 (1932); *Handb. der Phys.*, **24**, 515 (1933).

(3) F. Bloch: *Ann. der Phys.*, **16**, 285 (1933); *Zeits. f. Phys.*, **81**, 363 (1933).

of the field allows the particle to excite or ionize a larger number of atoms as it passes through the medium.

In 1938, SWANN ([4]), suggested that the presence of the medium through which the particle was passing would limit the relativistic extension of the electric field because of the polarizability of the atoms in the medium. In 1940 FERMI ([5]) calculated this polarization effect or density effect, as it is more commonly called, for the special case of a medium composed of dispersion oscillators of a single frequency. The conclusions of this theory indicated that the energy loss per unit path length should increase to some maximum value which depended on the density of the medium.

Fermi's theory has been extended by several authors ([5-9]) to multifrequency models of a dispersive medium, but the general conclusions as given above have not been altered. The disagreement between the theories now depends on detailed differences in the calculations, differences between dispersion models assumed and differences in the interpretation of the role played by Čerenkov radiation.

Accurate experimental results on the relativistic rise in ionization have been obtained by GHOSH, JONES and WILSON ([10]), who used μ-mesons in a cloud chamber, and a high resolution magnetic spectrometer. Their measurements extended over a momentum range from 500 MeV/c to about 30 GeV/c and showed a relativistic rise which agreed with theory and also showed the existence of the density effect, but did not reach the plateau. PRICE ([11]) has summarized other work on this problem.

Recently an experiment was performed by BARBER ([12]) in which he used intense beams of electrons having energies from 2 to 35 MeV and measured their energy loss by ionization in an ionization chamber. He measured the energy loss in hydrogen and helium at two pressures, one and ten atmospheres. The experimental points on the plateau, which were observable in both gases at ten atmospheres, were a little below the value predicted by STERNHEIMER but were not outside the experimental error.

([4]) W. F. C. SWANN: *Journ. Franklin Inst.*, **226**, 598 (1938).

([5]) E. FERMI: *Phys. Rev.*, **56**, 1242 (1939); **57**, 485 (1940).

([6]) O. HALPERN and H. HALL: *Phys. Rev.*, **57**, 459 (1940); **73**, 477 (1948).

([7]) G. C. WICK: *Ric. Scient.*, **11**, 273 (1940); **12**, 858 (1941); *Nuovo Cimento*, **1**, 302 (1943).

([8]) M. SCHÖNBERG: *Bull. Cent. Phys. Nucl. Bruxelles*, No. 20 (1950); *Nuovo Cimento*, **9**, 210, 372 (1952).

([9]) R. M. STERNHEIMER: *Phys. Rev.*, **88**, 851 (1952); **89**, 1148 (1953); **91**, 256 (1953); **93**, 1434 (1954); **93**, 351 (1954); **103**, 511 (1956).

([10]) S. K. GHOSH, G. M. D. B. JONES and J. G. WILSON: *Proc. Phys. Soc.*, A **65**, 68 (1952); **67**, 331 (1954).

([11]) B. T. PRICE: *Report on Prog. in Phys.*, **18**, 52 (1955).

([12]) W. C. BARBER: *Phys. Rev.*, **103**, 1281 (1956).

The possibility that the relativistic increase in ionization could be used in the measurement of the velocity of very high energy particles has led us to measure this rise in various gases.

We used a cloud chamber placed in a magnetic field so that the momentum of the particles could be determined by measuring the curvature of the track. The ionization was determined by stereoscopically counting drops along the track. In order to obtain measurements of ionization over the range from $\beta\gamma=3$ (minimum ionization) to $\beta\gamma=1000$ both μ-mesons and electrons were used. The measurements were carried out in helium at about 1.3 atm., in argon at about 0.2 atm., in argon plus helium each at about 0.2 atm., and in xenon plus helium each at about 0.1 atm. In each case there was in the cloud chamber, in addition to the inert gas, alcohol and water vapor at a partial pressure of about 5 cm Hg.

2. – Experimental procedure.

The magnet and cloud chamber used for the helium experiment have been described previously ([13]). In order to measure the ionization in argon and xenon it was necessary to construct a new cloud chamber to operate at pressures below atmospheric pressure. This chamber is slightly larger than the previous one but is very similar in construction and operating characteristics and fits into the same magnet.

3. – Photography.

During the helium experiment the camera was operated at $f/16$ and power for the flash tubes was supplied by about 300 μF charged to 2000 V. A delay of 140 ms between the expansion of the cloud chamber and the flashing of the lights was used to allow time for the drops to grow to a size large enough for photography. A 6 ms delay was added electronically to the unavoidable mechanical delay of 12 ms between detection of an event and complete expansion of the cloud chamber. This delay allowed the ions to diffuse sufficiently so that the drops which later formed on them could be counted readily.

During the argon experiment the camera aperture was opened to $f/11$ and the power for the flash tubes was increased by doubling the number of condensers connected to each lamp. In addition the delay was increased to 250 ms. These changes were made because the drops grew much more slowly in the argon atmosphere. The rate of drop growth is limited mainly by two things;

([13]) W. B. Fretter and E. W. Friesen: *Rev. Sci. Instr.*, **26**, 703 (1955).

by diffusion, because as the drop grows it depletes the vapor in the immediate vicinity and can grow only as rapidly as vapor diffuses to it, and by thermal conductivity, because as the vapor condenses heat is liberated, and the faster this heat can get away the faster the drop will grow.

In the argon experiment it was readily seen that diffusion was not causing the difficulty because the ions were diffusing about the same distance as they had in helium, because of the lower pressure of argon (0.2 atm.). Therefore, we assumed that the drop growth was being limited by thermal conductivity, and verified this by adding helium to the gas mixture which caused the drops to grow much more rapidly. The thermal conductivity of helium is about nine times as large as the thermal conductivity of argon.

In the argon-helium experiment (0.2 atm each), when the cloud chamber was filled with equal pressures of helium and argon, the camera aperture was $f/16$, and the flash lamp delay was 140 ms.

With the xenon and helium mixture (0.1 atm. each) the camera was set at $f/16$ and the light delay at 240 ms. It was desirable to use $f/16$ because the photographic depth of field was then sufficient to give good drop images to within about one centimeter of both the front glass and the back plate. With the aperture set at $f/11$ the depth of field is about 2/3 the total depth of the cloud chamber. Therefore, during the pure argon experiment each lens of the camera was focused on a slightly different plane in the chamber, and good drop images were obtained on either one view or the other over the full depth of the chamber.

4. – Operating procedure.

Since we desired to obtain the relative value of energy loss by ionization over the velocity range which covers from minimum ionization to the plateau value, we decided to use both μ-mesons and electrons. The μ-mesons cover the range from minimum ionization ($\beta\gamma=3$) to $\beta\gamma=80$. The electrons cover the range from $\beta\gamma=50$ to $\beta\gamma=1000$.

In order to compare the electron and μ-meson data it was necessary to take both types of pictures under exactly the same experimental conditions. To accomplish this the pictures were taken alternately, two μ-meson pictures and then one electron picture and this cycle was repeated automatically.

In a cloud chamber the condensation efficiency depends on the expansion ratio, the temperature, and possibly on the time after last expansion. Therefore, great effort was made to keep these factors unchanged from expansion to expansion during each experiment. The expansion ratio controller was not touched during each run and the magnet temperature, although automatically controlled, was checked frequently and found not to vary more than

0.2 °C, except at the beginning of the xenon experiment where it was 0.5° lower than the average temperature. A 23 minute dead time was used between pictures to smooth out the variation in the time between expansions due to fluctuations in the coincidence rate.

The argon and helium used was commercial grade, about 99.7% pure. The xenon that was used was considerably purer. The vapor was obtained from a mixture of ethyl alcohol and water placed in a cellulose sponge pad in the bottom of the chamber. In the helium experiment a mixture of 2:1 by volume ethyl alcohol to water was used, and in the argon and xenon experiments a mixture of 3:2 was used.

In order to eliminate the air from the cloud chamber prior to filling it for the helium experiment, the chamber was flushed ten times to a pressure of 1.5 atmospheres with helium. For the xenon and argon experiments the chamber was evacuated with a vacuum pump.

5. – Data analysis.

The momenta of the μ-mesons were measured by methods previously described ([13]), simplified where possible. For the low energy electrons the only difference in the momentum determination procedure was that instead of using comparator measurements to determine the curvature, the photographs were projected to full size and the track curvature was compared to arcs of circles of known radius.

We estimate that the above procedure for determining momentum was accurate to about 5% and since an error of 10% in the momentum corresponds to an error of only 1% in ionization, we considered this sufficiently accurate.

6. – Ionization measurement.

The ionization was measured by counting drops along the track with a stereoscopic microscope which magnified the images 40 times. The drops were counted between two easily recognized spots along the track (e.g., where the track crossed fiducial lines) and then later, during the projection of the event, the distance between these points was measured.

The drops were counted by pressing a switch connected to a counter for every drop seen. When a large cluster of drops was seen, the number of drops in the cluster or blob was estimated, and if it exceeded 40, none of the drops were included in the data; but the fact that a blob had been seen was noted. It was assumed that all of the ion pairs in one of these clusters were secondary ions produced by a single collision between the primary particle and

one of the electrons in the gas. Therefore, the forty drops were a measure of the maximum energy transfer in a single collision that was considered in the experiment. This maximum energy transfer is calculated below.

In order to be able to determine the variation of the consideration efficiency from the top to the bottom of the cloud chamber, the μ-meson tracks were divided into two sections for drop counting. The top half and the bottom half of the track were counted separately. It had been shown previously that the variation in the condensation efficiency was approximately linear, at least nearly enough for the purposes of this experiment ([13]); therefore, two points were enough to determine the curve. We corrected for this variation in the case of the electrons which were not centered in the cloud chamber.

Since the error in ionization was directly dependent on the error in the measurement of the length of the track counted, considerable care was taken to keep errors in this measurement at a minimum. For the mesons, which were full length tracks almost parallel to the back plate (the counter telescope limited the angle with respect to the plane of the back plate), the length was measured on the full scale reprojection of the event with a ruler. The radius of curvature of the lowest momentum μ-meson was large enough so that the track length differed from the chord length by less than one per cent. The length measured was then corrected for magnification, and a certain length was subtracted for each blob detected.

Since the electron tracks were so curved that the length of the chord was not a sufficiently accurate measurement of the length of the arc, and since the radius of curvature changed enough along the track (due to the inhomogeneous magnetic field) so that a correction could not be applied to the length of the chord, a calibrated wheel that is used in measuring distances on maps was rolled along the reprojected image of the track to measure their length. In addition to the corrections applied to the μ-meson track lengths, the electron track lengths had to be corrected for angle with respect to the back plate.

The number of drops per centimeter was then determined by dividing the total number of drops counted by the correct length of track. This number is a measure of the average amount of energy lost per centimeter by ionization in energy transfers less than a certain maximum.

7. – Systematic errors and corrections applied.

In order to eliminate as many systematic errors as possible, the following procedure was used in analyzing the data:

1) The particles were divided into three or four groups, depending on the experiment. Each group had an equal number of each kind of particle and an equal number of particles for each momentum range.

2) Each of the three or four groups was analyzed by a different individual.

3) Electrons and μ-mesons were intermixed during the drop counting, and the pictures were counted in a random order.

It was expected that there might be systematic differences in the absolute value of the drop counts between individuals, but this turned out not to be the case. In each experiment the average values of the minimum ionization determined for each of the groups were within one standard error of the overall average. Therefore, all of the grups were mixed together.

In each experiment it was found that the minimum level changed gradually during the course of the experiment. In the helium and xenon experiments it slowly decreased and in the argon experiments it decreased. The reason for these changes is not definitely known, but all effects that have been thought of that could produce such a result (i.e., a leak or a slow systematic change in the condensation efficiency) would have negligible or no effect on the relative ionization. It was assumed that the variations were a linear function of the event number and a least squares line was fitted to the variation. The original data were then corrected on the basis of the least squares line.

The time between expansions fluctuated from the 23 minutes dead time to over 60 minutes for some electron events. The data were examined to see if the different waiting times introduced any systematic difference in condensation efficiency between the electron showers and the μ-meson events. The minimum level determined from μ-mesons was plotted as a function of time after last expansion and no systematic variations were observed.

Another possible source of systematic error is the drop overlap correction. As the density of ions produced increases in general, the number of drops counted increases but not quite as fast. Previous work done in this laboratory shows that in the present experiments this effect is negligible. The tracks used for these experiments were 1.5 times as wide as those used in reference ([13]) which means that the density of drops was down by over a factor of two for the same number of drops per centimeter. Therefore, in the argon experiment where the drops were most dense (34 drops/cm) the correction as obtained from the previous work is of the order of 0.1 per cent.

The statistical fluctuations that were found to exist in the determination of the ionization of a 40 cm track at minimum ionization were calculated. In the helium experiment the standard deviation of a single measurement was found to be 8%, in the argon experiments it was 13%, and in the xenon-helium experiment it was 11%. The total number of drops in a 40 cm minimum ionizing track was, in each of the respective experiments, 788, 924 and 640. By comparing the standard deviation calculated from all electrons together to that calculated by taking the average standard deviation calculated from

the single pictures which contained several electrons, it was found that a large part of error was due to fluctuations in the minimum level from picture to picture. The standard deviation calculated from all electrons was about twice that obtained on the single picture basis for each of the experiments.

When the μ-meson data were compared with theory, care had to be taken in the high momentum region. In this region the momentum errors are large, and the number of mesons per momentum interval decreases rapidly as the momentum increases. Therefore, errors in measurement would throw low momentum mesons into high momentum groups and thus cause a systematic error.

The procedure used in this experiment to estimate this error was to calculate the curve of ionization versus momentum that would be expected, taking into account the differential spectrum of the mesons, the statistical error in a given momentum measurement, and the theoretical curve of ionization versus momentum. This was done as follows.

Let p_0 be the experimentally determined momentum for a particular μ-meson. In a cloud chamber momentum determination the error in the reciprocal of the momentum is a constant for all momenta and the error is gaussian. Therefore, in order to make the calculations easier, the inverse of the momentum is used. The relative probability that a particle actually has the momentum p when the experimentally determined momentum is p_0 can be written as

$$\exp\left[-k\left\{\frac{1}{p}-\left(\frac{1}{p_0}+\frac{1}{p'}\right)\right\}^2\right],$$

where $1/p'$ represents a systematic error in the momentum determination and k is a constant which determines the width of the guassian distribution in the error.

The quantities k and $1/p'$ are measured by periodically turning off the magnetic field and photographing a high energy μ-meson. The curvature of the tracks obtained is measured in the comparator in the same way that the curvature of a normal track is measured; and since the particle went straight through the chamber, any curvature detected is due to turbulence in the chamber and measurement errors. In our cloud chamber the maximum detectable momentum which is defined as that momentum which gives a curvature equal to the probable spurious curvature arising out of the turbulence and measurement errors, was 33 GeV for the argon experiment, 40 GeV for the argon experiment and 30 GeV for the xenon experiment. There was no significant systematic error in the momentum measurements of the helium experiment, but in the argon experiment p' was 55 GeV and in the xenon experiment p' was 21 GeV. The systematic error means that on the average a straight track would be measured to have the momentum p'.

In order to calculate the ionization that would be expected on the average for a μ-meson with an experimentally determined momentum of p_0, one has to sum over all possible momenta p, multiplying the probability that a meson with a measured momentum p_0 actually has momentum p times the relative number of that momentum and finally times the ionization produced by a particle with momentum p. The expression written in terms of the inverse momentum is:

$$\bar{I} = \frac{\int_{-\infty}^{\infty} I\,(1/p)\, n\,(1/p)\, \exp\left[-k\,\{1/p - (1/p_0 + 1/p')\}^2\right] \mathrm{d}(1/p)}{\int_{-\infty}^{\infty} n\,(1/p)\, \exp\left[-k\,\{1/p - (1/p_0 + 1/p')\}^2\right] \mathrm{d}(1/p)},$$

where the denominator is a normalizing factor and $n(p) = n(1/p)\left[(\mathrm{d}(1/p))/\mathrm{d}p\right]$ is the differential momentum spectrum of the μ-mesons incident on the cloud chamber. In the integral, negative momentum means that the charge of the particle with this momentum is opposite to the charge of a particle which has positive momentum of the same absolute value.

This expression was integrated numerically for each experiment using the experimental $n(p)$ as given by CARO et al [14]. In general it was found that the theoretical and experimental curves began to differ at about 8 GeV/c; therefore, no μ-mesons with momentum greater than this were included in the results.

8. – Comparison of results with theory.

The results of the present experiment have been compared with two theoretical expressions for the energy loss by ionization (see Fig. 1-4), one derived by STERNHEIMER (1952) and one by BUDINI [15].

The formula obtained by STERNHEIMER for the total energy loss in collisions with energy transfer less than a certain amount η is:

$$\left(\frac{\mathrm{d}E}{\mathrm{d}x}\right)_{<\eta} = \frac{2\pi N e^4}{mv^2}\left[\ln\frac{2mv^2\eta}{I^2(1-\beta^2)} - \beta^2 - \delta\right],$$

where N is the number of electrons per cm^3, m is the mass of an electron.

[14] D. E. CARO, J. K. PARRY and H. D. RATHGEBER: *Nature, Lond.*, **165**, 689 (1950).

[15] P. BUDINI: *Nuovo Cimento*, **10**, 236 (1953).

e is the electronic charge, and v is the velocity of the ionizing particle. I is an experimentally determined quantity called the average ionization potential and δ, which is the density effect correction, is given by STERNHEIMER in terms of the plasma frequency of the medium, the oscillator strengths and transition frequencies of the energy levels of the atoms in the gas. STERNHEIMER adjusts the observed optical frequencies and ionization potentials to give the experimentally observed value of the average ionization potential for a given material. Since these values are uncertain we used two different sets to compare with our data.

In order to compare the predictions of Sternheimer's theory with our results, a correction has to be made for the energy loss in the form of Čerenkov radiation which escapes to distances greater than the distance b from the track of the ionizing particle; b is chosen so that energy absorbed inside that distance would be counted experimentally.

Sternheimer's correction for energy loss in the form of Čerenkov radiation for the helium experiment lowers the plateau value less than one per cent for the mixture used in the cloud chamber; whereas for pure helium the plateau value would be lowered by $3\frac{1}{2}$ or 4 per cent. This happens because there are lower energy transitions possible for the outer electrons in the vapor atoms than in helium, and these outer electrons are the only ones which produce Čerenkov radiation which is not absorbed. (The absorption coefficient for the substance is small for frequencies below the frequency of the first transition but becomes large for frequencies above that.) Therefore, since there are relatively few weakly-bound electrons, little energy is lost in the form of Čerenkov radiation. In each of the mixtures used in the present experiment, the Čerenkov correction was neglected when drawing the curves in the figures.

The expression derived by BUDINI for the behavior of the energy loss by ionization beyond minimum energy loss is as follows:

$$\left(\frac{\mathrm{d}E}{\mathrm{d}x}\right)_{<\eta} = \frac{2\pi N e^4}{mv^2}\left[\ln \frac{mv^2\eta}{I^2[F(\beta)]^{\frac{1}{2}}} - \beta^2\right].$$

For the function $F(\beta)$ two possible cases were considered by BUDINI:

1) The absorption bands for ionization may be considered to be extremely broadened lines so that $\omega_i/g_i \approx 1$. ω_i is the frequency of the ith absorption and g_i is the half-width of the line. In this case $F(\beta)$ may be written in the form

$$[F(\beta)]^{\frac{1}{2}} = 1 - \beta^2 + \beta^2 \frac{\hbar^2\alpha}{I^2}(\tilde{\Delta}_{\mathrm{I}})^{\frac{1}{2}},$$

where $(\tilde{\Delta}_{\mathrm{I}})^{\frac{1}{2}} \approx 1$ and $\alpha = (4\pi N e^2/m)$.

2) The absorption bands are equivalent to moderately broadened absorption lines so that $(\omega_i/g_i)^2 \gg 1$. In this case

$$[F(\beta)]^{\frac{1}{2}} = \left[(1-\beta^2)^2 + \beta^4 \frac{\hbar^4\alpha^2}{I^4}\tilde{\Delta}_{II}\right]^{\frac{1}{2}},$$

where $\tilde{\Delta}_{II} \gtrsim 1$.

The main difference between case 1 and 2 is the manner in which the energy loss by ionization approaches saturation when $(1-\beta^2)$ becomes smaller than $\beta^2(\hbar^2\alpha/I^2)(\tilde{\Delta}_{II})^{\frac{1}{2}}$. In case 1 the approach to saturation is more gradual than in case 2.

The above expressions have been used to calculate the theoretical curves for the present experiment. Two sets of values for the ν_i' as given by STERNHEIMER (9) (1952,1956) have been used to calculate the average ionization potential for the mixtures and also to calculate the density effect corrections used by STERNHEIMER.

The maximum energy, η, was determined by a method of successive approximations using Sternheimer's theory. A value for η was assumed and used to calculate the amout of energy loss per centimeter at minimum ionization. Then, knowing the number of drops prduced per centimeter at minimum ionization, the amount of energy loss per drop was calculated. This number was multiplied by the number of drops in a blob (40) minus the average number of drops that would be in the blob due to collisions other than the high energy one. This gave a new estimate of η which was used for a new estimate of the energy loss per drop. This procedure was repeated until agreement was obtained between the assumed and the calculated one.

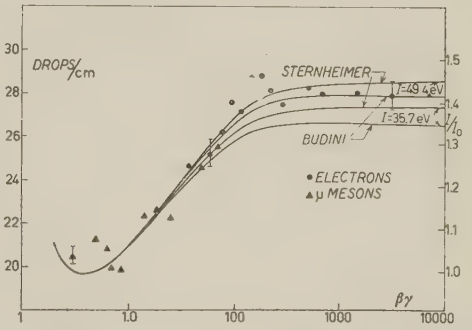

Fig. 1. – Ionization loss in helium. The theoretical curves are normalized to the μ-mesons with $\beta\gamma < 30$, and are calculated for different values of the average ionization potential for the mixture of gases in the cloud chamber. Standard deviations are indicated for a few of the experimental points.

The vapor pressure of the liquid used in the cloud chamber was calculated from tables in the International Critical Tables. The values of the various numbers used for the different experiments are in Table I.

Fig. 1 shows the results of the helium experiment. Each point on the graph represents an average of ten tracks. The two lower curves were calculated from the theories of Budini and Sternheimer using the ionization potentials as listed by STERNHEIMER in 1952. The upper curves are for the same theories using the higher ionization potentials recommended by STERNHEIMER

TABLE I. – *Cloud chamber operating conditions.*

Experiment	(eV) maximum energy transfer	I (eV) average ionization potential for the gas mixture	Noble gas pressure (cm Hg)	Operating temperature (°C)
Helium { Upper curves	740	49.4	91	24.0
Helium { Lower curves	740	35.7		
Argon	710	146	17.5	23.5
Argon + Helium	700	129.5	Argon 16.1 Helium 16.7	21.9
Xenon + Helium	960	277	Xenon 5.8 Helium 6.8	22.9

in 1956. Budini's approximation I for $\sqrt{F(\beta)}$ was used. The theoretical curves were normalized to the μ-mesons with $\beta\gamma < 30$. It is seen that the agreement between theory and experiment is excellent when the higher ionization potentials are used.

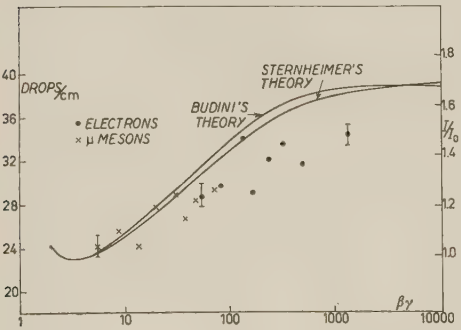

Fig. 2. – Ionization loss in argon.

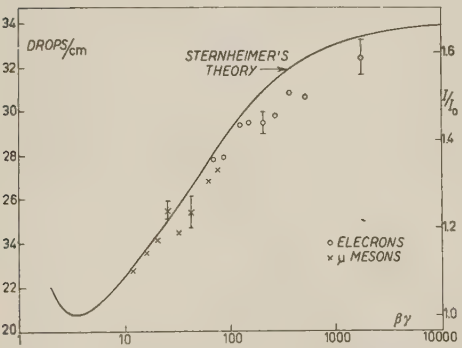

Fig. 3. – Ionization loss in argon-helium mixture.

Fig. 2 shows the results of the argon experiment. The two shown curves were calculated using the old ionization potentials and were normalized to the μ-mesons with $\beta\gamma < 30$. When the new (higher) ionization potentials are used, the curves are raised so that at $\beta\gamma = 10000$, the theoretical ionization is changed form 1.69 to about 1.72. Each point on the graph is again the average ionization of ten tracks. It is seen that there is an indication that the results disagree with theory, but the experimental errors are quite large because of the poor quality of the pictures obtained with argon without helium.

The argon plus helium results shown in Fig. 3 have lower experimental errors because of the better quality of the pictures. Normalizat-

ion to the μ-mesons with $\beta\gamma$ below 30 has the effect of causing almost all of the other experimental points to fall below the curve. If the theoretical curve is lowered by one standard deviation of an individual point the points above $\beta\gamma = 30$ fit quite well, but all four points below $\beta\gamma = 30$ are above the curve. The best fit, as with pure argon, and with xenon plus helium, is to a curve with a slope smaller than that predicted by the theory.

The xenon experiment results are shown in Fig. 4. On this graph each point represents the average of 20 tracks. Again the curves plotted are those calculated using the ionization potentials and normalized to the μ-mesons with $\beta\gamma < 30$.

In the comparison between theory and experiment so far, the theoretical expressions for energy loss have been used only to determine the relative variation of ionization with velocity, and no consideration has been given to the absolute energy loss. In order to estimate the absolute energy loss, one has to know the average energy loss per ion pair and assume that it is independent of velocity and one has to know the condensation efficiency in the cloud chamber during the experiment. The energy loss per ion pair is independent of velocity over quite wide velocity ranges in many gases ([12-16]), so this assumption may be justified. Difficulty is encountered, however, in estimating the energy loss per ion pair for a particular gas mixture in the cloud chamber. Even though this quantity has been measured for many gases, it is well known that the gas has a marked effect on the value obtained ([17]). For the present experiments it was assumed that the energy loss per ion pair in the vapor and in helium when mixed with the cloud chamber vapors was 30 eV. The values used for argon and xenon were 25.8 and 22 eV respectively ([18,19]).

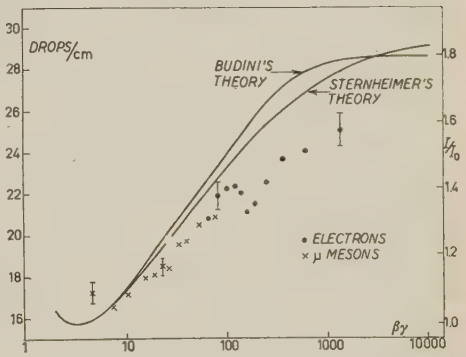

Fig. 4. – Ionization loss in xenon-helium mixture.

The condensation efficiency was estimated by counting tracks in which the positive and negative ions had been separated by the clearing field. The values obtained for the ratio of the number of drops on negative ions to the number of drops on positive ions were 0.4, 0.4 and 0.2 for the helium, argon

([16]) B. Rossi: *High Energy Particles* (New York, 1952).
([17]) W. P. Jesse and J. Sadauskis: *Phys. Rev.*, **88**, 417 (1952).
([18]) J. Weiss and W. Bernstein: *Phys. Rev.*, **103**, 1253 (1956).
([19]) W. P. Jesse and J. Sadauskis: *Phys. Rev.*, **97**, 1668 (1955); **90**, 1120 (1953).

and xenon experiments respectively. It was assumed that for the above ratios the condensation efficiency on the positive ions was essentially 100 per cent ([10]).

The energy loss at minimum determined experimentally for the helium experiment was 415 eV/cm compared to the theoretical value 392 eV/cm. For the argon experiment the experimental and theoretical values were 430 and 433 eV/cm respectively, and for the xenon experiment they were 320 and 425 eV/cm.

The agreement between theory and experiment for the helium and argon experiments is excellent, but the discrepancy in xenon led us to perform another experiment in xenon under better controlled conditions. A special counter triggering system was used to select μ-mesons in the range of $\beta\gamma$ from 2.4 to 4.9, so that μ-mesons in the range near minimum were observed. The magnetic field was cut off, and grids were placed at the sides of the chamber to provide an electric field to separate the positive and negative ion columns. Under these conditions it was possible to count the droplets formed in the positive and negative column independently, and to determine the ratio of these as a function of expansion ratio.

We found no significant variation of the number of drops in the positive column when the ratio of the number in the negative column to the number in the positive column varied from 0.15 to 0.4. We, therefore, assume that even when only 15 per cent of the ions in the negative column form drops, practically all the positive ions form drops. From this we can calculate the number of ions formed, and assuming the above values for energy loss per ion pair, can compare our experimental value with the theoretical value. For our particular conditions, the experimental value was (28.9 ± 0.6) drops cm. Theoretically the figures are (31.8 ± 0.4) drops cm for BAKKER-SEGRÈ ([20]) ionization potentials (STERNHEIMER,1952) and (29.6 ± 0.4) drops/cm using the CALDWELL ([21]) (STERNHEIMER, 1956) ionization potentials. The errors came from uncertainties in the energy loss per ion pair. We believe that the experimental and theoretical results are in agreement within the errors. The discrepancy in xenon was probably due to a bias in selection of doubled tracks where the conditions were not good for counting the negative column.

9. – Discussion of results.

The experimental results demonstrate clearly that the slope of the relativistic rise in the heavier gases is considerably smaller than that predicted theoretically, and seems to be approximately independent of the atomic number. The plateau in helium is, however, substantially lower than the plateau

([20]) C. J. BAKKER and E. SEGRÈ: *Phys. Rev.*, **81**, 489 (1951).

in argon or xenon. Previous experimental results have not been accurate enough or have not reached high enough velocities to have found this effect. We have explored various reasons for the difference between theory and experiment which may be summarized as follows:

1) The value of η, the maximum allowable energy transfer, may depend on the atomic number. Thus η, instead of being a fixed value depending only on the number of drops in a blob just countable, should perhaps be corrected for the binding energy of the struck electron. The actual energy transfer in the case of an electron in the K-shell of xenon, when a blob of 40 drops is formed, is approximately 40 KeV, rather than the assumed value $\eta = 960$ eV. A calculation was made, using Sternheimer's theory, but averaging over the various values of η for the different electron shells, to determine the effect on the slope of the curve. The slope was indeed reduced, but not sufficiently. For example in xenon, the value of the rise of energy loss above the minimum at $\beta\gamma = 100$ was lowered from 1.48 to 1.45, compared with the experimental value of 1.38. It seems clear, however, that this effect is valid and important and should be included when calculations of energy loss are made.

2) There has been discussion of the possibility that I, the average ionization potential, decreases with increasing velocity ([21]). Measurements are available, however, only as far as $\beta\gamma = 0.5$, and there are no experiments on dependence on $\beta\gamma$ at the very high velocities with which we are concerned. However, if I decreases as $\beta\gamma$ increases, the slope of the curve would be greater in contrast to the experimental result.

If η and I are independent of energy, the value of η/I^2 determines the slope of the relativistic rise, and together with the energy loss per ion pair, the absolute number of ion pairs per centimeter at minimum. Since the theory and experiment agree well up to values of $\beta\gamma$ near the minimum, it is difficult to reconcile theory with experiment beyond the minimum simply by changing the value of η/I^2. At minimum $\eta/I^2 = (960/(277)^2) = 0.013$. In order to fit the slope of the rising part of the curve, η/I^2 must be 2.73. We conclude that this ratio has no theoretical significance in the relativistic region.

Other possibilities have been considered but no detailed theoretical calculations have been made. Various possibilities are:

1) The ratio of energy loss to excitation and to ionization may not be independent of velocity and this dependence may vary with atomic number.

2) Shielding effects of the electron shells in the heavy elements may be important. The impact parameters in the region of the relativistic rise are orders of magnitude greater than those below the minimum of ionization,

([21]) D. O. Caldwell: *Phys. Rev.*, **100**, 291 (1955).

where the ionizing particle passes directly through the atom. Complete shielding of the K and L shells in xenon in the relativistic region produces a large effect (in the right direction) on the slope of the relativistic rise.

It seems clear that further calculations of ionization loss in heavy gases in the relativistic range should be made (*). Although the smaller slope will reduce the precision of velocity determination in the high momentum region, it seems probable that particle identification in this region may be made under sufficiently controlled conditions.

* * *

The authors are indebted to T. A. Aggson and R. W. Bierce who helped with the drop counting and data analysis. We also thank Dr. R. M. Sternheimer who sent us the results of his calculations for our helium experiment based on his theory and Prof. P. Budini for valuable discussions of the results. Prof. M. A. Ruderman participated in informative discussions on the theoretical implications of the results.

(*) Progress has been made recently in the theoretical calculations of Tidman [22] applying to oxygen, and Budini and Taffara [23] have also published the elements of a theory which should be applicable.

[22] D. A. Tidman: *Nuclear Physics*, **2**, 289 (1956) and in press.

[23] P. Budini and L. Taffara: *Nuovo Cimento*, **4**, 23 (1956).

RIASSUNTO (*)

In elio, argon e xenon si sono eseguite misure della ionizzazione prodotta da particelle relativistiche cariche. Nel caso dell'elio i risultati sperimentali si accordano bene con la teoria. Nell'argon e particolarmente nello xenon l'aumento relativistico della ionizzazione trovato sperimentalmente è inferiore a quanto la teoria lascia prevedere. Le misure furono eseguite col metodo del conteggio delle gocce in una camera a nebbia.

(*) *Traduzione a cura della Redazione.*

Absorption and Refraction of Some Polar Gases as a Function of Pressure at Microwave Frequencies (*).

A. Battaglia, F. Bruin (+) and A. Gozzini

Istituto di Fisica dell'Università - Pisa

(ricevuto il 9 Settembre 1957)

Summary. — Absorption and refraction of several polar gases has been measured, as a function of the pressure, at 32 mm wavelength and 0 °C. For ammonia, trimetilamine, ammonia-argon and ammonia-hydrogen mixtures a quadratic dependence has been found. For OCS and several amines the absorption increases less than quadratically. At the same pressure and concentration, we found the same absorption for ammonia-argon and ammonia-hydrogen mixtures. For absorbing gases, at low pressures, the refractive index is not proportional to the pressure.

1. – Theory.

The spectral absorption and refraction for a single transition in gases at microwave frequencies is usually described by the so called Van Vleck and Weisskopf formula (1) for the absorption coefficient α and refractive index n given by (1):

$$(1) \qquad \alpha = \frac{8\pi^2 Nf}{3ckT} |\mu_{ij}|^2 \nu^2 \left\{ \frac{1/2\pi\tau}{(\nu-\nu_0)^2 + (1/2\pi\tau)^2} + \frac{1/2\pi\tau}{(\nu+\nu_0)^2 + (1/2\pi\tau)^2} \right\},$$

$$(2) \qquad n^2 - 1 \approx 2(n-1) = \frac{8\pi Nf}{3kT} |\mu_{ij}|^2 \frac{\nu_0^2}{\nu_0^2 - \nu^2} \cdot \left[1 - \frac{\nu}{2\nu_0^2(2\pi\tau)} \left(\frac{\nu+\nu_0}{(\nu-\nu_0)^2 + (1/2\pi\tau)^2} + \frac{\nu-\nu_0}{(\nu+\nu_0)^2 + (1/2\pi\tau)^2} \right) \right] + \bar{\chi},$$

(*) The research reported in this paper has been made possibile by support extended by C.N.R. and Centro Microonde.

(+) Now at the Natuurkundig Laboratorium, Universiteit van Amsterdam.

(1) J. H. Van Vleck and V. F. Weisskopf: *Rev. Mod. Phys.*, **17**, 227 (1945).

in which α = absorption coefficient, in cm^{-1},

N = number of absorbing molecules, per unit volume,

f = fraction of molecules in the lower state i,

μ_{ij} = dipole moment matrix element of states i, j,

ν_0 = resonance frequency of the transition between states i, j,

τ = mean time between two molecular collisions,

c = $3 \cdot 10^{10}$ cm/s, $k = 1.38 \cdot 10^{-16}$ erg/K° and T absolute temperature,

and $\bar{\chi}$ represents the contribution to the refractive index of the $(1-f)N$ molecules that are not absorbing, being not in the lower state i.

In the far wing of a line, at moderate pressures, the quantity $(1/2\pi\tau)^2 \ll \ll (\nu_0 - \nu)^2$, and we may bring formula (1) into a more practical form:

$$\alpha_{\text{wing}} = 2\alpha_{\max} \frac{1 + (\nu/\nu_0)^2}{(\nu_0/\nu - \nu/\nu_0)^2} \left(\frac{\Delta\nu}{\nu_0}\, p\right)^2. \tag{3}$$

$\alpha'_{\max}$ being the absorption coefficient at the resonance frequency

$$\alpha_{\max} = \frac{8\pi^2 N f}{3ckT} |\mu_{ij}|^2 \frac{\nu_0^2}{p\,\Delta\nu}, \qquad (\approx \text{maximum absorption}).$$

$\Delta\nu$ the line half width constant $\Delta\nu = 1/2\pi\tau p$, and p the gas pressure. The central absorption $\alpha_{\max}$ is constant, if $1/\tau$ is proportional to the gas pressure. Therefore, at a fixed frequency, the absorption in the far wing of a spectral line, as a function of pressure, should be a quadratic parabola.

At the same pressure and frequency conditions, formula (2) can be put in the form

$$2(n-1) = \frac{c}{\pi} \alpha_{\max} \frac{p\,\Delta\nu}{\nu_0^2 - \nu^2} \left[1 - \frac{\nu}{2}\left(\frac{p\,\Delta\nu}{\nu_0}\right)^2 \left\{\frac{\nu + \nu_0}{(\nu_0 - \nu)^2} + \frac{\nu - \nu_0}{(\nu_0 + \nu)^2}\right\}\right] + \bar{\chi}, \tag{4}$$

$\bar{\chi}$ being proportional to the pressure, formula (4) predicts, that *at low pressures*, $(n-1)/p$ increases or decreases with pressure according as $\nu \gtrless \nu_0$.

At higher pressures, formula (2) shows that also the contribution of the resonant molecules tends to become proportional to the pressure. Therefore at higher pressures the Clausius-Mossotti law $(n-1)/p = \text{const}$ holds.

In the following both formulae (3) and (4) have been applied to measurements on a number of dipole gases.

2. – Measurements.

The apparatus used in the measurements discussed below was a slightly simplified version of the one previously described (2). The resonance frequencies of two equal adjustable cavities, each receiving half the klystron power, were compared by means of a sensitive pulse technique. Most of the measurements were performed at 0 °C. For this reason the cavities have been put in a bath of melting ice.

2·1. *Absorption of* NH_3 *and* NH_3 *mixtures.* – As was shown in the first section, the absorption in the low wing of a spectral line, for a fixed frequency ν, as a function of pressure, according to the simple theory should be a parabola. In Fig. 1 two parabolae of the type represented by formula (3) are given. The upper curve shows the absorption of NH_3 as a function of pressure at a wavelength of 32 mm and at a temperature of 0 °C. The lower curve is obtained from a similar measurement at 15 °C. As the centre of the absorption band of NH_3 is situated at a wavelength of 12.5 mm and measurements were performed at a wavelength of 32 mm, the quantity $2(1+(\nu/\nu_0)^2)/(\nu_0/\nu-\nu/\nu_0)^2$ in (3) for this case is equal to 0.528. The maximum absorption at a pressure of 100 mm and at room temperature is according to Bleaney and Penrose (3) equal to $49\cdot10^{-4}$ cm^{-1}, so that the lower curve of Fig. 1 should be

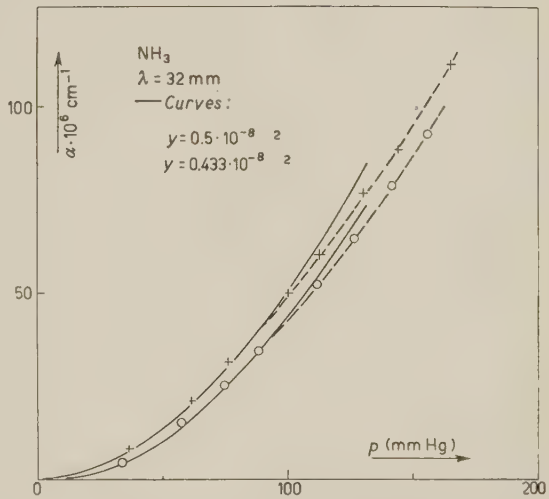

Fig. 1. – Absorption of NH_3 versus pressure at temperatuers of respectively 0 and 15 °C.

$$\alpha_{\text{wing}} = 2\,582\cdot10^{-6}\left(\frac{\Delta\nu}{\nu_0}p\right)^2 \text{cm}^{-1}. \tag{5}$$

At pressures below 150 mm Hg, the curves fitted to the observed points are given by

$$\alpha = 0.5\cdot10^{-8}\,p^2, \qquad \text{for the measurements at } 0\,^\circ\text{C}, \tag{6}$$

(2) A. Battaglia, F. Bruin and A. Gozzini: *Nuovo Cimento*,

(3) B. Bleaney and R. P. Penrose: *Proc. Phys. Soc.*, **59**, 418 (1947).

and

$$\alpha = 0.433 \cdot 10^{-8} p^2 , \quad \text{for the measurements at } 15\ ^\circ\text{C} . \tag{7}$$

It follows from (5) and (7) that the line width constant should be $\Delta\nu = 31$ MHz per mm Hg.

In order to obtain the theoretical value of $\Delta\nu$ one should average over all rotational quantum numbers J and K of ammonia. If this is done one finds ([1,5]) for $\Delta\nu$ about 26 MHz per mm Hg. This means that in the case considered here the observed absorption is 40% higher than expected. This discrepancy has been noted before ([6]).

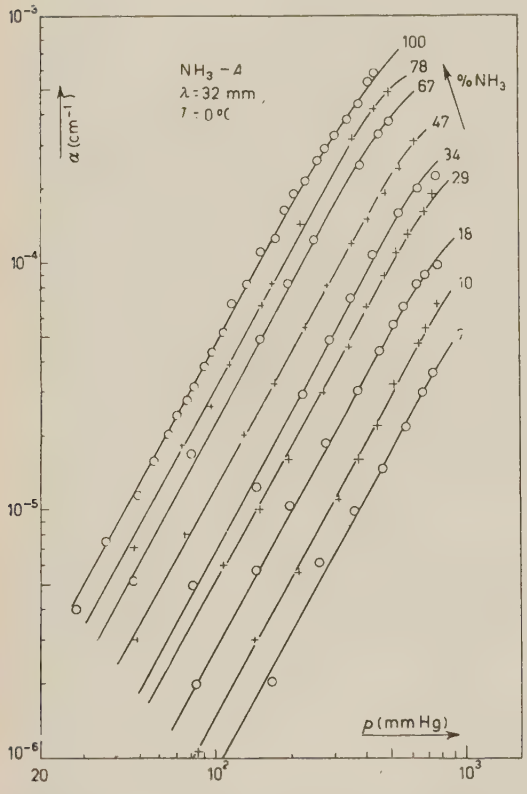

Fig. 2. - Absorption of pure NH_3 gas and of mixtures of NH_3 and argon as a function of pressure on a twofold logarithmic scale.

A second fact of interest which may be deduced from Fig. 1 is the dependence of the absorption on the temperature. From (6) and (7) we deduce a T^{-3} dependence. This agrees with the earlier and more detailed measurements performed by the group of N.B.S. Washinton ([6,7]) whereas other authors report a $T^{-\frac{5}{2}}$ dependence ([8,9]). No great value should be attached however, to this result, because the temperature of 15 °C has not been determined with great accuracy.

In order to check if the curves of Fig. 1 are indeed quadratic parabolae, in Fig. 2 we have plotted the absorption as a function of pressure on a twofold logarithmic scale. For quadratic dependence, the result should be a straight line having a slope of 2.

([4]) B. Bleaney and J. H. N. Loubser: *Proc. Phys. Soc.*, **63**, 483 (1950).

([5]) C. H. Townes and A. L. Schawlow: *Microwave Spectroscopy* (New York, 1955), p. 347.

([6]) G. Birnbaum and A. A. Maryott: *Journ. Chem. Phys.*, **21**, 1774 (1953).

([7]) G. Birnbaum and A. A. Maryott: *Journ. Chem. Phys.*, **22**, 1457 (1954).

([8]) H. Krishaji and P. Swarup: *Journ. Chem. Phys.*, **22**, 1456 (1954).

([9]) P. Swarup: *Journ. Scient. Ind. Res.*, **13** B, 389 (1954).

A number of diagrams of this kind is shown in Fig. 2. The upper curve in Fig. 2 represents the absorption of pure ammonia at 0 °C and at a wavelength of 32 mm. Up to a pressure of 200 mm Hg the curve is a straight line having a slope of 1.95, whereas at pressures below 100 mm Hg the slope is 2 within the limits of experimental error. At higher pressures the slope decreases, but this is not surprising as for increasing pressure the half width does not remain proportional to pressure ([10]).

In Fig. 2 is also shown the absorption as a function of pressure of mixtures of ammonia and argon for different fractions of NH_3. The curves all have the same slope, which simply means that we are each time in the far wing of an absorption line. A set of curves like in Fig. 2 may be used to determine the absorption as a function of concentration of NH_3 for some fixed pressure, after which the collision cross-section may be calculated. Such derived curves are shown in Fig. 3 for mixtures of ammonia and argon and of ammonia and hydrogen. It is seen that the results for both mixtures coincide.

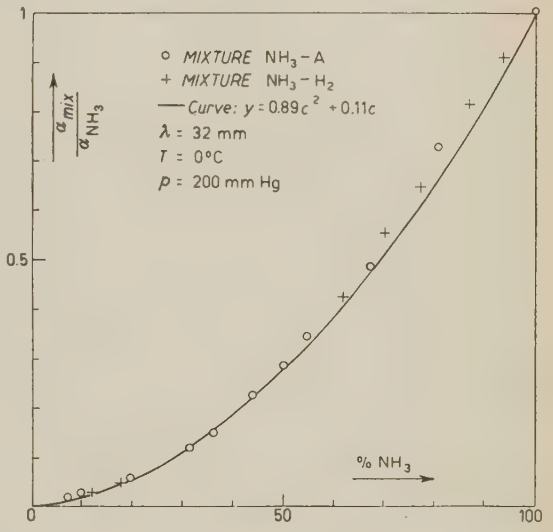

Fig. 3. – Relative absorption of NH_3-A and NH_3-H_2 mixtures as a function of concentration for a pressure of 200 mm Hg.

The analytic expression for the curve of Fig. 3 may be easily derived. Having a mixture of Nc molecules of ammonia and $N(1-c)$ molecules of argon, if v_1 and v_2 are the mean relative velocities of ammonia-ammonia and ammonia-argon molecules, and σ_1, σ_2 the cross-sections for ammonia-ammonia and ammonia-argon collisions, the collision rate for an ammonia molecule in the mixture is $1/\tau = Ncv_1\sigma_1 + N(1-c)v_2\sigma_2$. Putting $a = v_1\sigma_1/v_2\sigma_2$ the absorption relative to pure ammonia, as function of the concentration c may be easily shown to be:

$$y = c^2(1-a) + ca\,.$$

The curve of Fig. 3 is well represented, at concentrations below 80 %, by $y = 0.89c^2 + 0.11c$, therefore we obtain for a the value of 0.11.

([10]) G. Birnbaum and A. A. Maryott: *Phys. Rev.*, **92**, 270 (1953).

This is the same than that found for H_2, but higher than that found for A at resonance ([11]).

2·2. *Absorption of some amines and of carbonil sulfide.* – In Fig. 4 the absorption versus pressure curve of OCS and of $NH_2(CH_3)$; $NH(CH_3)_2$; $N(CH_3)_3$; $NH_2(C_2H_5)$; $NH(C_2H_5)_2$ are plotted in a twofold logarithmic scale. All measurements of figure are at 0 °C and 32 mm wavelength. The microwave spectrum of amines is little known. At low pressures, only methyl- and ethylamine have been investigated and many lines resolved in the frequency region between 15000 and 30000 MHz ([12,14]). At high pressures, HERSHBERGER ([15]) studied the absorption of amines, at 12 mm wavelength and at atmospheric pressure.

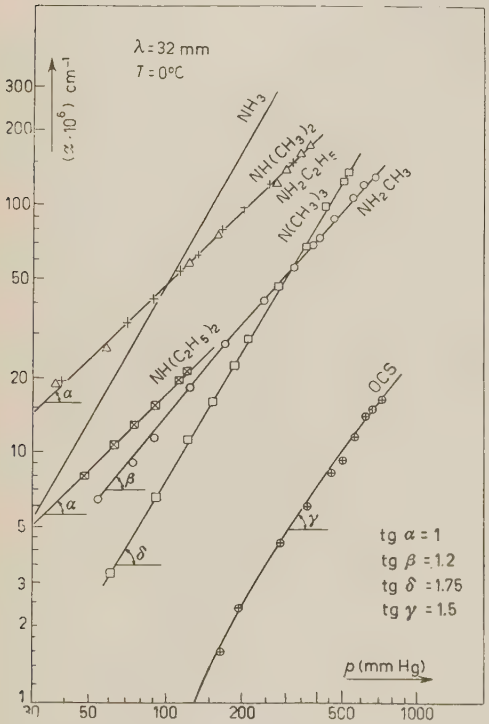

Fig. 4. – Absorption versus pressure for several gases, at 32 mm wavelength and at 0 °C.

Our investigation gave the following results. The absorption of the dimethyl-ethyl-, and diethylamine, at 32 mm wavelength is found to be proportional to pressure; the value of the coefficient of proportionality is $5 \cdot 10^7$ cm^{-1}/mm Hg, for the dimethylamine and the ethylamine; $1.7 \cdot 10^{-7}$ cm^{-1}/mm Hg for the diethylamine. The pressure interval for which this linear law holds, is (30 ÷ 300) mm Hg for the first two substances, and (30 ÷ 150) mm Hg for the diethylamine. Above these pressures, the substances (at 0 °C) begin to condense. At 12 mm wavelength, and at atmospheric pressure, HERSHBERGER ([15]) found that the ratio between the values of the absorption coefficients of the dimethil- and ethylamine is 7 to 11. According to our measurements, the two

([11]) C. H. TOWNES and A. L. SCHAWLOW: *Microwave Spectroscopy* (New York, 1955), p. 364.
([12]) K. SHIMODA and J. NISCHIKAWA: *Journ. Phys. Jap.*, **8**, 133 (1953).
([13]) K. SHIMODA and J. NISCHILAWA: *Journ. Phys. Jap.*, **9**, 974 1(954).
([14]) M. MATRICON and J. BONNET: *Journ. Phys. et Rad.*, **15**, 647 (1954).
([15]) W. D. HERSHBERGER: *Journ. Appl. Phys.*, **17**, 495 (1946).

coefficients have equal values at 32 mm wavelength, over the entire pressure interval investigated. The dimethylamine was studied at 12.5 mm wavelength also. We found that at this frequency the absorption coefficient depends on pressures less markedly than at 32 mm, while its value is appreciably higher (Fig. 5).

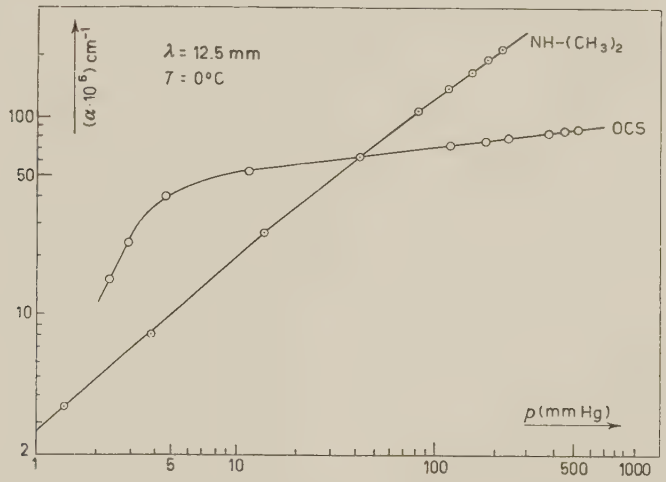

Fig. 5. – Absorption versus pressure for OCS and $NH(CH_3)_2$ at 12.5 mm wavelength and 0 °C.

The absorption of the methylamine, at 3.2 cm wavelength, is roughly proportional to the pressure, for pressures ranging from 400 to 700 mm Hg; at lower pressures, the increase is more steep.

Although the absorption of $N(CH_3)_3$ is seven times weaker than that of ammonia the dependence on pressure is about the same. This suggests that here also we are in the wing of an absorption band.

The absorption of carbonil sulfide, at 32 mm wavelength and 0 °C, is plotted against pressure in Fig. 4. Fig. 5 shows the results of similar measurements in the 12 mm region, at a frequency slightly below the frequency of the $J = 1$, $J = 2$ rotational transition. The first rotational line of this linear molecule is predicted to fall at 24.6 mm wavelength for the most abundant isotopic species $^{16}O\,^{12}C\,^{32}S$, so that, at 32 mm, we are in the far low wing of the resonance. From 300 mm Hg to atmospheric pressure, absorption is found to be proportional to the $\frac{3}{2}$ power of the pressure. Below 300 mm, the dependence is more pronounced and it approaches the quadratic law, but the absorption is too small to be measured with sufficient accuracy by our apparatus, at the time when the measurements were performed. The absorption measured at a frequency very close to that of the $J = 1$, $J = 2$ transition

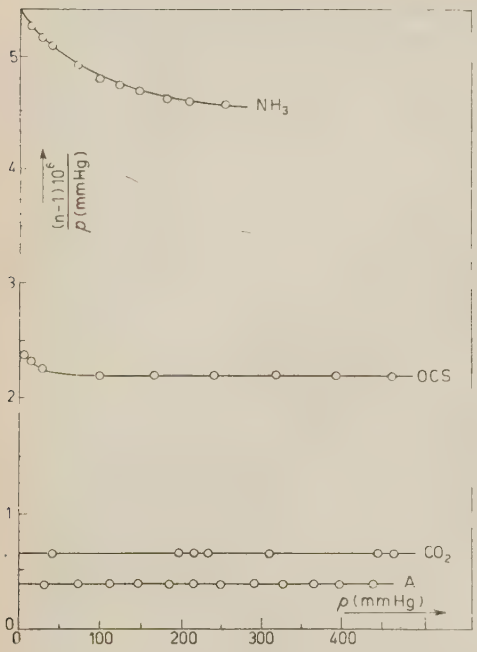

Fig. 6. – $(n-1)/p$ versus pressure for several gases.

raises quadratically with the pressure at very low pressures. According to the theory of collision broadening at higher pressures one expects the absorption to be independent of the pressure. However we observe a slight but definite increase of absorption. Both results of measurements at 32 and 12.5 mm indicate that the line width is less than proportional to the pressure.

2·3. *Refraction of* NH_3, OCS, CO_2 *and* A. – The Van Vleck and Weisskopf formula predicts that the refractive index of a gas in the wing of a line should not be, at low pressures, proportional to the pressure. This has been confirmed. The results are represented in Fig. 6 where $(n-1)/p$ is plotted versus pressure for several gases. For non absorbing gases as argon ad CO_2 the refractive index is strictly proportional to the pressure, whereas for ammonia and COS the curves show the behaviour predicted at low pressures by formula (5). Unfortunately with the klystrons at our disposal it was not possible to make measurements at frequencies in the high wing of the resonances, where formula (5) predicts that at low pressures, $(n-1)/p$ should increase with increasing pressure.

RIASSUNTO

Si riferiscono i risultati di misure sul coefficiente di assorbimento e sull'indice di rifrazione di diverse sostanze, alle lunghezze d'onda di 32 e 12 mm. Tali grandezze sono state misurate in funzione della pressione a frequenza e temperatura costante. A 32 mm di lunghezza d'onda il coefficiente di assorbimento dell'ammoniaca, di miscugli di ammoniaca ed argon ed ammoniaca ed idrogeno e della trimetilammina è proporzionale al quadrato della pressione. Alla stessa pressione e concentrazione di ammoniaca, il coefficiente di assorbimento di miscugli di ammoniaca con argon e di ammoniaca con argon e di ammoniaca con idrogeno è lo stesso. Per l'NH_3 e OCS, alle basse pressioni, l'indice di rifrazione non è proporzionale alla pressione.

The Interaction between Equilibrium Defects in the Alkali Halides: the «Ground State» Binding Energy of the Vacancy Pair (*).

M. P. Tosi and F. G. Fumi

Istituto di Fisica dell'Università - Palermo

(ricevuto il 10 Settembre 1957)

Summary. — The Born-Mayer model of ionic solids is used to calculate the binding energy of a positive-ion vacancy and a negative-ion vacancy at the distance of nearest neighbours in NaCl and KCl crystals: the results are 0.6 eV and 0.7 eV respectively. This leads one to expect in NaCl an equilibrium concentration of vacancy pairs ranging from 10% to 20% of the equilibrium concentration of Schottky defects between 500 °C and 700 °C. The available experimental data are compatible with the existence in the alkali halide crystals of an equilibrium concentration of vacancy pairs of this order of magnitude in the intrinsic temperature region.

1. – Introduction.

Mott and Gurney (1) were apparently the first to point out that positive-ion vacancies and negative-ion vacancies in an alkali halide crystal will tend to combine in pairs and Seitz (2) emphasized shortly afterwards that these pairs, and the larger vacancy agglomerates, will play an important role in the physics of these crystals. To a rough approximation, the binding energy of two oppositely charged vacancies at the closest lattice distance of approach, the binding energy of the ground state of the vacancy pair, may be taken equal to the

(*) The first paper of this series was published in *Nuovo Cimento*, **11**, 274 (1954).

(1) N. F. Mott and R. W. Gurney: *Electronic Processes in Ionic Crystals* (Oxford, 1940), p. 41.

(2) F. Seitz: *Rev. Mod. Phys.*, **18**, 384 (1946).

electrostatic interaction $-e^2/Kr_0$ of the effective charges of the two vacancies (K, static dielectric constant of the crystal; r_0, nearest-neighbour distance). It is obvious that an estimate of this sort of the binding energy cannot give an accurate value for the equilibrium concentration of vacancy pairs at a given temperature. In effect this equilibrium concentration is extremely sensitive to the value of the binding energy: for a NaCl crystal at 800 °K the ratio of the density m of vacancy pairs to the density n of Schottky defects (ref. (2), eqn. (26)) with (3) $n=1.2\cdot10^{23}\exp[-11700/T]$ cm^{-3} is 7.6 if the binding energy is Coulombic (0.91 eV), and only 0.085 if the binding energy is 0.6 eV. This estimate indicates clearly the necessity of having an accurate value for the binding energy of vacancy pairs to draw any conclusion on their equilibrium concentration at different temperatures.

We have computed the binding energy of the ground state of the vacancy pair in NaCl and KCl crystals using the Born-Mayer model as first applied to the study of point imperfections in the alkali halides by MOTT and LITTLETON (4). We find that the binding energy is smaller than the Coulombic value, as it is to be expected (5), and by several tenths of an electron volt. A similar, but less accurate, calculation had previously been performed for NaCl crystals by REITZ and GAMMEL (6).

2. – The binding energy of the ground state of the vacancy pair.

The binding energy of the ground state of the vacancy pair is equal to the difference between the work necessary to create a positive-ion vacancy in the perfect lattice, and the work necessary to create it in the position of nearest neighbour of a negative-ion vacancy. To take into account the electronic and displacement polarization of the lattice around the vacancy created, one writes the work of removal of the positive ion as the negative of the average of the potential energies in the position of the ion before and after it has been removed.

The important contribution to the potential energy of an ion in an alkali halide crystal are the electrostatic and repulsive energies, and these are the only terms that we shall consider. For the repulsive energy we adopt the exponential form proposed by BORN and MAYER (7,8).

(3) H. W. ETZEL and R. J. MAURER: *Journ. Chem. Phys.*, **18**, 1003 (1950).
(4) N. F. MOTT and M. J. LITTLETON: *Trans. Faraday Soc.*, **34**, 485 (1938).
(5) F. G. FUMI and M. P. TOSI: *Faraday Soc. Discussions*, **23**, 92 (1957).
(6) J. R. REITZ and J. L. GAMMEL: *Journ. Chem. Phys.*, **19**, 894 (1951).
(7) M. BORN and J. MAYER: *Zeits. f. Phys.*, **75**, 1 (1932); J. MAYER and H. HELMHOLZ: *Zeits. f. Phys.*, **75**, 19 (1932).
(8) F. BASSANI amd F. G. FUMI: *Nuovo Cimento*, **11**, 274 (1954).

3. – The work to create a positive-ion vacancy in a perfect crystal.

The MOTT and LITTLETON type of procedure to calculate the work to create a positive-ion vacancy in a perfect NaCl or KCl crystal has been described in detail in a previous paper ([8,9]). For the constants entering the calculation we use the same numerical values quoted in ref. ([8]), Table I except that we adopt for the electronic polarizabilities α_+ and α_- of cations and anions the values reported by TESSMAN, KAHN and SHOCKLEY (TKS) ([10]) for ions in crystal lattices, instead of the values given by PAULING ([11]) for free ions. This entails some numerical changes in the calculation previously described ([8]), and the new values for the work to create a positive-ion vacancy (4.78 eV in NaCl; 4.44 eV in KCl) are found to be somewhat larger, as the TKS polarizability for Cl^- ions is smaller than the Pauling polarizability. The net increase of the energy of formation of a Schottky defect caused by the change in polarizabilities is fairly small (0.09 eV in NaCl, 0.04 eV in KCl) as the work to create a negative-ion vacancy is somewhat reduced.

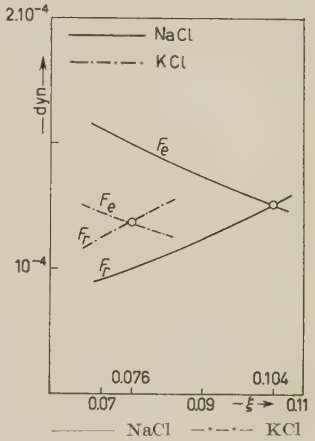

$$m(\mathrm{NaCl}) = \frac{\alpha(\mathrm{Na}^+)}{e^2 r_0(\mathrm{NaCl})}\, 1.263 \cdot 10^{-4} = 0.008$$

$$m(\mathrm{KCl}) = \frac{\alpha(\mathrm{K}^+)}{e^2 r_0(\mathrm{KCl})}\, 1.190 \cdot 10^{-4} = 0.022$$

Fig. 1. – Displacement and electronic polarization of the immediate neighbours of a negative-ion vacancy in NaCl and KCl.

4. – The work to create a positive-ion vacancy near a negative-ion vacancy.

To calculate the potential energy in the position of a positive ion which is nearest neighbour of a negative-ion vacancy we need to determine the polarization of the lattice due to the presence of the negative-ion vacancy. Of course the procedure is entirely analogous to that described for the positive-ion vacancy in a previous paper ([8]): the determination of the displacement ξr_0 and of the electronic dipole mer_0 of the immediate neighbours of the vacancy is illustrated in Fig. 1 ([12]). The electrostatic potential energy

([9]) Equation (7) of ref. ([8]) contains a misprint. The first term inside round brakkets should read $6\xi/(1+\xi)$, and not $6/(1+\xi)$.

([10]) J. R. TESSMAN, A. H. KAHN and W. SHOCKLEY: *Phys. Rev.*, **92**, 890 (1953).

([11]) L. PAULING: *Proc. Roy. Soc.*, A **114**, 181 (1927).

([12]) The equations at the bottom of Fig. 1, ref. ([8]) contain a misprint. A factor 10^{-4} was omitted from the numerical values of F_e introduced in the equations: however, the final values quoted for m(NaCl) and m(KCl) are correct.

neighbour distance):

$$
(8)\quad
\begin{cases}
\Delta E^{C} = \dfrac{e^2}{r_0}\Big\{\dfrac{8\sqrt{2}+2}{1+\eta} - \dfrac{1}{3+2\eta} - \dfrac{8}{[1+2(1+\eta)^2]^{\frac{1}{2}}} - \dfrac{8}{[(1+\eta)^2+(2+\eta)^2]^{\frac{1}{2}}} - \\
\qquad - \dfrac{4}{[1+4(1+\eta)^2]^{\frac{1}{2}}} - 8\sqrt{2} - \dfrac{5}{3} + \dfrac{8}{\sqrt{3}} + \dfrac{12}{\sqrt{5}}\Big\} + \\
\quad + 2\dfrac{e^2}{r_0}\Big\{|V_E(\eta 00)|\dfrac{r_0}{e} - \dfrac{1}{\eta} + \dfrac{1}{1+\eta} - \dfrac{1}{2+\eta} + \dfrac{1}{3+\eta} - \\
\qquad - \dfrac{4}{[1+(1+\eta)^2]^{\frac{1}{2}}} + \dfrac{4}{[1+(2+\eta)^2]^{\frac{1}{2}}} + \alpha_M - \dfrac{5}{6} + \dfrac{4}{\sqrt{2}} - \dfrac{4}{\sqrt{5}}\Big\} + \\
\quad + 8\dfrac{e^2}{r_0}\Big\{|V_E(\eta 00)|\dfrac{r_0}{e} - \dfrac{1}{\eta} + \dfrac{1}{1+\eta} - \dfrac{1}{2+\eta} + \dfrac{1}{[1+\eta^2]^{\frac{1}{2}}} - \\
- \dfrac{4}{[1+(1+\eta)^2]^{\frac{1}{2}}} + \dfrac{2}{[2+(1+\eta)^2]^{\frac{1}{2}}} + \dfrac{1}{[1+(2+\eta)^2]^{\frac{1}{2}}} + \dfrac{1}{[4+(1+\eta)^2]^{\frac{1}{2}}} + \\
+ \alpha_M - \dfrac{3}{2} + \dfrac{4}{\sqrt{2}} - \dfrac{2}{\sqrt{3}} - \dfrac{2}{\sqrt{5}}\Big\}.
\end{cases}
$$

$$
(9)\quad
\begin{cases}
\Delta E^{R} = b\exp\left(\dfrac{r_+ + r_-}{\varrho}\right)\cdot \\
\quad \cdot\Big\{10\exp\Big[-(1-\eta)\dfrac{r_0}{\varrho}\Big] + 32\exp\Big[-(1+\eta^2)^{\frac{1}{2}}\dfrac{r_0}{\varrho}\Big] - 42\exp\Big(-\dfrac{r_0}{\varrho}\Big)\Big\} + \\
+ 0.75b\exp\left(\dfrac{2r_-}{\varrho}\right)\Big\{20\exp\Big(-[1+(1-\eta)^2]^{\frac{1}{2}}\dfrac{r_0}{\varrho}\Big) + \\
+ 20\exp\Big[-(2+\eta^2)^{\frac{1}{2}}\dfrac{r_0}{\varrho}\Big] + 8\exp\Big[-(1+\eta)\sqrt{2}\dfrac{r_0}{\varrho}\Big] - 48\exp\Big(-\sqrt{2}\dfrac{r_0}{\varrho}\Big)\Big\}.
\end{cases}
$$

$$
(10)\quad
\begin{cases}
\Delta E^{P} = -\dfrac{1}{2}\dfrac{e^2}{r_0^4}(\alpha_+ + \alpha_-)\Big\{\Big[\dfrac{1}{(1+\eta)^2} - \dfrac{1}{(2+\eta)^2}\Big]^2 - \dfrac{9}{16}\Big\} - \\
\quad - 2\dfrac{e^2}{r_0^4}(\alpha_+ + \alpha_-)\Big\{\dfrac{1}{[1+(1+\eta)^2]^3} + \\
\qquad + \Big[\dfrac{1}{(1+\eta)^2} - \dfrac{1+\eta}{[1+(1+\eta)^2]^{\frac{3}{2}}}\Big]^2 - \dfrac{1}{8} - \Big(1 - \dfrac{1}{2\sqrt{2}}\Big)^2\Big\}.
\end{cases}
$$

In the formula for ΔE^C the first group of terms gives the change in electrostatic interaction energy amongst the ten nearest neighbours of the two vacan-

cies, while the second (and third) group of terms give the change in electrostatic interaction energy between the ions 1, 10 (and the ions from 2 to 9) and the rest of the lattice. In the formula for ΔE^P the first group of terms refers to the ions 1, 10 and the second group of terms refers to the ions from 2 to 9: the dipole-dipole interaction has been neglected. The numerical results are illustrated in Fig. 4: for ΔE^C and ΔE^P there is a direct correspondence between the values for NaCl and KCl as $r_0 \Delta E^C$ and $(r_0^4/(\alpha_+ + \alpha_-))\Delta E^P$ are functions of η which depend only on the type of structure and on the charge of ions. For NaCl, our numerical results agree with the results given by REITZ and GAMMEL (ref. (6), Fig. 4) but for KCl they show substantial deviations from the results reported by DIENES (ref. (13), Fig. 6): for ΔE^R this is to be imputed to the inclusion of the next-nearest repulsion which had been neglected by DIENES, but for ΔE^C the discrepancy is unexplained. The values that we find for the displacement ηr_0 of the immediate neighbours of the vacancy pair appear entirely reasonable. Indeed, if one considers that the nearest neighbours of each of the two vacancies are pushed out by the adjacent vacancy and pulled in by the other vacancy, it is clear that the uniform outward displacement of the ten nearest neighbours of the vacancy pair cannot be as large as the larger of the displacements around the isolated vacancies. This condition is verified by our values for the displacement ηr_0 in NaCl and KCl crystals, and by the value for ηr_0 reported by REITZ and GAMMEL for NaCl (6), but it is not verified by the value for ηr_0

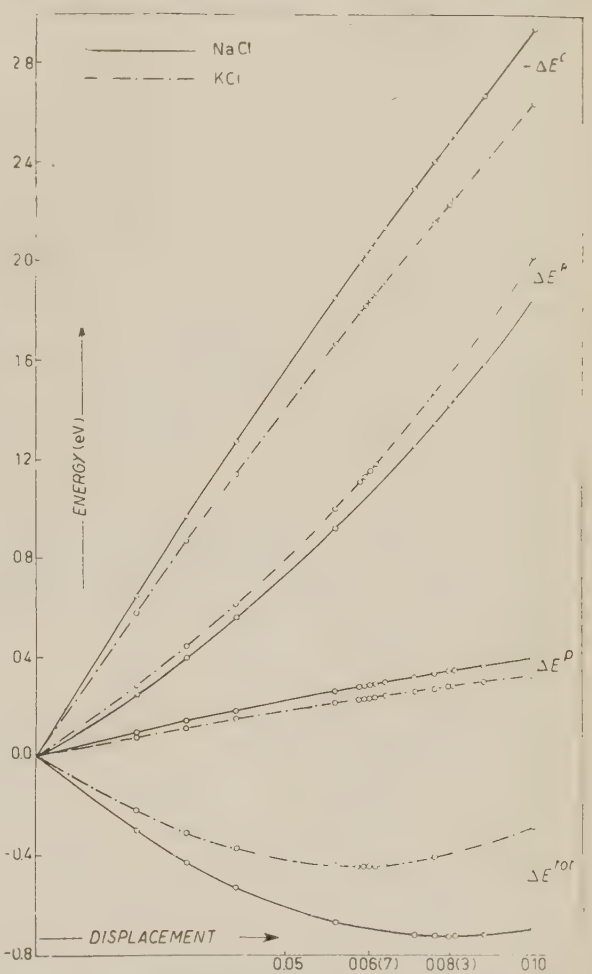

Fig. 4. – Determination of the displacement ηr_0 of the immediate neighbours of a vacancy pair.

reported by DIENES for KCl ([13]) (Table I). The fact that Dienes' distortion around the vacancy pair appears too large had already been noted by PRATT ([15]), who followed, however, an unreliable line of reasoning.

TABLE I. – *Displacements of the immediate neighbours of a vacancy pair and of isolated vacancies* ([a]).

		ξ^+	ξ^-	η
NaCl	PAULING	0.068 ([b])	0.104	0.083 ([c])
	TKS	0.070	0.104	0.083
KCl	PAULING	0.065 ([b])	0.077	(0.10) ([d])
	TKS	0.065	0.076	0.067

([a]) The quantity $\xi^+ r_0$ ($\xi^- r_0$) gives the outward displacement of the nearest neighbours of a positive-ion (negative-ion) vacancy and the quantity ηr_0 the *uniform* outward displacement of the ten nearest neighbours of the vacancy pair. The values reported were all computed with the Born-Mayer repulsive potential: they change slightly if one replaces the Pauling polarizabilities by the TKS polarizabilities.

([b]) These values were reported by BASSANI and FUMI [ref. ([8]), Fig. 1].

([c]) This value was reported by REITZ and GAMMEL [ref. ([6]), Fig. 4].

([d]) This value was reported by DIENES [ref. ([13]), Fig. 6], but it appears questionable.

The electrostatic and repulsive potential energies E_2 and Φ_2 at a positive-ion vacancy near a negative-ion vacancy are computed in the same sort of way as the energies E_1 and Φ_1. The relevant formulas are:

$$E_2^{RL} = E_1^{RL}, \tag{11}$$

$$E_2^D = \frac{e^2}{r_0}\left\{\frac{1}{2+\eta+\xi} - \frac{1}{2+\xi} + \frac{4}{[(1+\eta)^2+(1+\xi)^2]^{\frac{1}{2}}} - \right.$$
$$\left. - \frac{4}{[1+(1+\xi)^2]^{\frac{1}{2}}} - \frac{4}{[(1+\eta)^2+\xi^2]^{\frac{1}{2}}} + \frac{4}{[1+\xi^2]^{\frac{1}{2}}} - \frac{1}{1+\eta-\xi} + \frac{1}{1-\xi}\right\}, \tag{12}$$

$$\Phi_2 = b \exp\left(\frac{r_+ + r_-}{\varrho}\right) \cdot$$
$$\cdot\left\{4 \exp\left(-[(1+\eta)^2+\xi^2]^{\frac{1}{2}}\frac{r_0}{\varrho}\right) + \exp\left[-(1+\eta-\xi)\frac{r_0}{\varrho}\right]\right\}. \tag{13}$$

The polarization term of E_2 must be computed directly as the potential energy in the positive ion in question due to the dipoles induced on the ten ions which are immediate neighbours of the vacancy pair, and on the second

([15]) P. L. PRATT: *Report of the Conference on Defects in Crystalline Solids held at Bristol, in July 1954* (London, 1955), p. 402.

and third neighbours of the positive-ion vacancy by the field generated by the charges of the two vacancies, and by the displacements of the ten immediate neighbours of the vacancy pair. The polarization of the distant ions is neglected since the vacancy pair is neutral.

The various contributions to the work to create a positive-ion vacancy near a negative-ion vacancy in NaCl and KCl crystals are listed in Table II: in NaCl this work is equal to 4.18 eV, while in KCl it is equal to 3.72 eV. The numerical results for NaCl show substantial deviations from the results quoted by REITZ and GAMMEL (ref. [6]), Table II): for the initial configuration, the main source of discrepancy is the difference in the value for the displacement of the nearest neighbours of a negative-ion vacancy, while for the final configuration there is also an important effect of the replacement of the Pauling polarizabilities by the TKS polarizabilities. These effects concur to raise the work to create a positive-ion vacancy near a negative-ion vacancy in NaCl from the value 3.86 eV quoted by REITZ and GAMMEL to our value. The displacement $0.078\, r_0$ that REITZ and GAMMEL attribute to the nearest neighbours of a negative-ion vacancy in NaCl had been computed by MOTT and LITTLETON [4], using a repulsive potential rather different from the BORN-MAYER potential that REITZ and GAMMEL use in their calculations: the value that REITZ and GAMMEL should have used for this displacement is $0.104\, r_0$ (Table I).

TABLE II. – *Contributions to the work to create a positive-ion vacancy near a negative-ion vacancy* (eV).

	$E_1^{RL}(-E_2^{RL})$	E_1^D	$-E_1^P$	$-\Phi_1$	E_2^D	$-E_2^P$	$-\Phi_2$
NaCl	4.31	0.74	3.52	— 0.92	— 1.43	— 1.75	— 0.42
KCl	3.75	0.51	3.07	— 0.94	— 1.03	— 1.23	— 0.46

5. – Discussion of the results.

The values calculated in Sects. 3 and 4 for the work to extract a positive ion from a perfect lattice and from the displaced equilibrium position near a negative-ion vacancy give at once for the ground-state binding energy of a vacancy pair the values 0.60 eV in NaCl and 0.72 eV in KCl, which, of course, should not be taken literally, owing to the approximation inherent to this type of calculation (ref. [5]), sect. 4). The values that we compute are probably somewhat too large as the approximation involved in adopting with DIENES [13]) an *equal* outward displacement for the nearest neighbours of a vacancy pair reduces the work to extract a positive ion near a negative-ion vacancy. On the other hand, the slight uncertainty in the value of ηr_0, due to the flat minimum of ΔE^{tot} in Fig. 4, appears of little consequence for the binding energy of the

vacancy pair which is not affected by small changes in the value of η. Similarly, the replacement of the TKS polarizabilities by the Pauling polarizabilities has little effect on the binding energy of the vacancy pair, as the work to extract a positive ion from a perfect lattice and from the position of nearest neighbour of a negative-ion vacancy are reduced by comparable amounts ([16]): for NaCl, the binding energy becomes 0.66 eV, as previously reported ([17]), while for KCl it becomes about 0.76 eV, a value sizeably different from the one reported previously (0.85 eV) ([17]), which was based on Dienes' distortion around the vacancy pair. It should finally be stressed that the somewhat larger value of the binding energy in KCl appears quite reasonable as the outward distortion around a negative-ion vacancy is appreciably smaller than in NaCl.

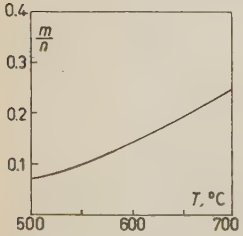

Fig. 5. - The «theoretical» ratio of the density m of vacancy pairs to the density n of Schottky defects in NaCl in the intrinsic temperature region.

The ratios of the density m of vacancy pairs to the density n of Schottky defects to be expected in NaCl crystals in the intrinsic temperature region on the basis of a simple association theory (ref. ([2]), eqn. (26)) with a binding energy of 0.6 eV taking[3] $n = 1.2 \cdot 10^{23} \exp[-11\,700/T]$ cm^{-3} are reported in Fig. 5. The corresponding values for KCl, which range from 0.19 at 500 °C to 0.82 at 700 °C, are not reported in the figure also because the available expression for the equilibrium concentration of Schottky defects in KCl, $n = 6.7 \cdot 10^{23} \cdot \exp[-13\,900/T]$ cm^{-3} ([18]), appears somewhat doubtful ([19]). The correction for the long-range Coulomb interaction between the two vacancies (ref. ([20]), pp. 300, 307-309) would reduce somewhat the ratio m/n both in NaCl and KCl, but not greatly owing to the small concentration of vacancies involved.

The available experimental evidence on the process of matter transport in alkali halide crystals is compatible with the existence of an equilibrium concentration of vacancy pairs in the intrinsic region of the order of the concentration that we compute for NaCl, but unfortunately the precision of the data is insufficient to allow firm conclusions to be reached ([19]). Some evidence on the role of vacancy pairs is provided by the studies of Mapother, Crooks

([16]) The replacement of the Pauling polarizabilities by the TKS polarizabilities has practically no effect also on the ground-state binding energy of the impurity complexes, and the values computed by Bassani and Fumi ([8]) with the Pauling polarizabilities remain valid. For Sr^{++} in NaCl and KCl, the new values are 0.43 eV and 0.38 eV respectively, while the values reported by Bassani and Fumi are 0.45 eV and 0.39 eV.

([17]) F. Bassani and F. G. Fumi: *Suppl. Nuovo Cimento*, **1**, 114 (1955).

([18]) H. Kelting and H. Witt: *Zeits. f. Phys.*, **126**, 697 (1949); F. Seitz: *Rev. Mod. Phys.*, **26**, 7 (1954).

([19]) R. J. Maurer: private communication.

([20]) A. B. Lidiard: *Handb. d. Phys.*, **20**, 246 (1957).

and MAURER [21], and ASCHNER and MAURER [22], on the validity of the Einstein relation between the diffusion coefficient and the ionic conductivity in NaCl, NaBr and KCl crystals, and by the measurements of SCHAMP and KATZ [23] on the diffusion of Br^- ions in NaBr. MAURER and his coworkers [21,22] report that the measured tracer diffusion coefficient for the cation in NaCl, NaBr and KCl in the intrinsic temperature region equals *within the experimental accuracy* the diffusion coefficient for the cation D_+ calculated from the measured conductivity σ by the Eistein relation

$$D_+ = \frac{kT\sigma}{N e^2} t_+ , \tag{14}$$

where t_+ is the transport number for the cation, and N is the number of molecules per cm^3. Actually, owing to correlation effects, the form of the Einstein relation to be used to calculate the *tracer* diffusion coefficient for the cation D_+^T is [24]

$$D_+^T = 0.78 \frac{kT\sigma}{N e^2} t_+ . \tag{15}$$

Thus the measured tracer diffusion coefficient for the cation in NaCl, NaBr and KCl [21,22] appears to be somewhat larger than it should be, suggesting that the vacancy pairs play some role. Similarly, if one keeps account of the correlation factor, the measurements of SCHAMP and KATZ [23] show that the tracer diffusion coefficient of Br^- ions in the intrinsic temperature region is of the order of one tenth of the diffusion coefficient deduced from the ionic conductivity, which refers essentially to the Na^+ ions. This is quite compatible with the existence of an equilibrium concentration of vacancy pairs of the order of 10%, especially if one considers that the mobility of a vacancy pair in an alkali halide crystal may be smaller than the mobility of an isolated cation vacancy [25,22]. The result of DIENES [13] that the theoretical migration barrier for a vacancy pair in KCl is lower than the theoretical migration barrier for an isolated cation vacancy in NaCl, as calculated by MOTT and LITTLE-

[21] D. MAPOTHER, H. N. CROOKS and R. J. MAURER: *Journ. Chem. Phys.*, **18**, 1231 (1950).

[22] J. F. ASCHNER: *Self-Diffusion in Sodium and Potassium Chloride*, Ph. D. Thesis (University of Illinois, 1954).

[23] H. W. SCHAMP and E. KATZ: *Phys. Rev.*, **94**, 828 (1954).

[24] J. BARDEEN and C. HERRING: *Imperfections in Nearly Perfect Crystals*, edited by W. SHOCKLEY (New York, 1952), p. 261; K. COMPAAN and Y. HAVEN: *Trans. Faraday Soc.*, **52**, 786 (1956); W. D. COMPTON and R. J. MAURER: *Journ. Phys. Chem. Solids*, **1**, 191 (1956).

[25] Y. HAVEN: *Report of the Conference on Defects in Crystalline Solids held at Bristol in July* 1954 (London, 1955), p. 261.

TON [4], cannot be considered as really probatory, also because the calculation of migration barriers, especially for negative ions, is yet the less settled side of lattice calculations on point imperfections in the alkali halides (ref. [5], Sect. 3).

* * *

It is a real pleasure to acknowledge the friendly discussions that the Authors have had on the subject-matter of this paper with Prof. SEITZ, and with Dr. HAVEN and Dr. LIDIARD, during the recent Varenna Summer School on Solid State Physics. The Authors are also indebted to Prof. MAURER for informative correspondence.

RIASSUNTO

Il modello di Born e Mayer dei solidi ionici è utilizzato per calcolare l'energia di legame di un posto vacante da ione positivo e di un posto vacante da ione negativo alla loro minima distanza reticolare in cristalli di NaCl e di KCl: i risultati sono rispettivamente 0.6 eV e 0.7 eV. Per il NaCl, questo porta ad una concentrazione di equilibrio di coppie di posti vacanti variabile fra il 10% ed il 20% della concentrazione di equilibrio di difetti Schottky nell'intervallo fra 500 °C e 700 °C. I risultati sperimentali disponibili sono compatibili con l'esistenza negli alogenuri alcalini di una concentrazione di equilibrio di coppie di posti vacanti di questo ordine di grandezza nella regione intrinseca di temperature.

On the Motion of Charged Particles in the Complex-Symmetric Unified Field Theory.

J. MOFFAT

Department of Mathematics, Imperial College - London

(ricevuto il 25 Agosto 1957)

In the complex-symmetric unified theory ([1,2]) the equations of motion of charged particles were derived from the field equations by an application of the EINSTEIN, INFELD and HOFFMANN approximation method ([3,4]), and the technique for deriving equations of motion introduced by INFELD ([5]). These equations of motion contained the Lorentz force.

However, at each stage of approximation in the general theory, the equations of motion proved to be incompatible. We wish to point out that by taking into account the conditions of integrability of the field equations this incompatibility is removed.

In the first treatment of this problem we used a source tensor expressed linearly in terms of the Dirac δ-function. The conditions of integrability of these field equations can be taken into account—and the incompatibility removed—by applying the « dipole procedure » introduced recently by INFELD and PLEBANSKI ([6]). The new treatment is based on the complex-symmetric field equations of empty space (*)

$$R_{\mu\nu} = 0 \,. \tag{1}$$

These field equations can be written

$$\Phi_{\mu\nu} + 2\Lambda_{\mu\nu} = 0 \,. \tag{2}$$

The $\Phi_{\mu\nu}$ are certain linear expressions in $\gamma_{\mu\nu}$, where $\gamma_{\mu\nu}$ is defined by

$$\gamma_{\mu\nu} = \varepsilon_{\mu\nu} - \tfrac{1}{2}\eta_{\mu\nu}\eta^{\alpha\beta}\varepsilon_{\alpha\beta} \tag{3}$$

and

$$\begin{cases} \eta_{mn} = -\delta_{mn} \,; \quad \eta_{0m} = 0 \,; \quad \eta_{00} = 1 \,, \\ \varepsilon_{\mu\nu} = g_{\mu\nu} - \eta_{\mu\nu} \,. \end{cases} \tag{4}$$

$g_{\mu\nu}$ is the complex-symmetric fundamental

([1]) J. MOFFAT: *Proc. Camb. Phil. Soc.*, **53**, 473 (1957).

([2]) J. MOFFAT: *Proc. Camb. Phil. Soc.*, **53**, 489 (1957).

([3]) A. EINSTEIN, L. INFELD and B. HOFFMANN: *Ann. Math., Princeton*, **39**, 66 (1938).

([4]) A. EINSTEIN and L. INFELD: *Can. Journ. Math.*, **1**, 209 (1949).

([5]) L. INFELD: *Acta Phys. Pol.*, **13**, 187 (1954).

([6]) L. INFELD and J. PLEBANSKI: *Bull. Acad. Pol. Sci.*, **11**, 763 (1956).

(*) Greek indices run from 0 to 3 and Latin indices from 1 to 3.

tensor (*) (7)

$$g_{\mu\nu} = {}^{*}g_{\mu\nu} + \hat{g}_{\mu\nu} . \tag{5}$$

The $\Lambda_{\mu\nu}$ are defined by certain linear and *non*-linear expressions in $\gamma_{\mu\nu}$.

Let us take a two-dimensional closed surface surrounding, say, the s-th singularity. We take a surface integral over this surface and obtain

$$\int^{s} (\Phi_{\mu r} + 2\Lambda_{\mu r}) n_r \, \mathrm{d}S = 0 , \tag{6}$$

where n_r are the components of the normal unit vector to the surface. Owing to the mathematical structure of $\Phi_{\mu r}$ we know that $\int \Phi_{\mu r} n_r \mathrm{d}S$ is *identically* zero (4). Therefore, we are left with

$$\int^{s} 2\Lambda_{\mu r} n_r \, \mathrm{d}S = 0 . \tag{7}$$

These equations tell us that the surface integral is independent of the shape of the surface.

Separating the field equations (2) according to the E.I.H. approximation method we obtain

$$\begin{cases} \underset{2l-2}{\Phi_{00}} + 2\underset{2l-2}{\Lambda_{00}} = 0 , \\ \underset{2l-1}{\Phi_{0m}} + 2\underset{2l-s}{\Lambda_{0m}} = 0 , \\ \underset{2l}{\Phi_{mn}} + 2\underset{2l}{\Lambda_{mn}} = 0 . \end{cases} \tag{8}$$

The integrability conditions of these field equations for the *known* $\Lambda_{\mu\nu}$'s are (because of the structure of $\Phi_{\mu\nu}$):

$$\begin{cases} {}^{*}\overset{s}{C}_{2l-1} = \int^{s} 2\Lambda^{*}_{0m} n_m \, \mathrm{d}S = 0 , \\ \overset{s}{\hat{C}}_{2l-1} = \int^{s} 2\hat{\Lambda}_{0m} n_m \, \mathrm{d}S = 0 , \end{cases} \tag{9}$$

and

$$\begin{cases} {}^{*}\overset{s}{C}_{2l} = \int^{s} 2\Lambda^{*}_{mn} n_n \, \mathrm{d}S = 0 , \\ \overset{s}{\hat{C}}_{2l} = \int^{s} 2\hat{\Lambda}_{mn} n_n \, \mathrm{d}S = 0 . \end{cases} \tag{10}$$

As pointed out by Einstein and Infeld (4), we can only insure the integrability of the field equations (8) by using the « dipole procedure ». The first set of equations (8) is of the form

$$\begin{cases} {}^{*}\underset{2l-2}{\gamma_{00,rr}} - 2\underset{2l-2}{\Lambda^{*}_{00}} , \\ \underset{2l-2}{\hat{\gamma}_{00,rr}} = 2\underset{2l-2}{\hat{\Lambda}_{00}} . \end{cases} \tag{11}$$

To force the integrability conditions (9) and (11) we must add to ${}^{*}\underset{2l-2}{\gamma_{00}}$ *gravitational* pole and dipole solutions and to $\underset{2l-2}{\hat{\gamma}_{00}}$ *electric* pole and dipole solutions. The additional single pole and dipole expressions contained respectively in ${}^{*}\gamma_{00}$ and $\hat{\gamma}_{00}$ are

$$\begin{cases} -\sum_{l} \lambda^{2l-2} \sum_{s=1}^{q} \left(4\overset{s}{m}(r)^{-1} + \underset{2l-2}{\overset{s}{S}_p}(r)_{,p}^{-1} \right) , \\ -\sum_{l} \lambda^{2l\ 2} \sum_{s=1}^{q} \left(4\overset{s}{e}(r)^{\ 1} + \underset{2l-2}{\overset{s}{D}_p}(r)_{,p}^{-1} \right) . \end{cases} \tag{12}$$

After the surface integrals are calculated we find that the integrability conditions are identically satisfied if we choose

$$\begin{cases} 4\underset{2l-1}{\overset{s}{\dot{m}}} = {}^{*}\overset{s}{C}_{2l-1} , \\ 4\underset{2l-1}{\overset{s}{\dot{e}}} = \overset{s}{\hat{C}}_{2l-1} , \end{cases} \tag{13}$$

and

$$\begin{cases} \underset{2l}{\overset{s}{\ddot{S}}_m} = {}^{*}\overset{s}{C}_{2l} , \\ \underset{2l}{\overset{s}{\ddot{D}}_m} = \overset{s}{\hat{C}}_{2l} . \end{cases} \tag{14}$$

Let us now remove all additional

(*) The * and $\hat{}$ denote real and imaginary quantities respectively.

(7) J. Moffat: *Proc. Camb. Phil. Soc.*, **52**, 623 (1956).

gravitational dipoles by putting

$$\sum_l \lambda^{2l-2} \overset{s}{S}_{p\,2l-2} = 0 \,. \tag{15}$$

On differentiation with respect to the « auxiliary time » τ we get

$$\sum_l \lambda^{2l} \overset{s}{\ddot{S}}_{m\,2l} = \sum_l \lambda^{2l} {}^*\overset{s}{C}_{m\,2l} = 0 \,, \tag{16}$$

which are the $3q$ equations of motion of the charged particles. In addition we have

$$\sum_l \lambda^{2l} \sum_{s=1}^{q} \overset{s}{\ddot{D}}_{m\,2l} = \sum_l \lambda^{2l} \sum_{s=1}^{q} \overset{s}{\dot{C}}_{m\,2l} \,, \tag{17}$$

and these equations determine the electric dipole moment of the system. By calculating ${}^*C_0$ and $\dot{C}_0$ we find the m's and e's from (13).

Thus in the case of the complex-symmetric field equations gravitational and electromagnetic dipoles are added at each stage of approximation to insure integrability. After the field equations have been solved the gravitational dipoles are equated to zero and this *restricts* the motion of the charged particles in the form of $3q$ equations of motion. The additional electromagnetic dipoles *cannot* be removed, because this would lead to inconsistent equations of motion, and in contrast to the gravitational dipoles these solutions are physically meaningful ([8]). At each stage of approximation the field equations determine the motion of the charged particles (by exclusion of gravitational dipoles), and specify in addition the type of singularity which is consistent with the motion; these equations of motion are *compatible*.

If we neglect non-linear gravitational effects and cross products in mass and charge we obtain in the sixth order the equations of motion previously deduced (see reference ([1]) Eq. (12.5)) together with additional electromagnetic dipole forces, and these equations of motion contain the Lorentz force.

Fuller details about this work and the calculation of the equations of motion will be published shortly.

* * *

I am grateful to Professor W. H. McCrea, Dr. W. B. Bonnor and Dr. D. J. Candlin for valuable criticisms and to my colleague Mr. R. Kerr for many stimulating discussions and suggestions.

([8]) L. Landau and E. Lifshitz: *The Classical Theory of Fields* (Cambridge, Mass., 1951).

Flux of Slow μ-Mesons and Protons Near the Geomagnetic Equator.

A. Subramanian, S. Naranan, P. V. Ramanamurthy,
A. B. Sahiar and Siddheshwar Lal

Tata Institute of Fundamental Research - Bombay

(ricevuto il 29 Agosto 1957)

In the course of an experiment on cosmic-ray particles stopping in a multiplate cloud chamber, it was possible to evaluate the vertical flux of slow μ-mesons and slow protons in air at Ootacamund (11.5° N, 76.7° E), 7500 ft above sea level, and about 2° N geomagnetic latitude. These flux values near the geomagnetic equator have been compared with those obtained by others [1-3] at higher latitudes near 50° N, to indicate the latitude effects.

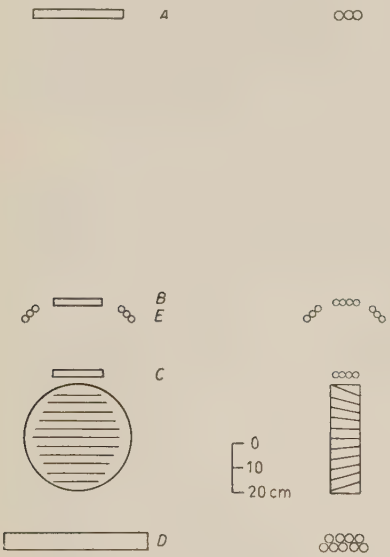

Fig. 1. – Experimental arrangement.

The experimental arrangement as shown in Fig. 1, consists of a circular cloud chamber, 45 cm in diameter, with a 10 cm illuminated depth, fitted with eleven quarter-inch thick brass plates, each equivalent to 4.2 g cm^{-2} of air. The chamber was triggered by a coincidence in the Geiger-Müller counter telescope ABC above the chamber, accompanied by an anticoincidence from Geiger-Müller trays D and E. Counters in tray E were used to reduce spurious triggerings due to side-showers. The half-angles of the counter telescope were 11° in one plane and 4° in the perpendicular plane.

The particles stopping in the plates of the chamber were classified as electrons, μ-mesons (*) or protons, from the visual estimates of ionizations of their tracks in the various compartments before stop-

(1) B. Rossi: *Rev. Mod. Phys.*, **20**, 537 (1948).
(2) M. Conversi: *Phys. Rev.*, **79**, 749 (1950).
(3) K. W. Ogilvie: *Can. Journ. Phys.*, **33**, 746 (1955).
(*) The number of locally produced π-mesons in our sample of stopping particles was estimated to be negligible.

ping, and their range in brass. Protons were easily identified since they ionized $\geqslant 3 I_{\min}$ in at least three compartments before stopping. For μ-mesons, if they traversed the plate vertically and stopped at the bottom of it, the ionization in the compartment above this quarter-inch plate could be as low as $2I_{\min}$, while that for an electron would be minimum. Due to the lack of comparison tracks of known ionization in the neighbourhood of the track of a stopping particle, it was difficult to distinguish visually between ionizations of $2I_{\min}$ and $I_{\min}$ in all conditions of chamber photography and throughout the illuminated region of the chamber. Therefore the electrons were separated from the μ-mesons by confining ourselves to particles stopping in the last four plates. The electrons could be identified by their scattering in the top seven plates, assuming that they did not loose energy by an undetected radiative process before stopping. For the determination of the proton flux, we have restricted ourselves again to the last four plates in order to separate from our sample, particles heavier than protons, such as deuterons, tritons etc. The number of particles which could not be unambiguously identified as protons or particles heavier (*) than protons is given in brackets in Table I. We have not been able to separate from this sample of protons, the possible very small number of K-mesons which on stopping did not give rise to any visible secondaries.

Table I gives the details of the data obtained, and the resulting flux values.

TABLE I.

Flux values of slow μ-mesons and slow protons near the geomagnetic equator (2° N).

Particles	Number of particles observed	Effective time of observation (hours)	Flux (*) $\cdot 10^6$ (particles g^{-1} air s^{-1} sr^{-1})
μ-mesons	272 + (49)	1072.2	$(3.7 \div 4.4) \pm 0.2$
Protons	94 + (18)	1072.2	$(0.9 \div 1.1) \pm 0.1$

(*) This flux refers to a range interval $47 \div 64$ g cm^{-2} air equivalent. The contribution of the matter in the roof, counter walls, chamber walls etc., is 17.4 g cm^{-2} air equivalent and has been included in the range limits.

The uncertain cases of mesons bracketted in Table I, are due to the difficulty in identifying them as μ-mesons or electrons in an unambiguous manner. In computing the area × solid angle factor for the acceptance of particles stopping in the bottom four plates, we have taken into consideration the loss of particles through scattering out of the illuminated region of the chamber, gain of particles through scattering into the illuminated region of the chamber, and the reduction in the solid angle of acceptance due to the dead space between adjacent counters in the trays A, B and C. We have also corrected for the loss of μ-mesons due to some of the positive mesons stopping in the plates and decaying into positrons which discharge the anticoincidence tray below. The corrections due to scattering and the decay (for mesons) decrease the area × solid angle factor by about 35% for μ-mesons, and about 9% for protons.

Comparing the above limits of the slow μ-meson flux with the value $1.2 \cdot 10^{-5}$ particles g^{-1} air s^{-1} sr^{-1} calculated for 800 g cm^{-2} (+) residual pressure at

(*) Seven definite cases of particles heavier than protons have been identified and so have not been included in the bracketted figure.

(+) At Ootacamund 7500 ft a.s.l.) the residual pressure is 800 g cm^{-2}.

50° N in the range interval $47 \div 64$ g cm^{-2} air equivalent, we are led to a latitude effect ranging from 2.6 to 3.4. In the calculation of the above flux value at 800 g cm^{-2} at 50° N, we have used the differential range spectrum of slow μ-mesons given by ROSSI [1] and the data on the rate of variation of slow μ-meson intensities with altitude given by CONVERSI [2]. In Table II we have collected the latitude effects of slow μ-mesons observed by different workers

effect suggested by OLBERT [7] and the geomagnetic latitude effect due to different energy cut-off's in the primary energy spectrum at the top of the atmosphere. The atmospheric latitude effect between 50° N and 0° as calculated by OLBERT [8] is of the order of only 10%. Hence the major portion of the latitude effects observed by various workers must be due to the geomagnetic latitude effect.

We have given in Table III, the latitude effect, between 2° N and 50° N for

TABLE II. – *Latitude effects of slow μ-mesons.*

Observers	Experimental technique	Residual ranges of mesons observed (g cm^{-2} air eq.)	Residual atmospheric pressure (g cm^{-2})	Latitudes compared	Latitude effect
CONVERSI [2] . . .	Delayed coincidence of G-M counters	$100 \div 117$	306	59° N, 9° N	1.87 ± 0.12
»		»	»	40 °N, 29° N	1.45 ± 0.1
DAVILA-APONTE and DEL ROSARIO [4]		~ 100	1030	51° N, 29° N	~ 1.35
KANEKO *et al.* [5] .	Nuclear emulsions	15 ± 5	1030	50° N *, 24° N	$1.9 \div 2.2$
TSAI-CHU and MAX MORAND [6] . . .		< 5	881	50° N *, 25° N	$3.5 \div 5.9$
» »		< 5	856	50° N *, 4° S	$3.0 \div 4.4$
Present authors . .	Multiplate cloud chamber	$47 \div 64$	800	50° N *, 2° N	$2.6 \div 3.4$

(*) The flux values at 50° N latitude were calculated from the literature [1,2].

[4] L. DEL ROSARIO and J. DAVILA-APONTE: *Phys. Rev.*, **88**. 998 (1952).

[5] S. KANEKO, T. KUBOZOE and M. TAKAHATA: *Journ. Phys. Soc. Japan*, **10**, 915 (1955).

[6] TSAI-CHU and M. MORAND: *Compt. Rend. Acad. Sci.*, **239**, 415 (1954); **235**, 1502 (1952).

and those deduced by us for latitudes where only flux measurements have been reported. We have deduced the latitude effects by comparing these flux measurements with the flux values calculated at 50° N for the appropriate atmospheric height and the relevant residual range interval.

The latitude effect of slow μ-mesons arises due to, the atmospheric latitude

slow protons at 800 g cm^{-2}, by comparing our flux value as given in Table I, with the value expected at 800 g cm^{-2} at latitude 50° N from the summary of the data [3] available on the slow proton intensity at sea level. We have used

[7] S. OLBERT: *Phys. Rev.*, **96**, 1400 (1954).

[8] S. OLBERT: *M.I.T. Technical Report*, **61** (1954).

TABLE III. – *Latitude effects of slow protons.*

Observers	Momentum interval (MeV/c)	Residual pressure (g cm^{-2})	Latitudes compared	Latitude effect
CONVERSI [2]	984 ÷ 1043	306	59° N, 9° N	3.2 ± 0.5
TSAI-CHU and M. MORAND [3]	724 ÷ 802	856	50° N *, 4° S	1.5 ÷ 2.4
Present authors	752 ÷ 830	800	50° N *, 2° N	2.7 ÷ 5.5

(*) The flux values at 50° N were calculated from OGILVIE's [3,8] data.

an absorption mean free path of (122 ± ± 12) g cm^{-2} for slow protons in air as measured by OGILVIE [9]. For protons in the momentum interval 752 ÷ 830 MeV/c (which corresponds to the residual range interval 47 ÷ 64 g cm^{-2} air equivalent), a vertical intensity of $(0.7 \div 1.0) \cdot 10^{-6}$ cm^{-2} s^{-1} sr^{-1} (MeV/c)$^{-1}$ is to be expected [3,9] at a latitude $\sim 50°$ N, at 800 g cm^{-2}. Taking our flux value per unit momentum interval as $\big((2.0 \div 2.4) \pm 0.2\big) \cdot 10^{-7}$ cm^{-2} s^{-1} sr^{-1} (MeV/c)$^{-1}$ we are led to a latitude effect ranging from 2.7 to 5.5 for slow protons. We have given in Table III, the latitude effects of slow protons, observed by different workers, and those deduced by us for latitudes where only flux values have been reported.

Our flux value of $\big((3.7 \div 4.4) \pm \pm 0.2\big) \cdot 10^{-6}$ particles g^{-1} air s^{-1} sr^{-1} for slow μ-mesons in the range interval (47 ÷ 64 g) cm^{-2} air equivalent at 2° N obtained with a multiplate cloud chamber, compares well with the value (*) $(3.3 \pm 0.6) \cdot 10^{-6}$ g^{-1} air s^{-1} sr^{-1} at 4° S, obtained in a lower range interval, viz. < 5 g cm^{-2} air equivalent by TSAI-CHU and M. MORAND [6] using nuclear emulsions. However, for slow protons, in the momentum interval 752 ÷ 830 MeV/c and at the residual pressure of 800 g cm^{-2}, we have a flux of $\big((2.0 \div 2.4) \pm 0.2\big) \cdot 10^{-7}$ particles cm^{-2} s^{-1} sr^{-1} (MeV/c)$^{-1}$ at 2° N, which is about half the value (+) $(4.5 \pm 0.4) \cdot 10^{-7}$ particles cm^{-2} s^{-1} sr^{-1} (MeV/c)$^{-1}$ obtained by TSAI-CHU and M. MORAND [6] at 4° S, using nuclear emulsions.

* * *

We have great pleasure in thanking Professor H. J. BHABHA for his encouragement, and keen interest in the work. We would also like to thank Messrs. A. R. APTE and K. F. DINSHAW for their assistance in running the chamber at Ootacamund.

Note added in proof.

BACCALIN, BASSI and MANDUCHI (*Nuovo Cimento*, **1**, 657 (1955)) have obtained a vertical flux of $(3.22 \pm 0.22) \cdot 10^{-7}$ particles cm^{-2} s^{-1} sr^{-1} (MeV/c)$^{-1}$ for slow protons in the momentum interval (890 ÷ 1200) MeV/c, at a residual atmospheric pressure of 820 g cm^{-2} and geomagnetic latitude 47° N, using a Čerenkov detector. Comparing our flux value of $((2.0 \div 2.4) \pm 0.2) \cdot 10^{-7}$ particles cm^{-2} · · s^{-1} sr^{-1} (MeV/c)$^{-1}$ with the value of BACCALIN *et al.* reduced to our altitude and momentum interval, we obtain a latitude effect of 3.0 ÷ 4.9 between 47° N and 2° N.

(8) K. W. OGILVIE: *Can. Journ. Phys.*, **33**, 555 (1955).

(*) This is the extrapolated value for our pressure of 800 g cm^{-2}.

(+) This is the value extrapolated for our pressure of 800 g cm^{-2} and corrected for the difference in the momentum intervals.

Note on the Properties of the μ-Meson.

S. Hirokawa and H. Komori

Institute for Theoretical Physics, Nagoya University - Nagoya, Japan

(ricevuto il 29 Agosto 1957)

In our previous work [1], we concluded from the analysis of cosmic ray bursts that the anomalous magnetic moment (δ) of the μ-meson does not exceed eighty percent of the normal Dirac moment. In the study of bursts, the cascade theory of showers and the problem of fluctuations are important points which should be carefully examined. As to the former, the Monte Carlo method [2] would be most reliable. In A, the ordinary cascade theory was corrected by the Monte Carlo method, though not so explicitly stated. Thus, at the footnote of page 741 of A, the factor of Christy and Kusaka 13.5 was reduced to 11.3. Hence, there would be no ambiguity in our cascade theory.

The theory of fluctuations is discussed by Mitra [3]. It is indicated that the Furry model by which we have dealt with fluctuations overestimates the frequency of bursts by a factor of about 1.5. Therefore, our conclusion that δ is less than eighty percent of the normal Dirac moment needs not be modified. The possibility of spin $-\frac{3}{2}$ of the μ-meson is also discussed by the same author [3]. On the other hand, the bremsstrahlung cross section in the case of spin $-\frac{3}{2}$ obtained by Matthews [4] exceeds the corresponding spin $-\frac{1}{2}$ cross section by a factor at least 3 at the photon energy 10^{10} eV. At the photon energy 10^{11} eV, the ratio is well over 10 and still increases rapidly with increasing energy. Because the spin $-\frac{1}{2}$ bremsstrahlung in this energy range accounts for nearly all of the bursts, it is expected that the curve of spin $-\frac{3}{2}$ bursts frequency in Fig. 2 of A would almost coincide with the curve of spin $-\frac{1}{2}$ and $\delta = 1$. Since the ambiguity of our cascade function is not significant and since the uncertainty of the Furry model is of the order of 50%, we conclude that the possibility of spin $-\frac{3}{2}$ is excluded.

Recently, the angular distribution of electrons produced by the decay of the polarized μ-mesons has been observed [5] in order to prove the non-conservation of parity. Simultaneously, the variation

---

(1) S. Hirokawa, H. Komori and S. Ogawa: *Nuovo Cimento*, **4**, 736 (1956), cited hereafter as « A ».

(2) R. R. Wilson: *Phys. Rev.*, **86**, 261 (1952).

(3) A. N. Mitra: *Nucl. Phys.*, **3**, 262 (1957).

(4) J. Mathews: *Phys. Rev.*, **102**, 270 (1956).

(5) T. Coffin, R. L. Garwin, L. M. Lederman, S. Penman and A. M. Sachs: *Phys. Rev.*, **106**, 1108 (1957),

of the counting rate of the decay electrons is also investigated by varying the magnetic field. From these experiments, it is concluded that the gyromagnetic ratio of the μ-meson is 2.00 ± 0.01. This means ([5,6]) that the spin of the μ-meson is $\frac{1}{2}$ and that δ is very small.

In conclusion, the assumption on the spin of the μ-meson made in A is justified and no modification is necessary of our previous conclusion.

([6]) The anomalous magnetic moment, $-0.4 < \delta < 0.2$ is obtained by Rawitscher making the assumption of spin $-\frac{1}{2}$ for the μ-meson, in which the cross section of the μ-meson pair creation by photons is estimated, G. H. RAWITSCHER, preprint. We wish to thank Dr. G. H. RAWITSCHER for sending us the manuscript before publication (*Phys. Rev.*, **107**, 274 (1957)).

ERRATA - CORRIGE

S. HIROKAWA, H. KOMORI and S. OGAWA – **On the Anomalous Magnetic Moment of μ-Mesons:** *Nuovo Cimento*, **4**, 736 (1956).

Line 15, page 743 of A: « uncertainty of the cascade function » should read « uncertainty of the fluctuations ».

Lines 9-14, page 745 of A: « But his reduction may not be ... » should read as follows ([1]): « According to Carmichael, the number of ion pairs in the experiment of Driggers is small; $3.0 \cdot 10^5 \div 1.2 \cdot 10^6$ ion pairs. So, the energy range covered by Driggers' experiment is different from that of Schein and Gill ».

([1]) W. D. WALKER: private communication. We are grateful to Professor W. D. WALKER for communicating us his valuable opinion on this point.

A Remark on a Paper by Barašenkov.

C. Hayashi

Department of Nuclear Science, Kyoto University - Kyoto

(ricevuto il 24 Settembre 1957)

In a recent paper Barašenkov [1] has made a remark that the integrability condition is not satisfied in the author's [2] Hamiltonian formulation of quantized fields with a non-local interaction. Such a conclusion cannot be true since the Hamiltonian in this formulation has originally been derived in accordance with a general scheme which contains a prescription completely equivalent to theintegrability condition. It will be shown in the following that the calculations made by Barašenkov are in fact misleading.

For the sake of comparison, the notation of Barašenkov will be used. The canonical variables $A_0[x;\sigma]$ and $\psi_0[x;\sigma]$ obey the equation of motion

$$\frac{\delta A_0[x;\sigma]}{\delta\sigma(x')} = i[H(x'/\sigma);\, A_0[x;\sigma]\,]. \tag{1}$$

The Hamiltonian has been expressed as space-time integrals of products of the operators A_0, ψ_0 and factors which depend on σ explicitly [2]. Then, we have for the Hamiltonian

$$\frac{\delta H(x/\sigma)}{\delta\sigma(x')} = \frac{\partial H(x/\sigma)}{\partial\sigma(x')} + i[H(x'/\sigma);\, H(x/\sigma)]\,, \tag{2}$$

where $\delta/\delta\sigma$ means a total derivative, and $\partial/\partial\sigma$ is a derivative with respect to σ which is included explicitly. The last term of (2) has been overlooked by Barašenkov. The contribution of this term to $[\delta/\delta\sigma(x'');\, \delta/\delta\sigma(x')]A_0[x;\sigma]$ just cancels the other contributions as calculated by Barašenkov [1] (*). Using eq. (1) and (2)

[1] V. S. Barašenkov: *Nuovo Cimento*, **5**, 1469 (1957).

[2] C. Hayashi: *Prog. Theor. Phys.*, **10**, 533 (1953); **11**, 226 (1954).

(*) His expression (29) itself should be corrected as follows. The last two terms on the right side of $[\partial H_2(x'/\sigma)/\partial\sigma(x'');\, A_0[x;\sigma]]$, that is, $\Delta_m(x_1 - x_1')\psi_0[x_3';\sigma]\psi_0[x_3;\sigma] + \Delta_m(x_3 - x_3')\psi_0^*[x_1;\sigma]\psi_0^*[x_1';\sigma]$ should be replaced by $\Delta_m(x_1 - x_3')\psi_0^*[x_1';\sigma]\psi_0[x_3;\sigma] + \Delta_m(x_3 - x_1')\psi_0^*[x_1;\sigma]\psi_0[x_3';\sigma]$. The expression for $[\delta/\delta\sigma(x'');\, \delta/\delta\sigma(x')]A_0[x;\sigma]$ should also be corrected correspondingly.

we have

$$(3)\qquad \left[\frac{\delta}{\delta\sigma(x'')};\frac{\delta}{\delta\sigma(x')}\right]A_0[x;\sigma] =$$

$$= i\left[\frac{\partial H(x'/\sigma)}{\partial\sigma(x'')} - \frac{\partial H(x''/\sigma)}{\partial\sigma(x')} + i[H(x''/\sigma);\, H(x'/\sigma)];\quad A_0\,[x;\sigma]\right],$$

and an expression of the same form for $\psi_0[x;\sigma]$. Each commutator on the right side of (3) has been calculated in the g^2-approximation ([1]). It is easily found that (3) really vanishes in this approximation. More generally, a direct calculation gives

$$(4)\qquad \frac{\partial H_2(x''/\sigma)}{\partial\sigma(x')} = -\frac{\partial H_2(x'/\sigma)}{\partial\sigma(x'')} = \frac{i}{2}\,[H_1(x''/\sigma);\, H_1(x'/\sigma)]\,,$$

which confirms that the equivalent integrability condition,

$$(5)\qquad \frac{\partial H(x'/\sigma)}{\partial\sigma(x'')} - \frac{\partial H(x''/\sigma)}{\partial\sigma(x')} + i[H(x''/\sigma);\, H(x'/\sigma)] = c\text{-number}\,,$$

is satisfied.

* * *

In conclusion, the author thanks Prof. S. Hiroishi for valuable discussions.

Theory of the Dirac Field as a Continuous Assembly of Small Rotating Bodies.

T. Takabayasi (*)

Institut Henri Poincaré - Paris

(ricevuto il 24 Settembre 1957)

The Dirac spinor ψ (in c-number theory) defines a Lorentz frame at each point of space with the set of four 4-vectors all real and mutually orthogonal. They are quantities related to ψ in bilinear manners, i.e. (+)

$$S_\mu = i\bar{\psi}\gamma^\mu\psi\,, \qquad \hat{S}_\mu = i\bar{\psi}\gamma^5\gamma^\mu\psi\,, \tag{1}$$

and the real and imaginary parts $\alpha_\mu^{(1)}$ and $\alpha_\mu^{(2)}$ of the *complex* vector

$$\Xi_\mu = \bar{\psi}^c\gamma^\mu\psi = \alpha_\mu^{(1)} + i\alpha_\mu^{(2)}\,, \tag{2}$$

where ψ^c denotes the charge conjugate spinor defined by

$$\psi^c = C\bar{\psi}^T\,, \tag{3}$$

with

$$C^\dagger C = 1\,, \qquad C^T = -C\,, \qquad (\gamma^\mu)^T = -C^{-1}\gamma^\mu C\,. \tag{4}$$

Accordingly Ξ_μ may also be written as

$$\Xi_\mu = -\psi^T C^{-1}\gamma^\mu\psi\,. \tag{5}$$

If we introduce the complex vector $\Xi_\mu^\times$ which is imaginary conjugate (−) to Ξ_μ,

(*) On leave of absence from Nagoya University (Japan).

(+) $\bar{\psi} = \psi^\dagger\gamma^4$. In this paper $+$ signifies adjoint, $*$ complex conjugate, and T transpose. A 4-vector is real when its space components are real while its time component is pure imaginary. Greek suffixes run from 1 to 4. Precisely, $\hat{S}_\mu$ is a pseudovector.

(−) Here « imaginary conjugate » means that $\Xi_\mu^\times = \Xi_\mu^*$ for $\mu = 123$, $= -\Xi_\mu^*$ for $\mu = 4$. Such $\Xi_\mu^\times$ can be written $\Xi_\mu^\times = \psi^\dagger\gamma^4\gamma^\mu\gamma^4 C\psi^* = -\bar{\psi}\gamma^\mu\psi^c$, and is shown to be a vector.

$\alpha_\mu^{(1)}$ and $\alpha_\mu^{(2)}$ are written in the form:

$$6) \qquad \alpha_\mu^{(1)} = \frac{1}{2}(\Xi_\mu + \Xi_\mu^\times), \qquad \alpha_\mu^{(2)} = \frac{1}{2i}(\Xi_\mu - \Xi_\mu^\times).$$

Actually, we can verify the identical relations

$$(7) \qquad \begin{cases} (\alpha_\mu^{(1)})^2 = (\alpha_\mu^{(2)})^2 = \hat{S}_\mu^2 = \varrho^2, \qquad S_\mu^2 = -\varrho^2, \\ \alpha_\mu^{(1)}\alpha_\mu^{(2)} = \alpha_\mu^{(1)} S_\mu = \alpha_\mu^{(2)} S_\mu = \alpha_\mu^{(1)} \hat{S}_\mu = \alpha_\mu^{(2)} \hat{S}_\mu = S_\mu \hat{S}_\mu = 0, \end{cases}$$

where ϱ is the scalar quantity defined by

$$(8) \qquad \varrho = (\Omega^2 + \hat{\Omega}^2)^{\frac{1}{2}},$$

with

$$(9) \qquad \Omega = \bar{\psi}\psi, \qquad \hat{\Omega} = i\bar{\psi}\gamma^5\psi.$$

Incidentally we note that $\{\Omega, \hat{\Omega}\}$ defines the other variable θ (pseudoscalar) by

$$(10) \qquad \operatorname{tg}\theta = \hat{\Omega}/\Omega.$$

If we introduce unitary vectors $a_\mu^{(\xi)}$ ($\xi = 1, 2, 3, 4$) in the directions of $\alpha_\mu^{(1)}$, $\alpha_\mu^{(2)}$, $\hat{S}_\mu$ and S_μ by

$$(11) \qquad \begin{cases} \alpha_\mu^{(\xi)} = \varrho a_\mu^{(\xi)}, \qquad (\xi = 1, 2) \\ \hat{S}_\mu = \varrho a_\mu^{(3)}, \qquad S_\mu = i\varrho a_\mu^{(4)}, \end{cases}$$

then $(a_\mu^{(\xi)})$ satisfies

$$(12) \qquad a_\mu^{(\xi)} a_\nu^{(\xi)} = \delta_{\mu\nu}, \qquad a_\mu^{(\xi)} a_\mu^{(\eta)} = \delta_{\xi\eta},$$

and exactly represents a Lorentz frame.

Furthemore we can show that the Dirac field ψ is represented equivalently by this Lorentz frame assigned to each point of space, together with two more variables ϱ and θ.

Also we take into account the fact that the existence of a Lorentz frame $(a_\mu^{(\xi)})$ is equivalent to the co-existence of a *translation* with a velocity v_μ (*) and a *rotational orientation* of spatial axes represented by a rotation matrix (C_{jk}), which naturally obeys

$$(13) \qquad C_{ij}C_{jk} = \delta_{jk}.$$

(*) v_μ is a unitary 4-velocity satisfying $v_\mu^2 = -1$, and is related to the 3-dimensional velocity $\boldsymbol{V}$ through

$$v_i = v_0 V_i/c, \qquad v_4 = iv_0, \qquad v_0 = (1 - \boldsymbol{V}^2/c^2)^{-\frac{1}{2}}.$$

Latin suffix runs from 1 to 3.

Explicitly $a_\mu^{(\xi)}$ are expressed in terms of v_μ and C_{ik} as follows:

$$(14) \qquad \begin{cases} a_{4\mu} = -iv_\mu\,, \qquad a_{i4} = iC_{ij}v_j\,, \\ a_{ik} = C_{ik} + \dfrac{C_{ij}v_jv_k}{1-iv_4}\,. \end{cases}$$

We have thus obtained the representation of the Dirac field in terms of the set of variables

$$(15) \qquad \{v_\mu,\ (C_{ik}),\ \varrho,\ \theta\}\,.$$

The above result shows that we can regard the Dirac field as a continuous assembly of very small rotating bodies (*) whose rotational orientation and translational velocity are specified by (C_{ik}) and v_μ, respectively, ϱ means simply the distribution of the number density of such bodies in the rest reference frame and θ is an additional internal variable possessed by the body, other than the rotational degrees of freedom.

At this point we remark the following. Under a gauge-transformation (+)

$$(16) \qquad A_\mu \to A_\mu + \partial_\mu \lambda\,, \qquad \psi \to \exp\left[\frac{ie}{\hbar c}\lambda\right]\cdot\psi\,,$$

ϱ, θ, $a_\mu^{(3)}$ and $a_\mu^{(4)}$ are invariant, while $a_\mu^{(1)}$ and $a_\mu^{(2)}$ are not so. It is therefore profitable to revise the definition of Ξ_μ slightly so that it becomes gauge-invariant. Namely we separate a phase factor such that

$$(17) \qquad \Xi_\mu = \exp\left(2iA/\hbar\right)\cdot\Xi'_\mu\,,$$

where A is a redundant scalar function with the property that it transforms, under (16), like

$$(18) \qquad A \to A + \frac{e}{c}\lambda\,.$$

Henceforth we adopt Ξ'_μ and corresponding $\alpha_\mu^{(\xi)\prime}$ and $a_\mu^{(\xi)\prime}$ $(\xi = 1, 2)$, and write them simply as Ξ_μ, $\alpha_\mu^{(\xi)}$, and $a_\mu^{(\xi)}$. They are all gauge-independent quantities and retain the properties in the original definitions. The Dirac field is then represented by the set of variables,

$$(19) \qquad \{a_\mu^{(\xi)},\ \varrho,\ \theta,\ A\}\,.$$

Finally the time evolution of the Dirac field is expressed as the equations of

(*) By « rotating body » we only mean a certain body whose rotational orientation of internal rotation has a definite meaning, but do not assume further properties concerning the usual concept of rigidity.

(+) A_μ is the potential of the electromagnetic field acting on the Dirac particle;

$$\partial_\mu = \frac{\partial}{\partial x_\mu}\,. \qquad x_4 = ict\,.$$

motion for our variables (19). They are derived from the following Lagrangian density (*),

$$\mathcal{L} = -\varrho\left\{mc^2(ia_\mu^{(4)}k_\mu + \cos\theta) + \frac{\hbar c}{2}(a_\mu^{(3)}\partial_\mu\theta - i\varepsilon_{\mu\nu\varkappa\lambda}a_\mu^{(4)}a_\nu^{(3)}\partial_\varkappa a_\lambda^{(4)})\right\} + \tag{20}$$

$$+ \lambda_{\mu\nu}(a_\mu^{(\xi)}a_\nu^{(\xi)} - \delta_{\mu\nu}),$$

where the derivations are to be taken with respect to the arguments

$$\{a_\mu^{(\xi)},\ \varrho,\ \theta,\ \Lambda,\ \lambda_{\mu\nu} = \lambda_{\nu\mu}\}, \tag{21}$$

while k_μ in (20) are dependent variables defined by

$$mck_\mu = -\frac{e}{c}A_\mu + \partial_\mu\Lambda - \frac{\hbar}{2}a_\nu^{(1)}\partial_\mu a_\nu^{(2)}. \tag{22}$$

This is also gauge-independent and has the meaning of a particle momentum-energy 4-vector. The equations of motion following immediately from (20) contain the redundant variables $\lambda_{\mu\nu}$, other than $\{a_\mu^{(\xi)},\ \varrho,\ \theta,\ k_\mu\}$, but $\lambda_{\mu\nu}$ can be easily eliminated therefrom. (+) Anyway we can actually verify that the set of our equations of motion resulting from (20) is equivalent to the original Dirac equation.

The present theory has close relationship with the hydrodynamical representation of the Dirac field previously constructed [1]. The variables ϱ, θ, v_μ and k_μ are exactly the same things as employed in the hydrodynamical scheme. Also $a_\mu^{(3)}$ is nothing but the spin pseudovector w_μ used there.

(*) $\varepsilon_{\mu\nu\varkappa\lambda}$ is the signature of the permutation $(\mu\nu\varkappa\lambda)$.

(+) The equations of motion are considered in a separate note.

[1] T. TAKABAYASI: *Nuovo Cimento*, **3**, 233 (1956); *Phys. Rev.*, **102**, 297 (1956); *Suppl. Prog. Theor. Phys. (Japan,)* No. 4 (1957).

Variation of Electron Mass with Velocity.

F. C. Champion
King's College, University of London

(ricevuto il 4 Ottobre 1957)

Faragó and Jánossy [1] have recently concluded that the experiments of Champion [2] failed to distinguish between the formula of Abraham and that of Lorentz, on the grounds that the experimental error was too large. Taking the most unfavorable case selected by them, where they represent the error as three times the standard error, amounting to 12% of the rest energy, I would point out that Fig. 1 of Faragó and Jánossy's paper indicates a ratio of 300% in the values predicted by the two theories for $(m_\parallel/m)^2$ at the energy considered by Champion. This was expressed by him in the form of expected collision angles of 58° and 75.2° according to the two theories respectively, the experimental angle being found to be $(75.2 \pm 1.5)°$, with a difference therefore of over 25%. Details of thirteen other independent and technically favorable instances of electron-electron collisions were given, all of which supported the relativity formula with the same order of experimental accuracy.

While I am entirely in agreement with Faragó and Jánossy that the accuracy of collision experiments cannot compare with that attainable by spectroscopic techniques such as the fine structure doublet separation of hydrogen-like spectra, I must insist that with the most unfavorable estimation of the errors involved in the collision experiment, there is no doubt whatever that they show that if one wishes to predict experimentally how momentum and energy will be shared during the elastic collision of two electrons in the energy range $(0.5 \div 1)$ MeV, a much more accurate forecast will result if the relativistic formulae are used in preference to any other existing relations. Whether this conclusion « proves » the validity of relativity theory, or to what degree of accuracy any experiment has to be carried to « prove » any theory, is a matter of definition and opinion.

[1] P. S. Faragó and L. Jánossy: *Nuovo Cimento*, **5**, 1411 (1957).

[2] F. C. Champion: *Proc. Roy. Soc.*, A **136**, 630 (1932).

On the Σ-Hyperon-Nucleon Interaction Cross-Section - II.

F. Ferrari and M. Tonin

Istituto di Fisica dell'Università - Padova
Istituto Nazionale di Fisica Nucleare - Sezione di Padova

(ricevuto il 22 Ottobre 1957)

As is well known, an apparent discrepancy exists between the data on K^- capture in hydrogen [1] and in emulsion nuclei [2] in so far as the interaction rates leading to different hyperons are concerned. In a previous paper [3] it was supposed that the figures of ~ 0.4 for the ratio $(\Lambda_p + \Sigma_p^0)/(\Sigma_p^- + \Sigma_p^+)$ as given by Alvarez *et al.* [1] and $\lesssim 3$ for the ratio $(\Lambda_{\mathcal{H}} + \Sigma_{\mathcal{H}}^0)/(\Sigma_{\mathcal{H}}^- + \Sigma_{\mathcal{H}}^+)$ obtained from photographic emulsion experiments, might be due to a large cross-section for the process

$$\Sigma + N \to \Lambda + N + Q \,, \tag{1}$$

transforming, inside nuclear matter, a large number of Σ's into Λ's. The fitting of the data with such an hypothesis leads to a reaction cross-section $\sigma_{\Sigma\Lambda}$ of about 50 mb, while the cross-section $\sigma_{\Sigma\Sigma}$ for the process

$$\Sigma^i + N \to \Sigma^i + N \qquad (i = +, -) \tag{2}$$

results much smaller.

This value however may be greatly modified if one takes into account that the hyperons are produced in nuclear matter and consequently, as suggested by various authors [4], may be subjected to a mean nuclear potential: the hyperons in the nucleus will be considered as being inside a nuclear potential V_Σ to which the Coulomb potential V_C has to be added for the charged hyperons [5]. In what follows we will consider a nucleus described by an ideal Fermi gas defined by $R = r_0 A^{\frac{1}{3}}$, where $r_0 = 1.4 \cdot 10^{-13}$ cm, and having the binding energy of the last nucleon equal to 8 MeV. Furthermore we will assume that the K particles are absorbed

(1) L. W. Alvarez, H. Bradner, P. Falk, J. D. Gow A. H. Rosenfeld and R. D. Tripp, F. T. Solmitz: *Nuovo Cimento*, **5**, 1026 (1957).

(2) W. F. Fry: *Phys. Rev.*, **100**, 950 (1955); D. W. Falla, M. W. Friedlander, F. Anderson, W. D. B. Greening, S. Limentani, B. Sechi-Zorn, C. Cernigoi, G. Iernetti and G. Poiani: *Nuovo Cimento*, **5**, 1203 (1957).

(3) N. Dallaporta and F. Ferrari: *Nuovo Cimento*, **3**, 743 (1957).

(4) *Padua-Venice Conference on «Mesons and recently discovered particles»* 1957.

(5) H. Capps: *Phys. Rev.*, **107**, 239 (1957).

by a single nucleon in the nucleus exclusively by the reaction

$$K^- + N \to Y + \pi \,. \tag{3}$$

In fact, as is experimentally known, this reaction is the predominant one; the probability that the absorption involves two nucleons,

$$K^- + N + N \to Y + N \tag{4}$$

being smaller than 10 %.

Taking into account the relative isotopic spin wave functions of the initial and final states of reactions (3), and the ratios observed in hydrogen by ALVAREZ *et al.* [1], i.e.

$$\Sigma_p^- : \Sigma_p^0 : \Sigma_p^+ : \Lambda_p = 4 : 2 : 2 : 0.5$$

we have that the ratios in nuclei are:

$$\Sigma_p^- : \Sigma_p^0 : \Sigma_p^+ : \Lambda_p = 6 : 4 : 2 : 1.5 \tag{5}$$

or

$$\frac{\Sigma_p^0 + \Lambda_p}{\Sigma_p^- + \Sigma_p^+} \sim 0.7 \,. \tag{6}$$

Let us now consider a hyperon produced at a point P distant ϱ from the center of the nucleus. As in reference [3] the probability that a charged Σ^i may be converted to Σ^0 or Λ is taken as being related to the strength of the reactions (1) and (2). However we have here the additional fact that the hyperon may be reflected from the nuclear surface: the reflection probability (or the transmission coefficient $\tau^i(E)$) is a function of the Σ-nucleus potential V_Σ, of the electrostatic potential V_C and of the kinetic energy of the hyperon itself.

The probability that a hyperon generated at a point P by a capture event, (*) will escape from the nucleus as Σ^i or Y^0, will be given by the following relations (see also formulae (4) and (5) of reference [3]):

$$\Pi_{\Sigma^i} = \int_{R-\varrho}^{R+\varrho} \mathrm{d}t\, W(R, \varrho, t)\, \Sigma_p^i \left\{ \int_{V_\Sigma - V_C}^{\infty} \mathrm{d}E\, P^i(E)\, \frac{\exp\left[-t/\lambda_{T\Sigma}\right]}{1 + 2\left[1 - P(R, R, \lambda_{T\Sigma})\right](1 - T^i)/T^i} + \right.$$

$$\left. + (1 - \bar{\eta}^i) \int_{V_\Sigma - V_C}^{\infty} \mathrm{d}E\, P^i(E) \left(1 - \frac{\exp\left[-t/\lambda_{T\Sigma}\right]}{1 + 2\left[1 - P(R, R, \lambda_{T\Sigma})\right](1 - T^i)/T^i} \right) \right\} , \tag{7}$$

and

$$\Pi_{Y^0} = \int_{R-\varrho}^{R+\varrho} \mathrm{d}t\, W(R, \varrho, t) \left\{ \Lambda_p + \Sigma_p^0 + \sum_i \left[\Sigma_p^i \int_0^{V_\Sigma - V_C} \mathrm{d}E\, P^i(E) + \right. \right.$$

$$\left. \left. + \Sigma_p^i \bar{\eta}^i \int_{V_\Sigma - V_C}^{\infty} \mathrm{d}E\, P^i(E) \left(1 - \frac{\exp\left[-t/\lambda_{T\Sigma}\right]}{1 + 2\left[1 - P(R, R, \lambda_{T\Sigma})\right](1 - T^i)/T^i} \right) \right] \right\} . \tag{8}$$

(*) In the derivation of expressions (7) and (8) we have supposed that the number of Σ^i which are converted into Σ^0 is approximately equal to the number of Σ^0 which are converted into Σ^i.

In the above, $P^i(E)$ represents the energetic distribution function of a hyperon with charge i inside the nucleus; $1-\bar{\eta}^i$ gives the probability that a hyperon Σ^i, after a collision, does not transform into a Λ and may have sufficient energy to escape from the nucleus. The function $P(R, \varrho, \lambda_{T\Sigma})$ which gives the escape probability, has been defined by CLEMENTEL and PUPPI (6) and T^i is given by:

$$T^i = \frac{\int_{V_\Sigma - V_c}^{\infty} dE\, P^i(E)\, \tau^i(E)}{\int_{V_\Sigma - V_c}^{\infty} dE\, P^i(E)}$$

The introduction of the potential V_Σ allows one to fit the experimental data assuming different values for the cross-sections $\sigma_{\Sigma\Lambda}$, $\sigma_{\Sigma\Sigma}$ and for the hyperon-nucleus potential V_Σ. In order to discriminate between the various possibilities which are thus presented, it is convenient to consider other experimental data. For this purpose we have also considered the ratio Σ^-/Σ^+ which in hydrogen turns out to be $\Sigma_p^-/\Sigma_p^+ \sim 2$, while from emulsion experiments it turns out to be $\Sigma\bar{\varrho}/\Sigma\bar{\varrho} \leqslant 2$.

The ratios $(\Sigma_{\varrho}^0 + \Lambda_{\varrho})/(\Sigma_{\varrho} + \Sigma_{\varrho}^+)$ and $\Sigma\bar{\varrho}/\Sigma_{\varrho}^+$ can easily be calculated from formulae (7) and (8).

The results are plotted in Fig. 1 and in Fig. 2, as functions of the total cross-section $\sigma_{T\Sigma}$ and for several values of the Σ-nucleus potential:

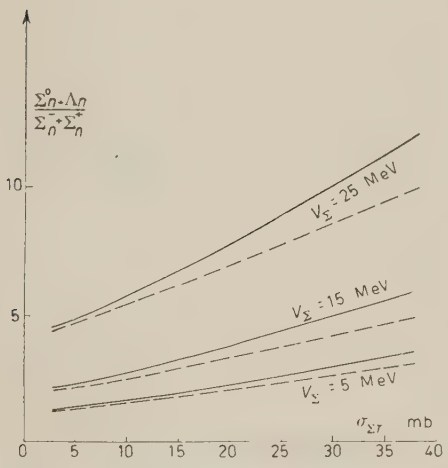

Fig. 1.

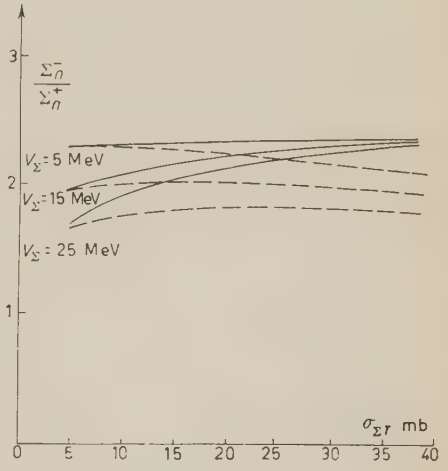

Fig. 2.

1) The full line has been obtained by assuming that the cross-section of reaction (1) is greater than the cross-sections of reactions (2), namely $\sigma_{\Sigma\Sigma} = 0.2\, \sigma_{T\Sigma}$.

2) The dotted line is obtained if one makes the inverse hypothesis, $\sigma_{\Sigma\Lambda} = 0.2\, \sigma_{\Sigma T}$.

(6) E. CLEMENTEL and G. PUPPI: *Nuovo Cimento*, **10**, 197 (1953).

From an inspection of the figures and taking into account that the observed ratios are $(\Sigma^0_{\mathcal{H}} + \Lambda_{\mathcal{H}})/(\Sigma^-_{\mathcal{H}} + \Sigma^+_{\mathcal{H}}) \lesssim 3$ and $\Sigma^-_{\mathcal{H}}/\Sigma^+_{\mathcal{H}} \leqslant 2$ (these values have been corrected for the loss of Σ^-), it can be seen that the Σ-nucleus potential must lie between ~ 10 MeV and ~ 20 MeV, unless one assumes very small $\sigma_{\Sigma\Lambda}$ or $\sigma_{\Sigma\Sigma}$ cross-sections, say smaller than 10 mb. These limits may not be considerably modified if one considers a more refined nuclear model (see H. Capps, reference [5]).

It is to be remarked that the hypothesis 1) leads to total cross-sections of the order of magnitude ~ 10 mb, while the hypothesis 2) can also lead (see Fig. 2) to greater total cross-sections.

As a consequence, in this last case one can obtain agreement with the experimental data with a quite small cross-section for the processes (1), say $\sigma_{\Sigma\Lambda} \sim 10$ mb, while the cross-sections for the processes (2) can be of the same order of magnitude as the geometric nucleon-nucleon cross-section, say $\sigma_{\Sigma\Sigma} \sim 40$ mb. (We have assumed $V_\Sigma \sim 10$ MeV). It is interesting to compare these values with the calculated total S-wave hyperon-nucleon scattering cross-sections given by Lichtenberg and Ross [7] (see Table I).

Energy in MeV	Cross-sections in mb						
	$\Lambda p \to \Lambda p$ $\Lambda n \to \Lambda n$	$\Sigma^+ p \to \Sigma^+ p$ $\Sigma^- n \to \Sigma^- n$	$\Sigma^- p \to \Lambda n$ $\Sigma^+ n \to \Lambda p$	$\Sigma^0 p \to \Lambda p$ $\Sigma^0 n \to \Lambda n$	$\Sigma^- p \to \Sigma^- p$ $\Sigma^+ n \to \Sigma^+ n$	$\Sigma^0 p \to \Sigma^0 p$ $\Sigma^0 n \to \Sigma^0 n$	$\Sigma^- p \to \Sigma^0 n$ $\Sigma^+ n \to \Sigma^0 p$
14	46	98	4.6	2.3	50	67	15
28	19	39	2.8	1.4	24	27	7.1

Although a detailed analysis cannot be made on the basis of our simple optical model, it is seen that at last qualitatively these results are not in disagreement with those derived by Lichtenberg and Ross from scattering data.

* * *

We are indebted to Prof. N. Dallaporta for many discussions and advices.

Note added in proof:

The most recent experimental values of the ratio Σ^-_N/Σ^+_N are considerably smaller than 2 [8]. Such a value can be explained by considering also the processes

$$\Sigma^0 n \to \Sigma^- p \,,$$

$$\Sigma^0 p \to \Sigma^+ n \,,$$

[7] D. Lichtenberg and M. Ross: *Pion Contribution to Hyperon-Nucleon Forces* (in press).

[8] F. C. Gilbert, C. E. Violet and R. S. White: *Phys. Rev.* **107**, 228 1957, K^- Stack collaboration; Padua-Venice *Conference* 1957.

which in our calculations have not been considered (see note at foot of page 2), If we include these processes and assume a cross-section $\sigma_{\Sigma^0\Sigma^-} = \sigma_{\Sigma^0\Sigma^+} = 15$ mb, and take into account the ratios given in formula (5) and the energetic distribution function of the hyperon after the collision (the hyperons are mainly of low energy owing to the Pauli principle), we have that, with $V_\Sigma = 10$ MeV, 80% of the Σ^- produced by Σ^0 are captured while 90% of the Σ^+ can escape from the nucleus. With these hypotheses we have

$$\frac{\Sigma_N^0 + \Lambda_N}{\Sigma_N^- + \Sigma_N^+} \cong 3 \qquad \text{and} \qquad \frac{\Sigma_N^-}{\Sigma_N^+} \cong 1.2 \,.$$

The figure of 1.2 is in good agreement with the latest experimental data quoted above. A detailed discussion on these topics will be published.

* * *

We wish to thank Dr. D. Evans and Dr. D. Prowse for discussions.

A Search for the Existence of Asymmetries in Positive K-Meson Decay.

A. Wataghin (*)
H. H. Wills Physical Laboratory - Bristol

G. Alexander and R. H. W. Johnston
Dublin Institute for Advanced Studies

(ricevuto il 23 Ottobre 1957)

1. – Introduction.

It is a consequence of the two component theory of the neutrino, that an asymmetry should exist in the angular distribution of the meson secondary to the K_{μ_2} decay mode, if: *a*) the spin of the K-meson is different from zero, and *b*) the beam is polarized, and *c*) serious depolarization does not take place in the focussing and analysing magnetic fields.

In the course of an experiment (1), the purpose of which was the determination of the relative abundances of the K-particle decay modes and the study of the 3 body decay-spectra, records were kept of angular data relating to 2 697 K_L decays. The angular distribution of the secondaries in this sample of 2 697, which may be regarded as being random, has been analysed in this work.

For reasons explained at length in (1), it is considered that the scanning bias is negligible. The number of K-particles coming to rest for which no secondary was visible is less than 2%.

2. – Conditions of exposure.

The experimental arrangements for the selection of the primary K-particles were those shown in Fig. 1 of Birge *et al.* (2). A beam of secondary particles from a copper target was selected at mo-

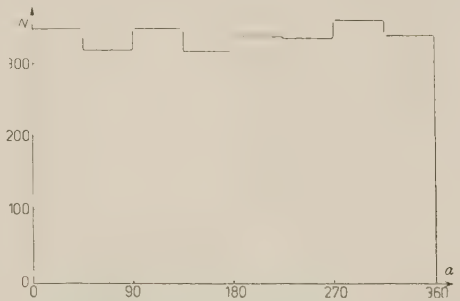

Fig. 1. – Angle α between initial secondary direction at edge of stack, projected on the emulsion plane. Distribution of values of α from 2 697 K^+ decays at rest.

(*) On leave of absence from Faculdade de Filosofia, S. Paulo University, with a fellowship from Conselho de Pesquisas of Brazil.

(1) G. Alexander, R. H. W. Johnston and C. O'Ceallaigh: *Nuovo Cimento*, **6**, 478 (1957).

(2) R. W. Birge, D. H. Perkins, J. R. Peterson, D. H. Stork and M. N. Whitehead: *Nuovo Cimento*, **4**, 834 (1956).

mentum 409 MeV/c at 90° to the circulating proton beam of the Berkeley Bevatron by a system of quadrupole focussing magnets followed by an analysing magnet. The field of the latter produced a deflection of the secondary beam through an angle of 45°.

The emulsion block was exposed with the pellicles perpendicular to the plane containing the 409 MeV/c focussed beam and the initial 6.2 GeV proton beam, so that the momentum, as defined in the analysing magnet, was constant in each plate but varied slowly across the stack.

3. – Depolarization of the beam.

In the event of the K-meson beam being polarized in the production process, one might expect a certain degree of depolarization to take place in the quadrupole focussing magnets; particles travelling along different rays within the cone of acceptance will encounter magnetic fields of widely differing strengths and orientations. However, over a wide central area of the magnetic lens-system the field is relatively small, so that to assume as an order of magnitude 10^4 G for the depolarizing magnetic field would appear to be reasonably conservative. The time of flight in the quadrupole focussing system is about $2 \cdot 10^{-9}$ s. Under these conditions one would expect precessions of the order of 10° to take place, so that the beam would not undergo serious depolarization.

The time of flight in the analysing magnet is of the same order of magnitude. The field in this case however being uniform, one expects precession of all the particles to take place by the same amount, so that the percentage polarization of the beam should not decrease.

The stray magnetic field in the region of the plate was found be ~ 50 G. After the K-meson has come to rest, the precession that one can expect due to this field in 10^{-8} s (mean lifetime of the K-meson) is of the order of 0.5°. Thus, the depolarization effect arising from this cause may be neglected.

4. – Possible spin effects.

If the K-mesons have spin different from zero and the beam were polarized, some anisotropy in the angular distribution of the particles emitted should exist unless the secondary particles from the K_{π_2} mode (abundance 23%) have possessed such asymmetry as to compensate the supposed asymmetry in the K_{μ_2} (61% abundance). Our results, given in the next section, on the identified K_{π_2}, K_{μ_2} and the total sample, do not lend support to such an assumption.

It should also be remarked that, if the angular distribution of the π in the K_{π_2} mode is supposed isotropic (there is no reason at the moment to suppose that it is not), an asymmetry of $\sim 15\%$ in the K_{μ_2} part of the total sample would be clearly seen as a $\sim 10\%$ asymmetry in our total sample.

It is of interest to note also that the observation of an asymmetry in the decay of μ-mesons in emulsion [3], in spite of possible triplet muonium formation, suggests that K-meson effects, if they exist, ought not to be obscured by the analogous process of K-mesonium formation.

5. – Experimental results.

Our results, given in Tables I, II, III and in Fig. 1, are consistent with isotropy in space of the direction of emission of the charged emitted particle. For the K_L sample, a peak to valley

[3] R. L. GARWIN, L. M. LEDERMAN and M. WEINRICH: *Phys. Rev.*, **105**, 1415 (1957).

excess ratio $\gtrsim 10\%$ in any direction in space should be seen either in the projected α distribution (Table I, Fig. 1) or in the data relating to dip given in Table III. The angle α is the projection on the emulsion plane of the angle between the direction of the K-beam when entering the stack and the direction of the charged particle emitted in the decay. The α distributions for identified cases of K_{μ_2} and K_{π_2} are given in Table II. The distributions of these samples, though smaller, are also consistent with isotropy.

TABLE I. – *Number of* K_L.

0° – 45°	348
45° – 90°	318
90° – 135°	348
135° – 180°	316
180° – 225°	336
225° – 270°	334
270° – 315°	359
315° – 360°	338
Total	2 697

TABLE II.

α	K_{μ_2}	K_{π_2}
0° – 60°	33	11
60° – 120°	28	16
120° – 180°	47	14
180° – 240°	23	12
240° – 300°	28	12
300° – 360°	36	12
Total	195	77

TABLE III.

Dip % (Processed emulsion).	Number (Experimental)	Percentage (Experimental)	Calculated on assumption of isotropy
$0 \leqslant \delta < 6$	408	13.4 ± 0.5	12.9
$6 \leqslant \delta < 20$	699	23.0 ± 0.9	25.0
$20 \leqslant \delta$	1936	63.6 ± 0.9	62.8
Total	3043	100.0	100.7
Toward glass	1169		
Toward surface	1153		

6. – Discussion and conclusion.

An investigation of the angular distribution in space the secondary of 436 cases of K_L-decay has been carried out by M.I.T.-Johns Hopkins Group (4). Further, F. and M. BRUIN (5) have analysed 500 K_L, (the projected angle distribution only). No evidence for anisotropy was found in either case.

The above analysis based on 2697 events enables an upper limit of about 10% to be placed on the anisotropy with 1% confidence on unresolved modes, or a $\sim 15\%$ limit on the K_{μ_2} part of the total sample, if the distribution of the other modes is supposed isotropic. There is no indication of any asymmetry in the identified K_{μ_2} and K_{π_2} beyond that expected through statistical fluctuations.

* * *

We wish to thank Prof. C. O'CEALLAIGH and Dr. D. PROWSE for useful discussions and constant interest in this work.

(4) Reported on behalf of M.I.T. - Johns Hopkins Group C. O'CEALLAIGH: *7th Rochester Conference Report.*

(5) F. and M. BRUIN: *Physica*, **23**, 553 (1975).

Direttore responsabile: G. POLVANI

Tipografia Compositori - Bologna

Questo fascicolo è stato licenziato dai torchi il 29-XII-1957